The HITRAN 2012 Molecular Spectroscopic Database

L.S. Rothman[a,*], I.E. Gordon[a], Y. Babikov[b], A. Barbe[c], D.Chris Benner[d], P.F. Bernath[e], M. Birk[f], L. Bizzocchi[ff], V. Boudon[g], L.R. Brown[h], A. Campargue[i], K. Chance[a], L. Coudert, V.M. Devi[d], B.J. Drouin[h], A. Fayt[j], J.-M. Flaud[k], R.R. Gamache[l], J. Harrison[m], J.-M. Hartmann[k], C. Hill[n], J.T. Hodges[o], D. Jacquemart[p], A. Jolly[k], J. Lamouroux[k,l], R.J. LeRoy[q], G. Li[a], D. Long[o], C.J. Mackie[a,†], S.T. Massie[r], S. Mikhailenko[b], H.S.P. Müller[rr], O.V. Naumenko[b], A.V. Nikitin[b], J. Orphal[s], V. Perevalov[b], A. Perrin[k], E.R. Polovtseva[b], C. Richard[a], M.A.H. Smith[t], E. Starikova[b], K. Sung[h], S. Tashkun[b], J. Tennyson[n], G.C. Toon[h], Vl.G. Tyuterev[c], J. Vander Auwera[u], G. Wagner[f]

[a]*Harvard-Smithsonian Center for Astrophysics, Atomic and Molecular Physics Division, Cambridge MA 02138, USA*
[b]*Institute of Atmospheric Optics, Tomsk 634055, RUSSIA*
[t]*Université de Reims-Champagne-Ardenne, Groupe de Spectrométrie Moléculaire et Atmosphérique, 51062 Reims, FRANCE*
[d]*The College of William and Mary, Department of Physics, Williamsburg VA 23187, USA*
[e]*Old Dominion University, Department of Chemistry and Biochemistry, Norfolk VA 23529, USA*
[f]*DLR, Remote Sensing Technology Institute, Wessling 82234, GERMANY*
[ff]*CAAUL, Observatório Astronómico de Lisboa, Lisboa, PORTUGAL*
[g]*CNRS-Université de Bourgogne, Institut Carnot de Bourgogne, 21078 Dijon, France*
[h]*California Institute of Technology, Jet Propulsion Laboratory, Pasadena CA 91109, USA*
[i]*Université Joseph Fourier/CNRS, Laboratoire de Spectrometrie Physique, 38402 Saint-Martin-d'Hères, FRANCE*
[j]*Université Catholique de Louvain, Lab. de Spectroscopie Moléculaire, 1348 Louvain-la-Neuve, BELGIUM*
[k]*CNRS et Universités Paris Est et Paris 7, Laboratoire Inter-Universitaire des Systèmes Atmosphériques, 94010 Créteil, FRANCE*
[l]*University of Mass Lowell, Dept. of Environmental Earth and Atmospheric Sciences, Lowell MA 01854, USA*
[m]*University of York, Department of Chemistry, York YO10 5DD, UK*
[n]*University College London, Dept. of Physics and Astronomy, London WC1E 6BT, UK*
[o]*National Institute of Standards and Technology, Gaithersburg MD 20899 USA*
[p]*UPMC Univ. Paris 06, UMR 7075, Laboratoire de Dynamique, Interactions et Réactivité, 75252 Paris, FRANCE*
[q]*University of Waterloo, Department of Chemistry, Waterloo ON, N2L 3G1, CANADA*
[r]*National Center for Atmospheric Research, Boulder CO 80307, USA*
[rr]*Universität zu Köln, I. Physikalisches Institut, Cologne 50937, GERMANY*
[s]*Karlsruhe Institute of Technology, Institute for Meteorology and Climate Research, Eggenstein-Leopoldshafen 76344, GERMANY*
[t]*NASA Langley Research Center, Science Directorate, Hampton VA 23681, USA*
[u]*Université Libre de Bruxelles, Service de Chimie Quantique et Photophysique, 1050 Brussels, BELGIUM*

Received:_____

[*]Corresponding author: Tel.: +1 (617) 495-7474; fax: +1 (617) 496-7519.
E-mail address: LRothman@cfa.harvard.edu (L.S. Rothman).

[†]Current address: *University of Western Ontario, Department of Physics and Astronomy London, ON,, N6A 3K7, CANADA*

Abstract

This paper describes the status of the latest edition of the HITRAN molecular spectroscopic compilation. The new edition is meant to replace the previous HITRAN edition of 2008 and its updates during the intervening years. The HITRAN molecular absorption compilation is comprised of six major components structured into folders that are freely accessible on the internet. These folders consist of the traditional line-by-line spectroscopic parameters required for high-resolution radiative-transfer codes, infrared absorption cross-sections for molecules not yet amenable to representation in a line-by-line form, ultraviolet spectroscopic parameters, aerosol indices of refraction, collision-induced absorption data, and general tables such as partition sums that apply globally to the data. The new HITRAN is greatly extended in terms of accuracy, spectral coverage, additional absorption phenomena, and validity. Molecules and isotopologues have been added that address the issues of atmospheres beyond the Earth. Also discussed is a new initiative that casts HITRAN into a relational database format that offers many advantages over the long-standing sequential text-based structure that has existed since the initial release of HITRAN in the early 1970s.

1. Introduction

This article describes the data that have been added, modified, or enhanced in the HITRAN (**Hi**gh Resolution **Tran**smission) compilation since the previous update of 2008 [1] (hereafter called HITRAN2008 in the text). The HITRAN compilation is comprised of several components that have been arranged into folders that include: (1) line-by-line spectroscopic parameters for high resolution molecular absorption and radiance calculations (from the microwave through visible region of the spectrum); (2) infrared absorption cross-sections (generally representing absorption by molecules that have very dense spectra or many low-lying vibrational modes); (3) ultraviolet datasets (both line-by-line and cross-sections); (4) tables of aerosol refractive indices; (5) collision-induced absorption datasets; and (6) global data and software for filtering and managing the data. The updates to these six portions of HITRAN will be discussed in the following sections.

It is necessary to call attention to some caveats. The units used throughout HITRAN and this paper do not strictly adhere to the SI system for both historical and application-specific reasons. Thus cm is seen throughout, as is atm for pressure. We also employ the symbol ν throughout for line position in cm^{-1}, thereby dropping the tilde ($\tilde{\nu}$) that is the official designation of wavenumber. We normally express the HITRAN unit for intensity as cm^{-1}/(molecule cm^{-2}) rather than simplifying to the equivalent cm/molecule. In this manner we emphasize the quantity as wavenumber per column density, which is consistent with the viewpoint of atmospheric radiative-transfer codes.

There are a number of transitions in the line-by-line portion of HITRAN that have not been fully assigned in terms of quantum identification. Their lower-state energy is not known, but these transitions have been carefully measured at room temperature (296K is the standard

HITRAN temperature). We have opted to retain many of these important lines in the database, using minus one (-1) as a flag to warn users; in some cases, a crude guess of the lower-state energy has been made for these unassigned lines.

The line positions in the microwave region can be measured with a great degree of precision. The previous HITRAN format for the transition wavenumber, while allowing for eleven significant digits, suggested a FORTRAN field of F12.6. This had the effect of often placing only six places after the decimal, and thus valuable information in the microwave region was being lost. Considering that the flexible decimal point in the line positions can cause serious issues with existing computer codes, we have changed this format for only two molecules (HNO_3 and PH_3), but are planning to make the changes throughout entire database in the future so researchers will start to have to prepare for this change now. For HNO_3 and PH_3, nine places after the decimal are given for line positions with $v \leq 1$ cm^{-1}, eight for $1 < v \leq 10$, seven $10 < v \leq 100$, and six everywhere else.

The data that enter HITRAN or replace previous entries go through a rigorous process. Figure 1 is a schematic of the general process. The vertical box on the left is a representation of the many sources that come to the attention of the HITRAN committee. This committee is formed of an international group of spectroscopists covering all the molecules and spectral regions encompassed by HITRAN. Sources selected (and that can include measurements or calculations of line positions, and/or intensities, line-shape parameters, etc.) are then cast into the format of the HITRAN line list, or cross-section sets if that is applicable. Basic rules are applied to the line list as shown in the legend, and errors and outliers are culled. If possible, the line list is then provided for comparison with independent observations, often long-path high-resolution atmospheric measurements. The results are then discussed with the committee at large. This

whole process is intensive; there are quality measurements and calculations appearing in the literature and at meetings that may not get into the source box and may later appear as updates to HITRAN editions. Finally, users play an important role in the process. Inevitably errors can appear in the database, or important newer information does not get incorporated. Users often conduct new laboratory or field measurements that provide additional input to the scheme.
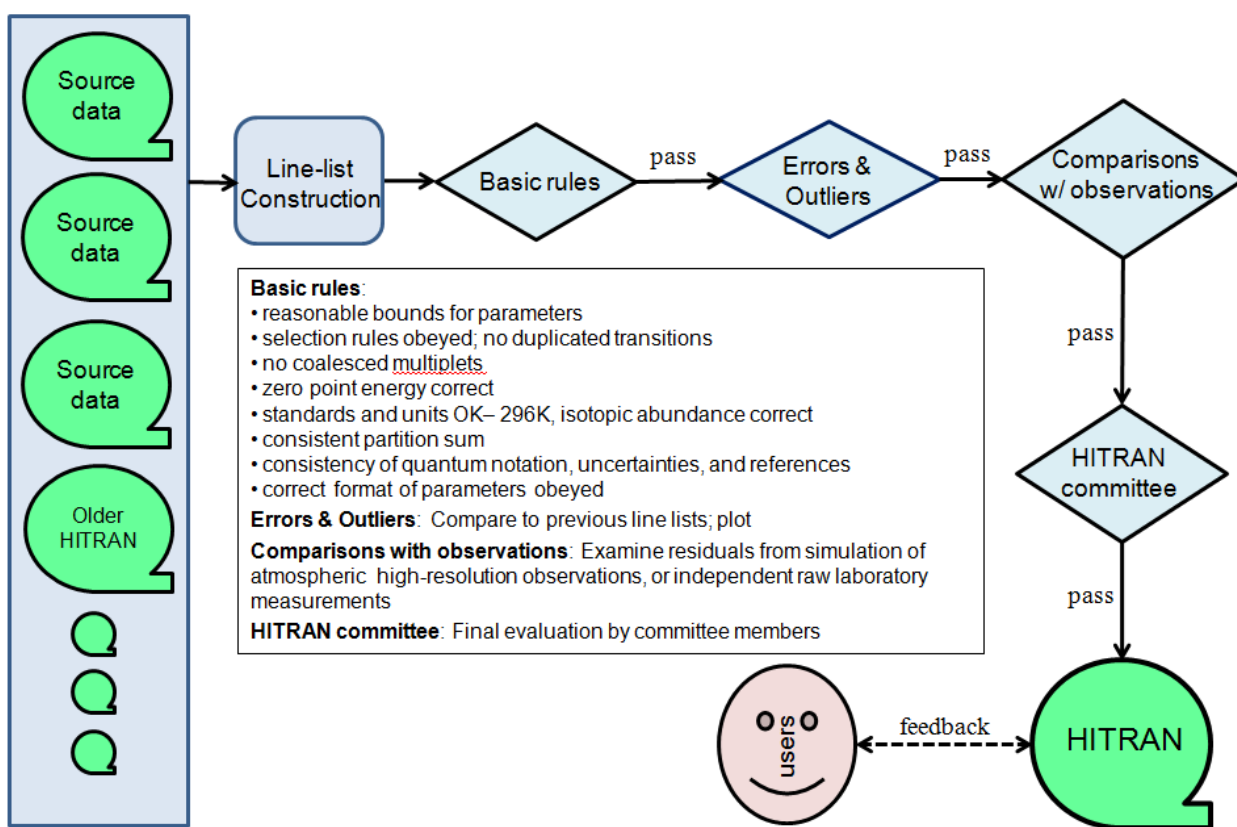
Approximate location of Fig. 1

Figure 1. Validation scheme for HITRAN line lists.

2. Line-by-line parameters

It has been over four years since the release of HITRAN2008, and during this time frame many significant improvements have been accomplished and incorporated into this new edition of HITRAN. The suite of spectral line parameters which have been represented since 2004 [2]

5

are displayed in Table 1. The improvements in the line-by-line parameters have been accomplished by vastly improved experimental techniques and analysis, as well as more sophisticated and robust theoretical treatments. In this section, we describe the changes, additions, and modifications of the molecules represented in the line-by-line portion of the HITRAN compilation in sub-sections ordered by the chronological HITRAN molecule number assignment; if no change was made, we still list the molecule in a sub-section. We emphasize that users of the molecular data should consult and reference the original sources of data. These sources are now easy to access (see Section 7 below).

Approximate location of Table 1

Table 1. Description of the quantities present in the 160-character records (transitions) of the line-by-line portion of the HITRAN database.

Para-meter	Meaning	Field Length	Type	Comments or units
M	Molecule number	2	Integer	HITRAN chronological assignment
I	Isotopologue number	1	Integer	Ordering by terrestrial abundance
v	Vacuum wavenumber	12	Real	cm^{-1}
S	Intensity	10	Real	$cm^{-1}/(molecule \cdot cm^{-2})$ at standard 296K
A	Einstein-A coefficient	10	Real	s^{-1}
γ_{air}	Air-broadened half width	5	Real	HWHM at 296K (in $cm^{-1}atm^{-1}$)
γ_{self}	Self-broadened half width	5	Real	HWHM at 296K (in $cm^{-1}atm^{-1}$)
E''	Lower-state energy	10	Real	cm^{-1}
n	Temperature-dependence coefficient	4	Real	Temperature-dependent exponent for γ_{air}
δ	Air pressure-induced line shift	8	Real	$cm^{-1}atm^{-1}$ at 296K
V'	Upper-state "global" quanta	15	Hollerith	see Table 3 in Ref. [2]
V''	Lower-state "global" quanta	15	Hollerith	see Table 3 in Ref. [2]
Q'	Upper-state "local" quanta	15	Hollerith	see Table 4 in Ref. [2]
Q''	Lower-state "local" quanta	15	Hollerith	see Table 4 in Ref. [2]
Ierr	Uncertainty indices	6	Integer	Accuracy for 6 critical parameters (v, S, γ_{air}, γ_{self}, n, δ), see Table 5 of Ref. [2]
Iref	Reference indices	12	Integer	References for 6 critical parameters (v, S, γ_{air}, γ_{self}, n, δ)
*	Flag	1	Character	Pointer to program and data for the case of line mixing
g'	Statistical weight of upper state	7	Real	See details in Ref. [3]
g''	Statistical weight of lower state	7	Real	See details in Ref. [3]

Table 2 provides an overview of the status of the high-resolution portion of the new edition of HITRAN. There are now 47 species and 109 isotopologues overall (additional species are covered by cross-section data, see Section 3.). The spectral coverage of the line-by-line portion ranges from the microwave region through the visible (UV transitions are discussed in Section 4).

Approximate location of Table 2

Table 2. Molecules and isotopologues represented in line-by-line portion of HITRAN.

Molecule	Isotopo-logue[a]	Spectral Coverage (cm^{-1})	Number of Transitions	Molecule	Isotopo-logue[a]	Spectral Coverage (cm^{-1})	Number of Transitions
(1) H_2O	161	0 — 25711	142 041	(19) OCS	622	0 — 4200	15 618
	181	0 — 19917	39 918		624	0 — 4166	6 087
	171	10 — 19946	27 546		632	0 — 4056	3 129
	162	0 — 22708	13 238		623	0 — 4164	2 886
	182	0 — 3825	1 611		822	0 — 4046	1 641
	172	1234 — 1599	175	(20) H_2CO	126	0 — 3100	40 670
(2) CO_2	626	345 — 12785	169 292		136	0 — 117	2 309
	636	406 — 12463	76 245		128	0 — 101	1 622
	628	0 — 11423	122 549	(21) HOCl	165	1 — 3800	8 877
	627	0 — 9560	27 724		167	1 — 3800	7 399
	638	461 — 8025	40 620	(22) N_2	44	11 — 9355	1 107
	637	494 — 8062	23 465		45	11 2578	161
	828	482 — 8161	10 411	(23) HCN	124	0 — 3424	2 955
	827	498 — 8194	14 729		134	2 — 3405	652
	838	539 — 6688	3 092		125	2 — 3420	646
(3) O_3	666	0 — 6997	261 866	(24) CH_3Cl	215	0 — 3173	100 293
	668	0 — 2768	44 302		217	0 — 3162	95 927
	686	1 — 2740	18 887	(25) H_2O_2	1661	0 — 1731	126 983
	667	0 — 2122	65 106	(26) C_2H_2	1221	604 — 9890	12 613
	676	0 — 2101	31 935		1231	613 — 6623	285
(4) N_2O	446	0 — 7797	33 074		1222	1 — 789	7 512
	456	5 — 5086	4 222	(27) C_2H_6	1221	706 — 3001	43 592
	546	4 — 4704	4 592		1231	726 — 919	6 037
	448	542 — 4672	4 250	(28) PH_3	1111	0 — 3602	22 190
	447	550 — 4430	1 705	(29) COF_2	269	696 — 2002	168 793
(5) CO	26	3 — 8465	1 019		369	685 — 815	15 311
	36	3 — 6279	797				
	28	3 — 6267	770				
	27	3 — 6339	728				

Molecule	Code	Range	Count
	38	3 — 6124	712
	37	1807 — 6197	580
(6) CH$_4$	211	0 — 11502	528 664
	311	0 — 11319	72 421
	212	7 — 6511	54 550
	312	959 — 1695	4 213
(7) O$_2$	66	0 — 15928	1 811
	68	1 — 15852	1 162
	67	0 — 14537	11 338
(8) NO	46	0 — 9274	103 701
	56	1609 — 2061	699
	48	1602 — 2039	679
(9) SO$_2$	626	0 — 4093	72 460
	646	0 — 2501	22 661
(10) NO$_2$	646	0 — 3075	104 223
(11) NH$_3$	446	0 — 5295	27 994
	456	0 — 5180	1 090
(12) HNO$_3$	146	0 — 1770	903 855
	156	0 — 923	58 108
(13) OH	61	0 — 19268	30 769
	81	0 — 329	295
	62	0 — 332	912
(14) HF	19	24 — 46985	10 073
	29	13 — 47365	24 303
(15) HCl	15	8 — 34250	11 879
	17	8 — 34240	11 907
	25	5 — 33284	29 994
	27	5 — 33258	29 911
(16) HBr	19	13 — 16034	3 039
	11	13 — 16032	3 031
	29	7 — 8781	1 455
	21	7 — 8778	1 55
(17) HI	17	10 — 13908	3 161
	27	5 — 7625	1 590
(18) ClO	56	0 — 1208	5 721
	76	0 — 1200	5 780
(30) SF$_6$	29	580 — 996	2 889 065
(31) H$_2$S	121	2 — 11330	34 329
	141	5 — 11227	10 166
	131	5 — 11072	5 466
(32) HCOOH	126	10 — 1890	62 684
(33) HO$_2$	166	0 — 3676	38 804
(34) O	6	68 — 159	2
(35) ClONO$_2$	5646	763 — 798	21 988
	7646	765 — 791	10 211
(36) NO$^+$	46	1634 — 2531	1 206
(37) HOBr	169	0 — 316	2 177
	161	0 — 316	2 181
(38) C$_2$H$_4$	221	701 — 3243	18 097
	231	2947 — 3181	281
(39) CH$_3$OH	2161	0 — 1408	19 897
(40) CH$_3$Br	219	794 — 1706	18 692
	211	796 — 1697	18 219
(41) CH$_3$CN	2124	890 — 946	3 572
(42) CF$_4$	29	594 — 1313	60 033
(43) C$_4$H$_2$	2124	0 — 758	124 126
(44) HC$_3$N	1224	0 — 760	180 332
(45) H$_2$	11	15 — 36024	4 017
	12	3 — 36405	5 129
(46) CS	22	1 — 2586	1 088
	34	1 — 1359	396
	32	1 — 1331	396
	23	1 — 156	198
(47) SO$_3$	2666	0 — 2778	10 881

a. AFGL shorthand code for isotopologues

2.1. H$_2$O (molecule 1)

The spectrum of water vapor has significant transitions throughout the complete spectral range of HITRAN. A detailed knowledge of the spectral parameters of water is paramount not only to remote sensing of planetary atmospheres, but to disentangle their effect as interferents in the detection and characterization of other species. The techniques of experiment and of theory

have steadily advanced, and new results often disagree with HITRAN2008 values as well as among themselves. We have conducted a thorough investigation regarding which parameters need to be updated or included in the database. Below we describe deficiencies identified in the HITRAN2008 water line list and the improvements introduced into the HITRAN2012 data for water vapor.

2.1.1 Deficiencies in the HITRAN2008 H_2O line list

Several deficiencies related to the water-vapor line list were identified and addressed:

(1) Due to the difficulties associated with measurements of water-vapor line intensities, some values given in HITRAN were reported to have problems. For instance, intensities in the 8000-9000 cm^{-1} spectral region were reported to have been systematically in error (10-15%) by authors of more recent experiments [4], theoretical calculations [5], and atmospheric retrievals [6, 7]. Less dramatic, but still noticeable (5-10%) inconsistencies were identified below 8000 cm^{-1} (see, for instance Refs. [8-10]) where a majority of intensities down to 1750 cm^{-1} (for stronger lines) originated from the unpublished SISAM database of Toth [11]. It is worth pointing out that the SISAM database tabulates intensities obtained both experimentally and using a semi-empirical model. However, only the calculated ones were adopted into the HITRAN database, and it was later determined that the experimental values were often superior to the calculated ones. In fact, the water vapor line list used by the TCCON (Total Carbon Column Observing Network) community [12] employs the measured values from Toth when the retrievals using HITRAN were not satisfactory.

(2) Air-broadened half widths in HITRAN2008 employed a rather sophisticated scheme, explained in Ref. [13], that determines and eliminates the experimental outliers and then either uses the experimental values or their averages if they exist, theoretical values calculated using

the complex Robert-Bonamy (CRB) method (see for instance Refs. [14, 15]), or if no experimental or theoretical value exists, semi-empirical values from Ref. [16]. There is room for improvement of these values. For instance, it was found that the CRB calculations should have included a larger number of correlation functions, higher-order cut-offs for convergence, and exact trajectories [17]. Failure to do so resulted in underestimation of the widths of some of the lines.

(3) The temperature dependences in HITRAN2008 originated from CRB calculations [14, 15] and suffered from the same problems as CRB air-broadened half-widths, as identified by Ma et al. [17]. This problem was also confirmed experimentally by Birk and Wagner [18].

(4) Partly in order to save disk storage and due to limited knowledge of reliable spectral parameters for weak lines, the previous versions of HITRAN employed a nonlinear (with wavenumber of the transition) intensity cutoff designed to provide transitions that would contribute to absorption over very long paths at telluric temperatures. However, the current cutoff criterion has been found to be over restrictive for remote-sensing applications [6]. Since disk storages have significantly increased in their capacity in recent years and due to the development of new sensitive experimental techniques (e.g. cavity ring-down spectroscopy) on par with advances in theoretical calculations, it was decided that the cutoff criterion established in the first HITRAN edition needed to be relaxed.

2.1.2 Construction of $H_2^{16}O$ line list

Figure 2 represents a flow diagram of the construction of the $H_2^{16}O$ line list (only for line positions and intensities) for this edition of HITRAN, while a detailed description is given below.
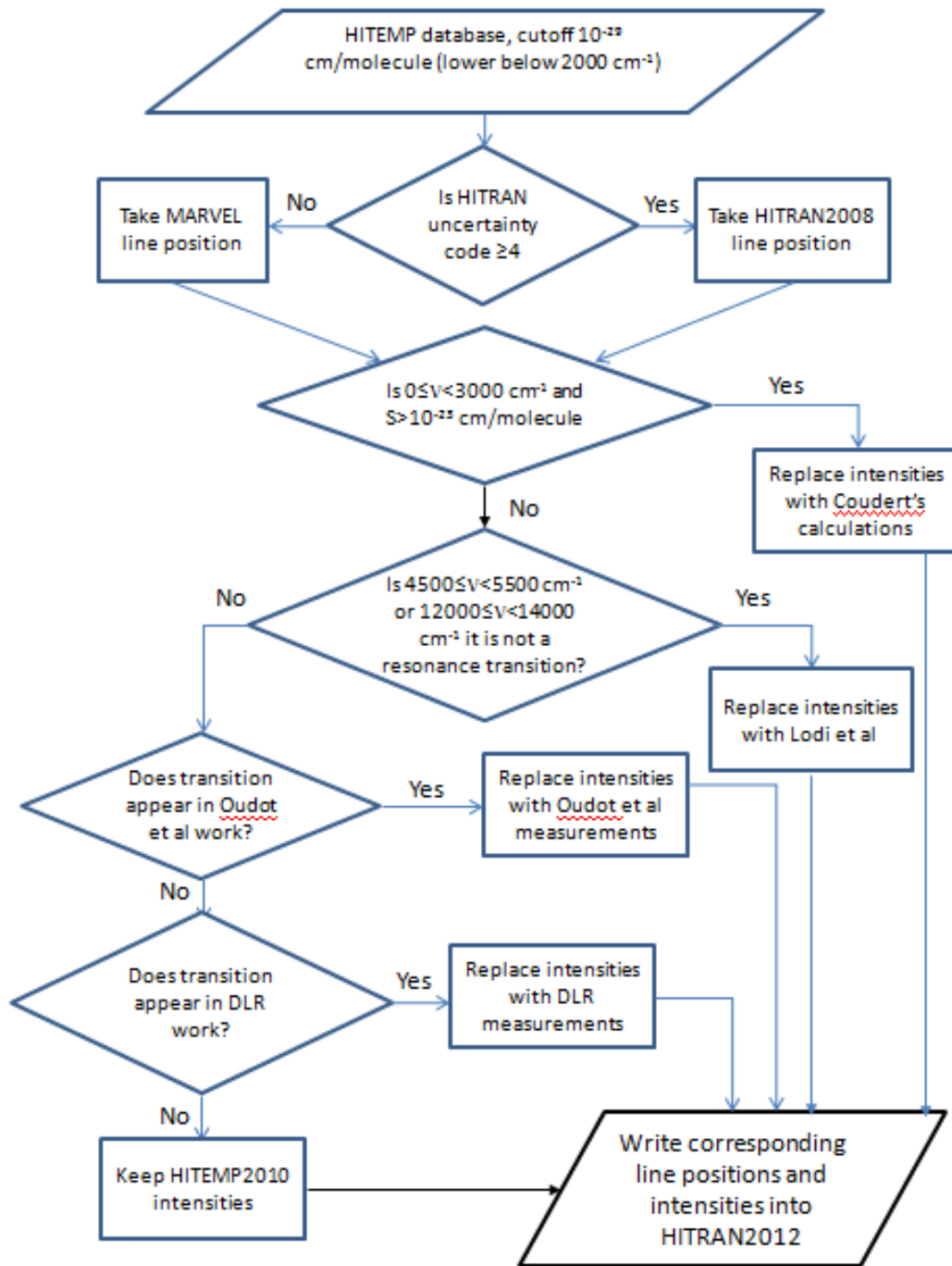
Figure 2. Flow diagram for the construction of the $H_2^{16}O$ line list.

(1) The asymptote of the previous formula for the intensity cutoff has been changed to S_{crit} = 10^{-29} cm^{-1}/(molecule cm^{-2}) (from the previous value of 3×10^{-27} cm^{-1}/(molecule cm^{-2})). The new formula for the cutoff is

$$S_{cut}(T) = \frac{S_{crit}\nu}{\nu_{crit}}\tanh\left(\frac{c_2\nu}{2T}\right) \qquad 0 < \nu \leq 2000 \text{ cm}^{-1} , \tag{1a}$$

$$S_{cut}(T) = S_{crit} \qquad \nu > 2000 \text{ cm}^{-1} , \tag{1b}$$

where c_2 is the second radiation constant and $T = 296$ K. Lines with intensities greater than S_{crit} above ν_{crit} =2000 cm^{-1}, as well as weaker lines below 2000 cm^{-1}, are now able to enter the database. We applied this cutoff to the HITEMP2010 [19] database water file which has intensities originating from the BT2 ab initio line list [20] with corresponding HITRAN2008 transitions, as well as empirically-derived transition wavenumbers replacing ab initio values whenever possible. In other words, instead of starting with a HITRAN2008 dataset we started to work from the reduced HITEMP database which is essentially the HITRAN2008 database supplemented with weaker lines. Whenever a rotational quantum number could not be determined unambiguously, the index of symmetry (1, 2, 3, and 4 as defined in Ref. [20]) accompanied with a negative sign was used. Note that 1 and 2 indicate para states, whereas 3 and 4 indicate ortho states. For the case of unassigned vibrational quanta, a "-2" label has been adopted.

Owing to this approach, the database not only became more complete but also does not have any unassigned lines (contrary to HITRAN2008 which contained over 800 of such lines).

(2) The line positions in HITEMP are either a) from HITRAN, or b) from a rather outdated collection of empirically derived wavenumbers, or c) from ab initio origin with uncertainty occasionally reaching 0.3 cm^{-1}. For HITRAN2012, some of these line positions were improved using following procedure.

A very extensive international effort was recently carried out to derive empirical energy levels of water vapor from the available measured transition wavenumbers [21] using a procedure known as MARVEL [22, 23] which involves inverting a cleansed and weighted set of transitions. This database of energy levels is then used to generate a dataset of all allowed transitions between these levels. Here "allowed" refers to transitions with $\Delta J = 0, \pm 1$, and ortho-ortho and para-para transitions. These transition wavenumbers replaced the HITEMP values, unless these values originated from HITRAN and have uncertainty indices larger than 4 (i.e. good to 0.001 to 0.0001 cm^{-1}). It is important to note that previous versions of HITRAN had erroneously assigned an uncertainty code "3" to *all* of the line positions originating from SISAM [11]. We have reassigned uncertainty codes for the line positions from the SISAM database in HITRAN before introducing MARVEL values.

(3) In HITRAN2008, experimental intensities from the work of Coudert et al [8] were employed wherever available and the quality of these intensities has proved to be superior to HITRAN2004 data from SISAM [11] available in this region. We now employ calculated intensities from the work of Martin et al. [24] that now extend to higher wavenumber. Considering that only strong lines in the 0-3000 cm^{-1} region from that work were evaluated, we adopted intensities stronger than 10^{-23} cm^{-1}/(molecule cm^{-2}) from that work in the 800-3000 cm^{-1} region, and intensities stronger than 10^{-26} cm^{-1}/(molecule cm^{-2}) below 800 cm^{-1}.

(4) Newer ab initio intensities from the work of Lodi et al [5] were incorporated in the 4500-5500 cm^{-1} and 12000-14000 cm^{-1} regions. These are the only regions from this work that were thoroughly evaluated and these theoretical intensities are superior not only in comparison with BT2 ab initio values but also with the available experimental data (for most of the transitions). The ab initio intensities improve on previous studies by (a) using high-quality ab initio

calculations specifically designed to converge the dipole moment and (b) using sensitivity analysis to identify those transitions involved in intensity borrowing via resonances, for which the computed results are not reliable [19]. Figure 3 clearly demonstrates that there is substantially better consistency among the bands in Lodi et al than the BT2 work. Intensities shown in the figure span the 4700-5000 cm^{-1} region. In particular, one can see that in the BT2 work, line intensities calculated for the $3\nu_2$ band were consistently poor, while the $\nu_1+\nu_2$ and $\nu_2+\nu_3$ bands agreed very well with experimental data. We also evaluated the 4500-5000 cm^{-1} region using retrievals from the solar pointing FTS at Park Falls, WI and found the Lodi et al data superior to other publicly available data sets [25]. A separate publication describing this work is planned. Note that in the 12000-14000 cm^{-1} region, a rather large number of resonance lines occur for which reliable theoretical predictions are not yet available; for those lines the previous HITRAN entries have been retained.
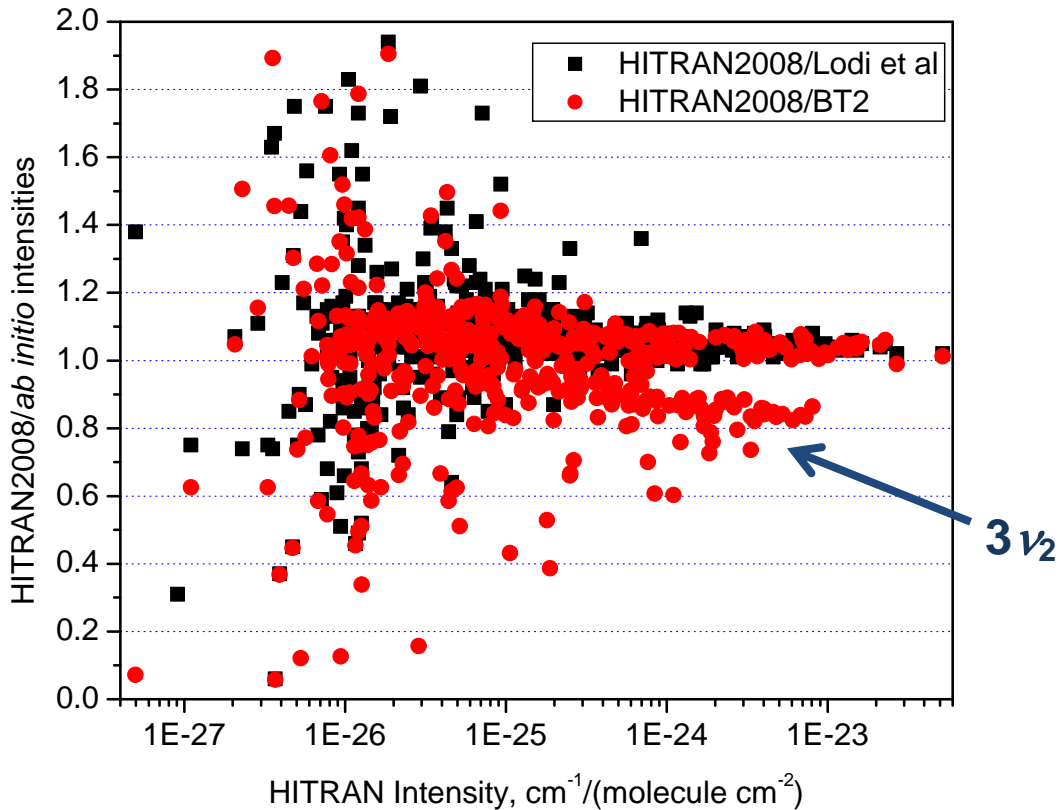
Approximate location of Figure 3

Figure 3. Comparison of HITRAN2008 with the values of BT2 [20] (red circles) and with the values of Lodi et al [5] (black squares) in the 4700-5000 cm^{-1} region.

(5) Intensities from the work of Oudot et al [4] were adopted in the 8000-9000 cm^{-1} spectral region wherever available. Also, intensities from unpublished, high-accuracy work by Wagner and Birk [26] in the 1-μm region were taken wherever available. The quality of the intensity data was confirmed by intercomparison with cavity ring-down results [27]. Agreement in intensities with [27] was better than 1%. For the vibrational band (2 0 1 $\leftarrow$ 0 0 0), agreement with Lodi and Tennyson [3] is better than 1%.

2.1.2 Construction of $H_2^{18}O$ and $H_2^{17}O$ line lists

Line positions and intensities were taken from the line lists of Lodi and Tennyson [28] for the entire HITRAN2012 line list of the $H_2^{18}O$ and $H_2^{17}O$ isotopologues. In Ref. [28], line

positions and intensities were calculated using the potential energy surface of Shirin et al [29] and the dipole moment function of Lodi et al [5]. Line intensities in the case of the ν_2 band of $H_2^{18}O$ were compared to experimental data which are an unpublished part of the line intensities [5] and line broadening [15] work of Birk and Wagner. Agreement better than 1% was found. The line positions were supplemented with transition wavenumbers derived from the corresponding MARVEL dataset [30].

For HITRAN2012, line positions from the SISAM database [11] with uncertainties better than 0.001 cm^{-1} were substituted in place of those from Lodi and Tennyson list [28]. Finally, we made full quantum assignments for just under a hundred unassigned lines from the Lodi and Tennyson list [28].

2.1.3 HDO line list corrections

An error was discovered in the transcription of the intensities of HDO line parameters above 11500 cm^{-1}. They were a factor of 10 too large in the 2008 release of HITRAN, and have now been corrected.

2.1.4 Line-shape parameters for the $H_2^{16}O$, $H_2^{18}O$ and $H_2^{17}O$ line lists

The air-broadened half widths for the first three isotopologues of water continue to be derived using the procedure described by Gordon et al. [13], with some experimental outliers identified and removed. Some of the outliers were identified in the work of Ma et al. [31]. It is worth noting that recent measurements by Birk and Wagner [18] in the ν_2 band region were given a priority and were written into the database directly. These data were checked using the partner transition scheme [32] which indicates transitions with the upper and lower rotational quantum numbers reversed should have half widths that agree to within several percent in the ν_2

band region. This fact was confirmed for most of the two hundred pair transitions in the data indicating the high quality of the data. In fact the data are so good it is possible to see partner scheme differences between ν_2 and $2\nu_2$-ν_2 transitions.

In the work of Birk and Wagner, a large effort was undertaken to deliver data with consolidated error bars. Agreement of measured and modeled data of the nadir-sounding satellite instrument IASI was significantly improved with the new pressure broadening data [33].

A new procedure has been developed for the temperature dependences of air-broadened half widths. For all the transitions in different bands that had the same rotational quantum assignments with those measured in Birk and Wagner [18], these measurements were used. Next, the temperature exponents from new CRB calculations using a 20 4 4 potential expansion, "exact" trajectories and full velocity integral for rotational band transitions were added to the database. While the CRB potential is not fully optimized, these temperature exponents are better than J-averaged values. Lastly, for those transitions for which no data are available from the above procedures, experimental values from Ref. [18] averaged as a function of J were employed.

2.1.5 Future work

Further evaluation of the ab initio intensities from Lodi et al [5] is ongoing, and in the future they may be recommended to be the main source of intensities throughout the entire database for the principal isotopologue of water vapor, with the exception of the resonant lines. So far, differences up to 8% between experimental data and ab initio work for entire vibrational bands are known [8, 26].

As mentioned above, it was found that the quality of the CRB calculations of line shape parameters should increase significantly, especially for narrower lines, if one uses a larger number of correlation functions, higher-order cut-offs for convergence, and exact trajectories [17]. The quality of calculations can also be improved by using the better-determined intermolecular potential constants and wavefunctions from ab initio calculations to replace the currently implemented Hamiltonian approach. This work is currently underway. Some of the semi-empirical values of Jacquemart et al [16] employed some of the outdated CRB and experimental values in their derivation and therefore will also need to be reevaluated.

A line list similar to that of Lodi and Tennyson for $H_2^{18}O$ and $H_2^{17}O$ [28] is being constructed for HDO using the VTT ab initio dataset [34] supplemented with line positions derived from the corresponding MARVEL levels [35]. Although in this edition some of the HDO line shifts were introduced from the work of Jenouvrier et al [10], most of the line shifts are still missing above 2000 cm^{-1} for this isotopologue and more experiments and calculations are needed, while some of the existing line shifts, including those from Ref. [36] need to be assessed.

2.2. CO$_2$ (molecule 2)

High-quality reference spectroscopic data for the carbon dioxide molecule remains one of the top priorities for the HITRAN database, due in part to its importance for the environmental satellite missions, including OCO-2 [37] and GOSAT [38] and its importance to the studies of the atmospheres of Mars and Venus [39].

HITRAN2008 featured an extensive update in the operational region of the OCO-2 satellite (4300-7000cm^{-1}). Spectral parameters for the strong and intermediate lines were taken from Toth et al [40], while weak lines were adapted from the Carbon Dioxide Spectroscopic Databank

CDSD-296 [41] or experimental values from more sensitive CRDS experiments (see Fig. 4 in the HITRAN2008 paper). For the lines outside that range, only a few bands were updated with more recent results, while the CDSD values were used to fill in the missing lines to accommodate a low intensity cut-off of 4×10^{-30} cm^{-1}/(molecule cm^{-2}).

In this edition we replaced all parameters taken from the previous version of CDSD with its newer edition. We also used new CDSD values to replace a majority of the line parameters throughout the CO_2 dataset unless these lines originated from very accurate experiments (including those from Ref. [40]). It is therefore important to give some background on the new version of the CDSD databank.

In 2003 the first version of the Carbon Dioxide Spectroscopic Databank, CDSD-296, aimed at atmospheric applications, was created [42]. CDSD-296 line positions and energy-level wavenumbers were calculated values based on the effective Hamiltonian and the effective dipole moment models. Later, in 2008, this version was updated and enlarged [41]. The enlarged CDSD-296 included 419610 transitions of the seven most abundant CO_2 isotopologues covering the 5.9 to 12784.1 cm^{-1} spectral range. A large portion of CDSD-296 data was included into HITRAN2008.

Since that time a large number of experimental studies of CO_2 line positions and intensities have been performed. In particular, a considerable amount of new experimental information on rare isotopologues has become available [43, 44].

Measured line positions and intensities previously collected [41] from the literature were augmented with measurements from recent papers (including those from [43-58]). In total more than 140,000 measured line positions and nearly 44,000 measured line intensities belonging to the 12 isotopologues $^{12}C^{16}O_2$, $^{13}C^{16}O_2$, $^{16}O^{12}C^{18}O$, $^{16}O^{12}C^{17}O$, $^{16}O^{13}C^{18}O$, $^{16}O^{13}C^{17}O$, $^{12}C^{18}O_2$,

$^{17}O^{12}C^{18}O, {}^{12}C^{17}O_2, {}^{13}C^{18}O_2, {}^{17}O^{13}C^{18}O, {}^{13}C^{17}O_2$ were used to form the line position and intensity data files. The data files of the measured positions were critically evaluated and the sets of experimental energy levels for each isotopologue were obtained. Details of this approach as applied to the CO molecule are given in Ref. [59]. The data files of the measured line intensities were also critically evaluated and cleansed of bad measurements. The resulting data files were used as input data to fit parameters of the effective Hamiltonians and effective dipole moment operators. Then the fitted models were used to calculate all possible transitions whose intensities are greater than 10^{-30} cm^{-1}/(molecule cm^{-2}) at 296 K. Finally, calculated transition frequencies were systematically substituted (where possible) by differences of the upper and lower experimental energy levels. The final line list covers the 3.68 - 12784 cm^{-1} spectral range.

The line-shape parameters now originate from the recent theoretical and semi-empirical calculations [60-62], which are in excellent agreement with high-quality experimental data. The resultant dataset was then used to update the line-mixing algorithm developed by Lamouroux et al. [63].

2.3. O₃ (molecule 3)

Ozone is one of the most important molecules for atmospheric and environmental applications of spectroscopic data. Apart from the well-known issues concerning the control of the ozone pollution in the troposphere and the ozone layer in the upper-atmosphere, a detection of ozone in the atmospheres of exosolar planets might be an indicator of the presence of oxygen. In this HITRAN edition, a major improvement has been made concerning ozone bands corresponding to highly excited vibration states which are required for validation of the molecular potential energy surfaces (PES) [64, 65] and for a correct account of non-local

thermodynamic equilibrium effects [66] in the modeling of emission and absorption properties of the middle and upper atmosphere.

The information concerning the changes in HITRAN parameters is summarized in Table 3 and Table 4. In total, seven updated bands between 3297.46 and 5526.30 cm^{-1} (Table 3) and 28 new bands between 3492.69 and 6996.68 cm^{-1} (Table 4) were added to the line-by-line ozone list using a two-step procedure. First, the parameters of spectroscopic models, line positions, intensities, and lower-state energy levels resulting from analyses of experimental spectra [67-75] have been introduced to the S&MPO (Spectroscopy and Molecular Properties of Ozone) information system [76] which offers various tools for spectra simulations and their comparison with experimental records. After the validation via S&MPO, the line-list in the HITRAN format has been generated with an appropriate cut-off. An overview of the resulting line list is presented in Fig. 4.

<p style="text-align:center; color:red;">Approximate location of Table 3</p>

Table 3. Updated bands for $^{16}O_3$.

Band	Number of lines	Spectral range (cm^{-1})	S_v	References for v, S
022 – 000	1336	3297.46 – 3478.53	9.936	[68], [68]
121 – 000	1611	3383.04 – 3483.38	62.720	[68], [68]
113 – 100	658	3490.53 – 3565.76	4.038	[69], [68]
014 – 001	1136	3520.70 – 3605.15	12.251	[69], [68]
014 – 100	13	3533.85 – 3562.08	0.029	[69], [68]
113 – 001	12	3543.34 – 3604.91	0.036	[69], [68]
213 – 000 [a]	954	5447.73 – 5526.30	9.627	[68], [68]

Notes: a. This band was labeled as 015 – 000 in the previous version of HITRAN. S_v is the sum of line intensities in units of 10^{-23} cm^{-1}/(molecule × cm^{-2}) at 296K for the corresponding bands included in the line list, v is the line position, and S is the line intensity.

<p style="text-align:center; color:red;">Approximate location of Table 4</p>

Table 4. Newly included $^{16}O_3$ bands.

Band	Number of lines	Spectral range (cm^{-1})	S_v	References for v, S
320 – 100	20	3492.69 – 3562.58	0.058	[69], [68]

$220 - 000$	553	$3500.08 - 3635.88$	2.629	[68], [68]
$114 - 000$	538	$5443.69 - 5574.11$	2.206	[68], [68]
$080 - 000$	7	$5474.65 - 5524.06$	0.018	[68], [68]
$321 - 000$	123	$5532.36 - 5569.38$	0.521	[68], [68]
$105_1 - 000$	730	$5708.95 - 5790.90$	4.943	[70], [70]
$421 - 010$	303	$5815.58 - 5873.74$	0.036	[71], [71]
$133 - 000$	702	$5852.44 - 5931.22$	0.472	[72], [72]
$411 - 000$	444	$5895.17 - 5956.76$	0.138	[72], [72]
$233_1 - 010$	528	$5941.73 - 6021.44$	0.079	[73], [73]
$034 - 000$	264	$5956.88 - 6078.00$	0.085	[74], [74]
$105_2 - 000$	678	$5983.44 - 6071.43$	0.210	[74], [74]
$124_1 - 000$	999	$6019.98 - 6201.30$	0.294	[74], [74]
$223_1 - 000$	954	$6031.75 - 6130.78$	1.179	[74], [74]
$510 - 000$	39	$6067.96 - 6136.40$	0.013	[74], [74]
$331 - 000$	168	$6163.49 - 6207.75$	0.014	[74], [74]
$025 - 000$	1003	$6225.12 - 6311.46$	0.770	[75], [75]
$124_2 - 000$	78	$6246.40 - 6363.42$	0.034	[75], [75]
$430 - 000$	111	$6284.63 - 6395.38$	0.031	[75], [75]
$501 - 000$	749	$6301.80 - 6365.48$	0.637	[75], [75]
$223_2 - 000$	777	$6318.03 - 6393.74$	0.679	[75], [75]
$421 - 000$	409	$6503.67 - 6574.40$	0.087	[71], [71]
$205_1 - 000$	570	$6525.82 - 6593.61$	0.197	[71], [71]
$233_1 - 000$	754	$6641.08 - 6722.18$	0.158	[73], [73]
$242 - 000$	457	$6665.49 - 6822.32$	0.029	[73], [73]
$520 - 000$	33	$6677.10 - 6771.82$	0.002	[73], [73]
$511 - 000$	317	$6945.09 - 6989.76$	0.024	[71], [71]
$233_2 - 000$	417	$6950.18 - 6996.68$	0.045	[71], [71]

Note: S_v is the sum of line intensities in units of 10^{-23} cm^{-1}/(molecule × cm^{-2}) at 296K for the corresponding bands included in the line lists, v is the line position, and S is the line intensity.
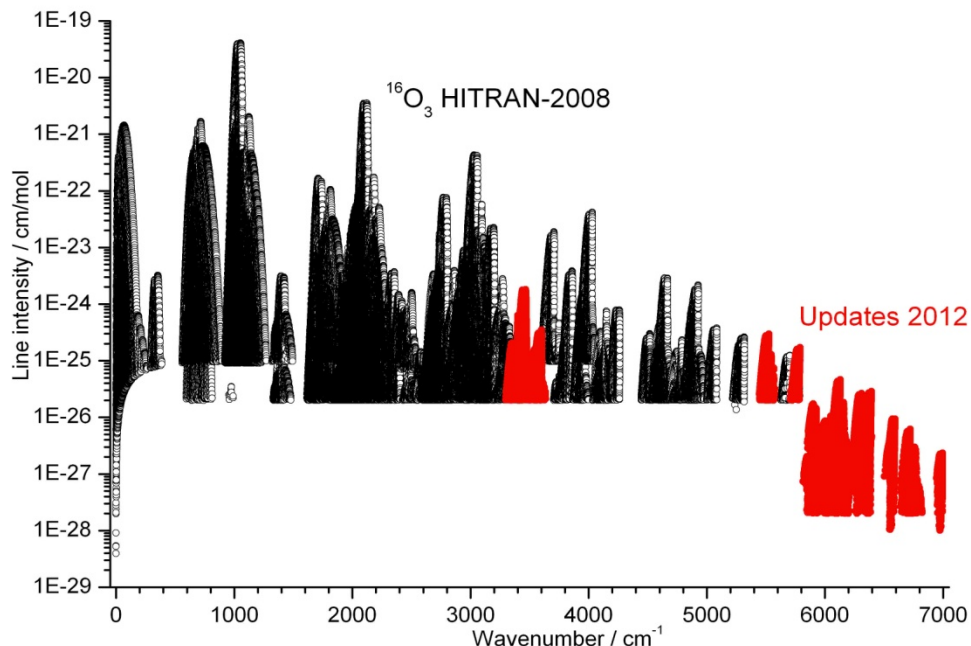
Approximate location of Figure 4

Figure 4. Schematic overview of the ozone $^{16}O_3$ transitions in the HITRAN2012 edition. Each of the 261886 lines corresponds to a circle or a triangle on the log intensity scale. New data added since the 2008 edition are marked with red full circles.

The data for updated bands (Table 3), as well as for newly provided bands up to 5800 cm^{-1} (Table 4), are based on analyses of FTS spectra [67-70] recorded by the Groupe de Spectrométrie Moléculaire et Atmosphérique (GSMA) laboratory of Reims University with improved signal-to-noise ratio. Spectral parameters of two bands, $v_1 + 2v_2 + v_3$ and $2v_2 + 2v_3$ from Ref. [67] were replaced by new data of Ref. [68] completed by the previously unobserved band $2v_1 + 2v_2$. The analysis of this [(022), (121), (220)] triad has been improved due to better characterization of resonance coupling parameters (using the PES of Ref. [65]) which was not well defined in the previous studies. The drastically increased number of assigned transitions has allowed a significant improvement in line intensities of $2v_2 + 2v_3$ and of the Q-branch of $v_1 + 2v_2 + v_3$ as well as for transitions corresponding to large values of rotational quantum numbers. An example of the improvement of the spectra modeling is given in Fig. 5.

Approximate location of Figure 5

23

Figure 5. Example of an improvement of the Q branch for the $\nu_1 + 2\nu_2 + \nu_3$ ozone band. The top panel is a comparison of the observed spectrum (in red) with calculations using HITRAN2008 data (in green); the bottom panel is a calculation with new data from S&MPO (including a few impurity lines marked in blue in the stick diagram).

The line positions of all four hot bands in Table 3 and of the $3\nu_1 + 2\nu_2 - \nu_1$ band (Table 4) have been calculated by using effective Hamiltonian parameters of Ref. [69]. Line strengths of these five bands were improved from a fit of the corresponding dipole transition moment parameters to experimental intensities [68], whereas they were extrapolated from cold bands in previous studies.

The new dataset covers the spectral range up to 6996.68 cm^{-1} (Table 4). All data above 5800 cm^{-1} are based on analyses of very sensitive cavity ring down spectroscopy (CRDS) spectra [71-75] recorded in the Laboratoire Interdisciplinaire de Physique (LIPhy) of Grenoble University providing information on weak bands which were missing in previous HITRAN editions. For this data set, we have slightly extended the format of vibration quantum numbers because the normal mode assignment for the corresponding excited vibrations is ambiguous for some states (a local mode assignment not being universally applicable as well). Following the original works [71-75], the vibrational assignment has been provided by the decomposition of the effective wavefunctions in the normal mode basis set as computed from the PES of Ref. [64] using the MOL_CT program suite [77]. As a result, the same normal mode basis function could give major contributions to two different vibration states. This occurs when the normal modes are strongly mixed due to anharmonic resonance interactions. In these cases, an additional (lower case) ranking index was thus added according to increasing vibration energy. Because of these considerations, the vibration labels for some states have been changed with respect to previous intuitive assignments: the band in the range 5625.97 – 5704.62 cm^{-1} previously labeled as (213) – (000) is now reassigned as (015) – (000).

The line lists were generated by the teams of GMSA (Reims) and of the Laboratory of Theoretical Spectroscopy of the Institute of Atmospheric Optics (Tomsk) following the corresponding analyses of experimental spectra [67-75]. In the high wavenumber range above 5000 cm^{-1}, the line position fits using effective models gave a satisfactory agreement (rms ~ 0.003 – 0.015 cm^{-1}) but did not reach the experimental accuracy (~ 0.001 – 0.003 cm^{-1}). This concerns particularly the CRDS range. In these cases, the empirical corrections on line positions were applied as follows: the corresponding line list contained all allowed transitions computed as

differences among energy levels derived from experimental spectra measured in Grenoble. All line intensities were computed from effective dipole transition parameters. The intensity cut off was fixed to 10^{-26} and 2×10^{-28} cm^{-1}/(molecule $\times$ cm^{-2}) below and above 5800 cm^{-1}, respectively.

Altogether for this edition, 5720 ozone lines were updated (Table 3) and 12725 lines of new bands (Table 4) were added for the $^{16}O_3$ list. The lesser ozone isotopologue line lists were not changed. The current state-of-art of the ozone high-resolution studies is described in the review paper of this Special Issue [78].

2.4. N$_2$O (molecule 4)

The line parameters of nitrous oxide have not undergone a revision and remain the same as in HITRAN2008.

2.5. CO (molecule 5)

The line parameters including line intensities, self- and air-broadening parameters, temperature dependence and air-induced line shifts, of the first overtone band of the three most abundant CO isotopologues $^{12}C^{16}O$, $^{13}C^{16}O$, $^{12}C^{18}O$, have been updated, based on the experimental works of [79], and of [80]. The fitting of the experimental data in these works has employed the speed-dependent Voigt profile and took into account the line-mixing. Based on these works, for $^{12}C^{16}O$, the speed dependence of the broadening, self and air off-diagonal line-mixing, as well as Rosenkranz [81] self and air line-mixing parameters, and the temperature dependence of line shift were introduced in a separate file that lists HITRAN molecule and isotopologue numbers, quantum numbers and the new parameters in the order shown in Table 5.

Approximate location of Table 5

Table 5. The format used for the additional spectroscopic parameters for CO and its isotopologues.

Parameter	Speed dependence	Air line-mixing	Rozenkranz air line-mixing	Temperature dependence of line shift	Self line-mixing	Rozenkranz self line-mixing
Field Length	7	8	8	9	8	8
Data type	Real	Real	Real	Real	Real	Real

Note: For the line-mixing pair P(J)~P(J+1) or R(J)~R(J+1), the corresponding line-mixing parameters are listed with the P(J) or R(J) line.

For the bands where no measurements of air-induced line shifts are available, the values were derived indirectly from the high-accurate measurements of the line shifts of the 2-0 band, using the approach based on the theory of Ref. [82].

The line list of the 0-0 bands of the three most abundant CO isotopologues $^{12}C^{16}O$, $^{13}C^{16}O$, $^{12}C^{18}O$, and the 1-1 band of $^{12}C^{16}O$, have been updated and extended to higher-J lines, based on the Cologne Database for Molecular Spectroscopy (CDMS) [83] and HITEMP [19]. The 2 - 2 and 3 - 3 bands of $^{12}C^{16}O$ have been added to the HITRAN line list for the first time.

2.6. CH$_4$ (molecule 6)

An unprecedented update in terms of extent and quality of methane molecular line parameters was implemented for the HITRAN compilation by including new global analyses and measurements for $^{12}CH_4$, $^{13}CH_4$ and $^{12}CH_3D$. Details of the update can be found in Brown et al. [84]; here we summarize the major changes since the last edition of HITRAN [1].

High-resolution spectroscopy of methane and the generation of accurate line lists, especially as one moves up the polyad ladder to shorter and shorter wavelength (necessary for many applications) is extremely challenging. Fortunately, the experimental techniques and the theoretical modeling continue to make great strides. Each new edition of the HITRAN database has witnessed major improvements for methane; Table 6 provides an overview of the evolution.

The latest methane line list is a significant expansion of information (and in the near-infrared, of quality).

Table 6. Overview of growth of the methane line list during the past 20 years of HITRAN editions.

HITRAN Year	Number of lines	Minimum IR intensity[+]	ν_{max} (cm^{-1})	Number of isotopologues[++]
2013	659848	1×10^{-29}	11500	4
2008	290091	1×10^{-29}	9200	4
2004	251440	1×10^{-29}	9200	3
2001	211465	8×10^{-29}	6185	3
1996	48032	1×10^{-24}	6185	3
1992	47415	4×10^{-24}	6107	3
1986	17774	4×10^{-24}	6107	3
1982	11803	3×10^{-24}	4667	3

[+] The minimum intensity for the far-IR is several orders of magnitude weaker than the value selected for the IR. Units of cm^{-1}/(molecule $\times$ cm^{-2}).
[++] The four isotopologues are $^{12}CH_4$, $^{13}CH_4$, $^{12}CH_3D$, and $^{13}CH_3D$ (the last one added in 2008).

A rough graphical overview of the spectral coverage now available for the four isotopologues of methane is shown in Fig. 6. To visualize the spectral lines in the line list, the plot is of absorption cross-sections generated at 0.05 cm^{-1} resolution, assuming one atmosphere and 296K. Of course the effects of the line-shape parameters and the density of lines cannot be fully appreciated in this figure.
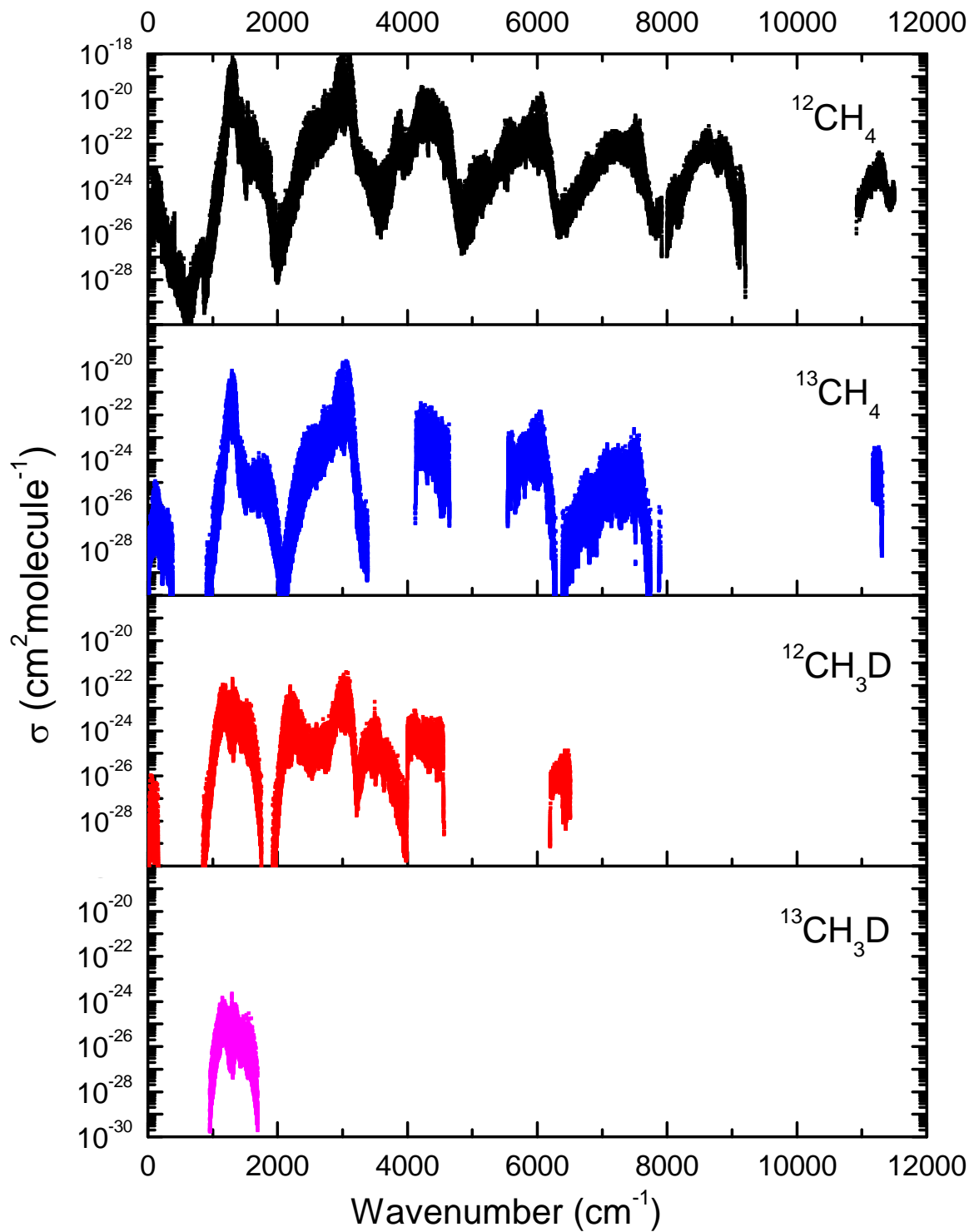
Figure 6. Log plot of the cross-sections generated from the line list for the four isotopologues of methane from 0 to 12 000 cm^{-1} (generated at 0.05 cm^{-1} resolution, one atmosphere, and 296K).

For the new compilation, three fourths of HITRAN 2008 methane transitions have been replaced. Only about 74000 existing lines were retained: CH_4 in two regions (4800 – 5550 cm^{-1} and 8000 – 9200 cm^{-1}), the dyad of $^{13}CH_4$ (6 – 8 µm), $^{12}CH_3D$ (7 – 4076 cm^{-1}), and the v_6 band of $^{13}CH_3D$ near 8.7 µm. With a minimum intensity (at 296 K) set to 10^{-37} cm^{-1}/(molecule × cm^{-2}) for the far-IR and 10^{-29} cm^{-1}/(molecule × cm^{-2}) for the mid- and near-IR, the new database more than doubled the number of lines in the 2008 compilation. Part of the size increase occurred because the minimum intensity criterion for $^{12}CH_4$ and $^{13}CH_4$ transitions above 600 cm^{-1} was lowered by two orders of magnitude. In addition, global analyses for $^{12}CH_4$ [85] and $^{13}CH_4$ [86, 87] obtained a better characterization of the dyad, pentad and octad polyads up through 2.2 µm. As a result, many weaker high-J and hot band transitions, important for outer planet and exoplanet atmospheres, could be compiled, including for the first time the Octad – Pentad difference bands whose transitions fall between 5 and 9 µm. Accuracies of some calculated positions were further improved by forming "empirical upper-state levels" based on secure quantum assignments and re-computing the line positions; entries changed in this manner are flagged by the position accuracy code set to be greater than 1. For the first time, the database (in the 2.2 – 4.0 µm region) added one $^{12}CH_4$ hot band $2v_3$–v_4 [88], the three strongest bands of the $^{13}CH_4$ octad (v_1+v_4, v_3+v_4, v_2 v_3) [87] and eleven bands of $^{12}CH_3D$ [89].

For the most part, the predicted infrared transitions arising from the ground state are expected to be very similar to prior calculated values. However, in HITRAN2008, the far-IR intensities of the ground state to ground state lines had been scaled by 1.15 based on new measurements of cold methane manifolds [90]. Later, Boudon et al. [91] reported new line-by-line intensities that were within 1% of the original intensities. The newer far-IR results were applied for HITRAN2012.

Above 5550 cm^{-1}, the new database was formed using observed line positions and intensities, some with empirical lower-state energies determined from cold spectra. Some 20,000 entries from the prior laboratory measurements [92] were replaced with 68,000 new values reported from extensive new FTIR analysis (5550 – 5852 cm^{-1}) [2.6.8] combined with differential absorption spectroscopy (DAS) and cavity ringdown spectroscopy (CRDS) from 5852 to 7912 cm^{-1}. The latter study, by Campargue et al. [93] relied on intensities at cold and room temperatures to provide empirical lower-state energies for many observed $^{12}CH_4$, $^{13}CH_4$ and $^{12}CH_3D$ features.

While no methane parameters between 8000 and 9200 cm^{-1} were altered, over 11000 measured positions, intensities, and empirical lower-state energies from cold CH_4 were added for the first time between 10923 and 11502 cm^{-1} [94]. However, the Tetracontad polyad near 10100 cm^{-1} is still not included in the compilation.

There were some special modifications to the database that should be noted. To enable the use of methane line positions as frequency calibration standards, a few hundred high-accuracy (10^{-6} to 10^{-5} cm^{-1}) values replaced predicted lines for selected transitions of v_3 near 3000 cm^{-1} [95] and $2v_3$ near 6000 cm^{-1} [96].

Available Voigt pressure broadening measurements from HITRAN2008 were transferred into the new compilation, but most of the lines were given crudely-estimated half widths, as described in Brown et al. [84]. For stronger far-IR transitions, new measured nitrogen and self broadening half widths [97] were adopted.

Much of the extensive updates occurred because experimental and theoretical research was undertaken specifically to support the analyses of Saturn and Titan by the Cassini mission **[98]**.

However, there is still much work to be done to have the comprehensive database required for remote sensing of all atmospheres (Earth, planets, exoplanets, moons, etc).

Our knowledge of pressure broadening of methane by air, N_2, H_2, and He is incomplete, particularly for the near-infrared. Basic coefficients of Lorentz broadening (widths, shifts, temperature dependence) all vary as a function of the transition quantum numbers, and values obtained for two fundamentals are not easily applied to the very complicated polyads having dozens of underlying vibrational states. Good theoretical models, confirmed by measurements, must be implemented in order to have accurate values, not the rough estimates used here for 99% of the present database. However, for applications that require the highest accuracies for intensities and broadening, Voigt line shapes are inadequate. Studies of line mixing, speed dependence and narrowing are required to provide the basic parameters for future methane compilations in the most utilized spectral regions.

Theoretical analyses of measured positions and intensities are required to identify the quantum numbers and produce models that predict all transitions that are likely to be required by applications, not just the ones seen in laboratory spectra. The extensive new cold and room temperature measurements between 5850 and 7900 cm^{-1} may successfully be reproduced in this decade using current Hamiltonian methods, but adequately characterizing the methane spectra at even shorter wavelengths still seems intractable. For this reason, ab initio methods are being investigated to interpret near-infrared methane. Forming a complete database requires predictions of both positions and intensities, and as usual, the accuracies of individual line intensities in the present effort will vary greatly. Intensity measurements are needed to confirm and improve the quality of predicted weak lines, particularly for the new hot-band transitions to support studies of exoplanet atmospheres.

2.7. O₂ (molecule 7)

In HITRAN, molecular oxygen is represented by both magnetic dipole and electric quadrupole transitions. Although these type of transitions are intrinsically weaker than electric dipole transitions, the large abundance of oxygen in the terrestrial atmosphere produces noticeable absorption. Another aspect of oxygen in HITRAN is that the transitions also involve several different electronic states. Owing to its uniformly mixed constituent profile, it is often used as a benchmark in satellite retrieval algorithms. It is thus critical to provide highly accurate spectroscopic constants for oxygen. In the past, classic laboratory measurements were lacking in accuracy as well as not sufficiently covering high rotational levels nor isotopologues. Recent experiments have made significant progress, and we have made use of these for improvements in HITRAN, as discussed below.

2.7.1. Microwave region

A detailed description of the update in the microwave region is described in Mackie et al. [99]. Here a brief summary is given.

The line positions for the $X^3\Sigma_g^-$ (v = 0) - $X^3\Sigma_g^-$ (v = 0) and $X^3\Sigma_g^-$ (v = 1) - $X^3\Sigma_g^-$ (v = 1) bands for $^{16}O_2$ and the $X^3\Sigma_g^-$ (v = 0) - $X^3\Sigma_g^-$ (v = 0) band for $^{16}O^{18}O$ and $^{16}O^{17}O$ were recalculated using spectroscopic constants derived by Leshchishina et al. [100, 101]. HITRAN line-shape parameters for the microwave bands of oxygen were previously estimated from the data from electronic bands and in particular did not distinguish between $\Delta N = 0$ and $\Delta N = 2$ transitions. Here we applied a semi-empirical model for calculating air-broadened half width values. This was derived based on N_2-broadening measurements of Tretyakov et al. [102] and Golubiatnikov

and Krupnov [103] and self-broadening measurements in Refs. [102-105]. The self-broadened values are now based on Refs. [102-105].

Transitions with $N' = 1$ were given a temperature-dependence of 0.97, transitions with $N' = 2$ were given a temperature-dependence of 0.86, and transitions with $N' \geq 3$ were given a temperature-dependence of 0.72 based on measurements by Drouin [106].

Finally, the quantum assignments were corrected for some of the lines in the MW region.

This update of line parameters in the MW region is a substantial improvement, especially for the line-broadening parameters.

2.7.2. $a^1\Delta_g$ - $X^3\Sigma_g^-$ transitions (around 1.27 μm)

In 2009 an update to the HITRAN2008 oxygen file was issued featuring substantial improvements based on the work of Newman et al. [107] and Washenfelder et al. [108].

For the 2012 release, further improvements for this band are made. A detailed description of the update for the $a^1\Delta_g$ - $X^3\Sigma_g^-$ transitions is also described in Mackie et al. [99] with a brief summary given here.

Recent CRDS measurements of line positions and intensities in this band [100, 101, 109, 110] for all stable isotopologues of molecular oxygen allowed a significant advance in extent and quality of the spectroscopic parameters in HITRAN.

The isotopologue line positions of $^{16}O_2$, $^{16}O^{18}O$, and $^{16}O^{17}O$ for the $a^1\Delta_g$ (v = 0, 1)- $X^3\Sigma_g^-$ (v = 0, 1) transitions were calculated using spectroscopic constants taken from two papers by Leshchishina et al [100, 101]. Note that $^{16}O^{17}O$ lines are made available for this band for the first time. Gordon et al. [109] have shown that in atmospheric retrievals one needs to account not only for magnetic dipole transitions traditionally provided in HITRAN for that band, but also

for electric quadrupole transitions. The quadrupole transitions were therefore included into HITRAN2012 with the intensities calculated using a model described by Mishra et al. [111] with the input parameters based on experimental intensities reported in Gordon et al. The intensities of magnetic dipole transitions were recalculated using intensities from the work of Leshchishina et al. as input parameters.

The intensities in the $a^1\Delta_g$ (v = 0) - $X^3\Sigma_g^-$ (v = 1) band were recalculated using input parameters from new experiments of Kassi and Campargue [112].

A new set of air- and self-broadening parameters and air-broadening temperature dependence was derived based on experimental data reported by Newman et al. [107].

2.7.3. A-band region near 762 nm

The line list for the O_2 A-band, $b^1\Sigma_g^+ \leftarrow X^3\Sigma_g^-(0,0)$ magnetic dipole transitions near 762 nm (13120 cm^{-1}) for the $^{16}O_2$, $^{16}O^{18}O$, and $^{16}O^{17}O$ isotopologues has been updated due to recent frequency-stabilized cavity ring-down spectroscopy (FS-CRDS) measurements [113-119]. Detailed discussions on the construction of this line list can be found in Refs. [118] and [119] for $^{16}O_2$ and the less abundant isotopologues, respectively.

These spectra were all fit with Galatry line profiles [120] which account for Doppler and pressure broadening as well as Dicke narrowing. The use of Galatry line profiles for the A-band is of critical importance in many applications and has been discussed extensively in the literature [113, 118, 121, 122]. Dicke narrowing parameters for each of the included isotopologues can be found in the last two columns of the auxiliary A-band input file supplied as part of the HITRAN2012 update. These last two columns are the air- and self-broadened collisional

(Dicke) narrowing parameters (in cm^{-1} atm^{-1} at 296 K), respectively. These parameters were taken from Refs. [118] and [119] for $^{16}O_2$ and the lesser isotopologues, respectively.

As these measurements were performed at low pressures (generally below 20 kPa), line mixing and collision-induced absorption (CIA) were unobservable and not included in the spectral fitting. These effects have, however, been shown to be important at atmospheric pressures (and above) [123-125]. We note that CIA has been added to HITRAN for the *A*-band [126] as measured with Fourier-transform spectroscopy measurements [123, 124] (see Section 6 below). Line mixing parameters can be calculated for a range of temperatures using the code of Tran et al. [124] with the auxiliary *A*-band input file provided as part of this update.

For the $^{16}O_2$ *A*-band magnetic dipole transitions, the most significant updates were to the transition wavenumbers, line intensities, self-broadening parameters, and lower-state energies. The intensities found in the present database are based upon FS-CRDS measurements and differ from those found in the HITRAN2008 database by >1% at high *J*. These measurements include a Herman-Wallis-like interaction and removed a calculation error in the HITRAN2008 *A*-band intensities. The self-broadening parameters were updated due to FS-CRDS measurements of high *J* (up to *J* = 50) transitions [117]. The included parameters differ from those in HITRAN2008 by more than 10% for high-*J* transitions but are very similar at low *J*. Finally, the transition wavenumbers and lower-state energies have been improved based upon a global fit of FS-CRDS measurements [115] and a large ensemble of ground-state measurements (see Ref. [127] for more details on this fit). At high *J*, differences exceeding 0.008 cm^{-1} for the transition wavenumbers and lower-state energies are seen between the present database and HITRAN2008.

Similarly, for the $^{16}O^{18}O$ and $^{16}O^{17}O$ *A*-band magnetic dipole transitions, the transition wavenumbers, line intensities, and lower-state energies were improved. In comparing to

36

HITRAN2008, the largest differences are seen for the line intensities which differ by ~3% for $^{16}O^{18}O$ transitions and up to 10% for $^{16}O^{17}O$ transitions. In addition, the transition wavenumbers and lower-state energies are now based on a global fit of FS-CRDS measurements [116, 119] and an ensemble of ground-state measurements (see Ref. [119] for more details on this fit). Large differences are seen for the transition wavenumbers found in the two databases of up to 0.001 cm^{-1} for $^{16}O^{18}O$ and 0.04 cm^{-1} for $^{16}O^{17}O$.

The line list for hot band transitions of $b^1\Sigma_g^+ \leftarrow X^3\Sigma_g^-(1,1)$ was also updated based upon the recent reevaluation of spectroscopic constants in the $b^1\Sigma_g^+$, v=1 state by Gordon et al. [128]. The new line positions are significantly improved over those found in the HITRAN2008 database.

Finally, A-band electric quadrupole transitions have been added to the database. The electric quadrupole line list is taken from Miller and Wunch [129] and is based upon recent FS-CRDS measurements [127]. These very weak transitions ($S = 1\times10^{-28}$ to 3×10^{-31} cm^{-1}/(cm^{-2} $\times$ molecule)) have been observed in atmospheric spectra [129, 130] and failure to include them in low uncertainty atmospheric retrievals can limit the resulting measurement precision.

2.7.4. B- and γ-*bands*

An extensive update of the so-called B- and γ-bands ($b^1\Sigma_g^+ \leftarrow X^3\Sigma_g^-(1,0)$ and $b^1\Sigma_g^+ \leftarrow X^3\Sigma_g^-(2,0)$) of oxygen around 0.69 and 0.63 μm respectively is described in the work of Gordon et al. [128]. These bands (in particular the B-band) are now being considered for future satellite missions. In this light, it is important to make sure that the reference spectroscopic parameters are accurate enough to provide means of deducing important physical characteristics from the atmospheric spectra. It was found that the HITRAN2008 parameters could not produce satisfactory fits of the observed high-quality spectra. In order to improve the database, we have collected the best available measured line positions that involve the $b^1\Sigma_g^+$ (v=1 and v=2) states

for the three most abundant isotopologues of oxygen and performed a combined fit to obtain a consistent set of spectroscopic constants. These constants were then used to calculate the line positions. A careful review of the available intensity and line-shape measurements was also carried out, and new parameters were derived based on that review. In particular, line-shift parameters, that were not previously available, were introduced. The new data have been tested in application to high-resolution atmospheric spectra measured with the Fourier transform spectrometers at Park Falls, Wisconsin (B-band) and Kitt Peak, Arizona (γ-band) and have yielded substantial improvement [128]. No experimental data were available for $^{16}O^{18}O$ in the γ-band and line positions were determined from the atmospheric spectra and then fitted to provide new spectroscopic constants.

2.7.5. Future work

Recently, Yu et al [131] carried out a global fit of all available experimental line positions for all the bands and isotopologues from the microwave to UV region. The constants derived in that fit may be used to update line positions throughout the entire HITRAN oxygen line list in the future.

2.8. NO (molecule 8)

Unchanged.

2.9. SO₂ (molecule 9)

The line positions and intensities of the pure-rotational transitions (with $J < 100$) in the ground and v_2 states of $^{32}SO_2$ and in the ground state of $^{34}SO_2$ have been adopted from the Cologne Database for Molecular Spectroscopy [83].

38

Several bands of $^{34}SO_2$ (second isotopologue by abundance in HITRAN) have been added to the database in the 4 and 7.2-10 μm regions based on the recent high resolution work of Flaud et al. [132] and Lafferty et al. [133, 134]. All the previous data that existed for $^{34}SO_2$ in HITRAN2008 have been replaced.

2.10. NO$_2$ (molecule 10)

Unchanged.

2.11. NH$_3$ (molecule 11)

Ammonia is an important atmospheric trace species with global emissions having increased very significantly due to the spread of intensive agriculture based on the use of fertilizers which has augmented the natural sources of ammonia from oceans, animal respiration, and soil microbial processes. Livestock, waste management, biomass burning and industry also lead to anthropogenic contributions to atmospheric ammonia. However, the actual ammonia emission budget remains uncertain [135]. Successful ammonia retrievals have been performed with the IASI/MetOp [136], MIPAS [137] and TES [138] remote-sensing satellites. Such observations are heavily dependent on the availability of reliable spectroscopic data. The ammonia line list in HITRAN has not been revised since the 2000 edition [139] and, as discussed below, is in need of improvement. The present edition is based on a complete reanalysis of the previous $^{14}NH_3$ data [140], new spectroscopic experiments [141], and some new bands generated using empirical energies and *ab initio* line intensities [140].

The lower-state energy levels up to $J = 20$ have all been replaced by those derived by Chen et al. [142]; energies for states with $J = 21$ and 22 were not changed and are in line with more recent measured values [143]. Down et al. [140] used these energy levels, combination

differences, and direct comparison with the computed BYTe line list for ammonia [144] to re-analyze and re-assign the previous HITRAN data resulting in 229 newly assigned lines, 324 assigned lines, and a significant number of other corrections to the quantum number labels. Down et al. also recommended the use of a newly defined and consistent set of quantum numbers as most of the previous sets employed contained insufficient quantum numbers to uniquely identify all the levels. These new quantum labels are adopted in the present edition. The new quantum notation is given as follows. The symmetry quantum numbers can be A_1', A_1'', A_2', A_2'', E' and E'' except for Γ_{tot} for which the A_1 states do exist. For Γ_{vib}, $'$ and $''$ denote even or odd inversion symmetry respectively (see Table 7 for definitions).

Approximate location of Table 7

Table 7. Definition of quantum labels for ammonia.

Quantum label	Definition
v_1	Quanta in vibrational mode 1 (symmetry stretch)
v_2	Quanta in vibrational mode 2 (symmetric bend)
v_3	Quanta in degenerate vibrational mode 3 (asymmetric stretch)
L_3	$|l_3|$ absolute vibrational angular moment for mode 3
v_4	Quanta in degenerate vibrational mode 4 (asymmetric bend)
L_4	$|l_4|$ absolute vibrational angular moment for mode 4
L	$|l|$ absolute total vibrational angular momentum
Γ_{vib}	Vibrational symmetry
J	Total angular momentum
K	$|k|$ projection of $\mathbf{J}$
i	s or a for symmetric or anti-symmetric inversion symmetry
Γ_{rot}	Rotational symmetry
Γ_{tot}	Total symmetry

A number of recent experimental studies [145-148] observed intensities differing significantly from those in the previous editions of HITRAN for the v_2 band. Comparisons

performed by Down et al. [140] found that the newer intensities agreed closely with the BYTe intensities [144] which are based on the use of ab initio dipoles [149]. Intensities for the ν_2 band have therefore been replaced by the newly measured values, where available, or by the values from BYTe. Down et al. found that both the frequencies and the intensities for the $2\nu_2 - \nu_2$ hot band were not reliable and lines for this band have been replaced with a new line list generated using frequencies from empirical energy levels and BYTe transition intensities. These new intensities agree well with the measured values of Chu et al. [150]. Down et al. employed the same technique to synthesize line lists for the $\nu_2 + \nu_4 - \nu_4$, $\nu_4 - \nu_2$, $\nu_4 - \nu_4$, and $2\nu_2 - 2\nu_2$ bands, all of which are included in HITRAN for the first time. Further details of all the above changes can be found in the paper by Down et al. [140] included in this issue.

Sung et al. [141] recently measured ammonia spectra in the 6300 to 7000 cm^{-1}, a region not previously considered in HITRAN. These data have been included into HITRAN with the quantum number labels, where available, changed to the form recommended by Down et al. [140]. Two studies were combined to provide an ammonia HITRAN database for the first time in this region. Sung et al. [141] reported an extensive empirical line list of 4800 $^{14}NH_3$ lines (positions, intensities, empirical lower-state energies with some quantum assignments) from 6300 – 7000 cm^{-1}; this study used FTIR to characterize 99.7% of observed opacity in this region. Concurrently, Cacciani et al. [151] reported 313 line positions with empirical lower-state energies between 6626 – 6669 cm^{-1} using laser spectra down to 130 K. Lacking near-IR pressure broadening studies (see Ref. [152]), information for the ν_2 band from Nemtchinov et al. [147] was applied. Details about the sources of parameters and the ascribed uncertainties are given below.

Almost all of the line positions listed in the 6300 – 7000 cm^{-1} region are adopted from Sung et al. [141], who analyzed a series of Kitt Peak FTS spectra recorded at temperatures 296 – 185 K. Among them, however, positions for six lines were replaced with values from Cacciani et al. [151], namely 6626.6553, 6628.2738, 6629.2148, 6635.6400, 6635.6602, and 6642.7091 cm^{-1}. There are another three lines (6650.9102, 6662.8051, 6667.3572 cm^{-1}), whose positions and intensities were adopted from Cacciani [153]. There are another five lines (6634.5034, 6644.7300, 6650.9102, 6662.8113, 6667.3554 cm^{-1}) listed in the Supplement of Ref. [151], but not observed by Sung et al. [141]. We have not included them in this update since we have no intensity information for them.

Line position uncertainties were estimated by taking into account multiple aspects that included root-mean-square of individual measurements of line positions, the number of the spectra averaged, and their line intensity range. For instance, the best uncertainty of 0.0005 cm^{-1} (HITRAN error code = 4) was given to strong lines (whose line intensity $S \geq 1 \times 10^{-22}$ cm^{-1}/(molecule × cm^{-2})) and well-measured unblended lines. Worse values were selected for blends or lines retrieved in less than 4 different laboratory spectra as shown in Table 8.

<p style="text-align:center; color:red;">Approximate location of Table 8</p>

Table 8. Three factors considered in the estimation of ammonia line position uncertainties.

rms of ν_{obs} (cm^{-1})	Number. of spectra averaged	Line intensities cm^{-1}/(molecule × cm^{-2})	Uncertainties assumed (cm^{-1})	error codes
< 0.01	1	$S \leq 5 \times 10^{-24}$	< 0.01	3
< 0.005	2 or 3	$1 \times 10^{-23} \leq S < 1 \times 10^{-22}$	< 0.01	3
< 0.0005	4 or more	$S \geq 1 \times 10^{-22}$	< 0.001	4

In this 1.5-μm region, all the line intensities were adopted exclusively from Sung et al. [141]. For intensity uncertainty estimates, similar factors were considered: 1) the rms of the

averaged intensity, 2) the number of individual spectra averaged, and 3) the level of strength itself (associated with peak height of the absorption features in the observed spectrum), as listed in Table 9. For instance, for a line whose intensity is averaged over only two spectra, no better than 10% uncertainty is assumed. For unblended strong lines, $S \geq 1 \times 10^{-22}$ cm^{-1}/(molecule cm^{-2}), uncertainties are expected to be as good as 2%, while the uncertainties for most of the other lines are in the range of 5 – 10%.

<p style="text-align:center; color:red;">Approximate location of Table 9</p>

Table 9. Three factors considered in the estimation of ammonia line intensity uncertainty estimates.

rms of S_{obs} (%)	Number of spectra averaged	Line intensities cm^{-1}/(molecule $\times$ cm^{-2})	uncertainties claimed (%)	error codes
> 5	1	$S < 5 \times 10^{-24}$	< 20	4
≤ 5	2	$5 \times 10^{-24} \leq S < 1 \times 10^{-23}$	< 10	5
≤ 2	3 or more	$1 \times 10^{-23} \leq S < 1 \times 10^{-22}$	< 5	6

Sung et al. [141] reported quantum assignments for ~1000 transitions by (J, K, l_3, l_4, s/a), almost doubling the number of transitions whose assignments are available from early work, including Lundsberg-Nielson et al. [154], Xu et al. [155], Li et al. [156], Lees et al. [157], and references therein. Recently, additional assignments for lower state J and K were suggested by Cacciani et al. [151] for 313 transitions between 6626 and 6669 cm^{-1} in the supplement. They exploited very cold spectra (130 K) to substantially diminish interferences or blending by neighboring high-J features and reveal transitions belonging to low-J transitions. As in Sung et al, they also reported empirical lower-state energies and used that information to assign the lower-state quantum numbers, J and K.

For the new HITRAN list, composite assignments and measured lower-state energies from Refs. [141, 151] were selectively adopted after comparing synthetic spectra based on the lists

against selected cold and room temperature FTIR spectra. If lower-state assignments were validated, the empirical lower-state energies were replaced by corresponding calculated ground-state energies from Urban et al. [158]. For unassigned features for which empirical lower-state energies were given by either Ref. [141] or Ref. [151], the closest values among the calculated ground-state energies [158] replaced the estimates, as summarized along with their sources in Table 10. Some of the empirical lower-state energies may later be found to be inaccurate.

Approximate location of Table 10

Table 10. Sources of lower-state energy, E'', for ammonia.

Transitions	quantum numbers	E'' used	References
Fully assigned	J', K', l', a/s' J'', K'', l'', a/s''	calc. E'' in Ref. [158]	[141]
Only lower state assigned	J'', K''	Empirical E'' rounded to nearest calc. E''	[151]
Unassigned with measured E		empirical E'' rounded to nearest calc. E''	[141] [151]
Unassigned, no measured E		E'' (= 333 cm^{-1}) assumed	

The vibrational dependence of the pressure broadened widths is expected to be smaller than measurement uncertainties for NH_3 line widths currently available. Therefore, the pressure broadening coefficients and their temperature dependence exponents measured in the ν_2 band by Nemtchinov et al. [147] were extrapolated for the 1.5-µm region. In cases where their quantum assignments are suggested in Ref. [141], air- and self-broadening half widths, γ_{air} and γ_{self}, for given rotational quantum numbers, J and K, were computed by

$$\gamma(J, K) = \beta_0 + \beta_1 m + \beta_2 K + \beta_3 m^2 + \beta_4 K^2 + \beta_5 mK. \tag{2}$$

Here $m = -J, J, J + 1$ for $P, Q,$ and R branch, respectively, and β_i are the polynomial coefficients by Nemtchinov et al. [147] derived from the asymmetric v_2 state. Uncertainties for the widths of assigned transitions were assumed to be 10% by taking into account their measurement and modeling uncertainties. For unassigned transitions or those assigned only in part, a best set of quantum numbers (i.e., $J, K, a/s$), at which the calculated ground-state energy by Urban et al. [158] is nearest to the empirical lower-state energy estimates, was employed to compute the broadening coefficients in Eq. (2) with uncertainties being no better than 10%. Finally, γ_{air} and γ_{self} were assumed to be 0.065 and 0.45 $cm^{-1}atm^{-1}$, respectively, for transitions whose E'' are not determined or derived.

Temperature dependence exponents are also adopted from Nemtchinov et al. [147]. Taking their temperature dependence exponents for N_2 and O_2 broadening given at J and K less than 8 in the v_2 band, we have computed air-pressure broadening temperature exponents, n_{air}, by

$$n_{air} = 0.79 \times n_{N2} + 0.21 \times n_{O2} \tag{3}$$

Finally, the range of computed exponents was confined to be either greater than 0.51 or less than 0.95 for all other J and K. The uncertainty of the temperature exponent, 0.11, was adopted by taking their realistic estimate from Ref. [147].

To summarize, the uncertainties and temperature dependence exponents are listed in Table 11 along with their error codes.

Approximate location of Table 11

Table 11. Uncertainty determination for ammonia pressure-broadened widths.

Transitions	Empirical lower-state E''	quantum number	Pressure-broadened width (cm^{-1} atm^{-1})	Uncertainties	code
assigned	Assigned	J, K	Computed	< 10 %	4

| unassigned | E'' estimate | determined J, K candidates | Estimated | < 20 % | 3 |
| unassigned | E'' estimates not available | | $\gamma_{air} = 0.065$ $\gamma_{self} = 0.45$ | Constant | 1 |

Highly reliable pressure-shift measurements are rare because these are challenging parameters to measure for transitions found in the dense NH_3 manifolds. Moreover, the line positions are perturbed by line mixing effects at higher pressures; the presence of an intrinsic limitation in measured pressure shifts based on the Voigt line-shape model cannot be overestimated. This being said, we estimated a crude magnitude of pressure shifts by applying a "rule-of-thumb" notion that shifts are smaller than line width coefficients at the corresponding J and K by an order of magnitude. In observing that pressure shifts are more likely to be red shifts (i.e., negative shifts) in the near infrared region for isolated lines of polyatomic molecules, we assumed the pressure shifts by the following expression [141]:

$$\delta_{air}(J, K) = -0.1 \times \gamma_{air}(J, K), \tag{4}$$

where $\gamma_{air}(J, K)$ was obtained as described above. Uncertainty for the assumed pressure shifts should be no better than 0.005 cm^{-1}. It should be noted, however, that the true sign of the shift is not known until their measurements are available.

Finally, in Table 12, these computed air-broadening and air-pressure shifts are compared to four measured shifts reported by Bell et al. [152]. Such agreement may not be true for the whole line list, however, so an error code of 3 was selected for the shifts.

Approximate location of Table 12

Table 12. Comparison of air-broadened widths and air-pressure frequency shifts of NH_3 measured by Bell et al. [152] in the 1.5-µm region to those adopted in this work.

	Ref. [152]	Ref. [141]	Ref. [152]	HITRAN2012	Ref. [152]	HITRAN2012
Transitions	v_{obs} (cm^{-1})	v_{obs} (cm^{-1})	γ_{air} (cm^{-1} atm^{-1})	γ_{air} (cm^{-1} atm^{-1})	δ_{air} (cm^{-1} atm^{-1})	δ_{air} (cm^{-1} atm^{-1})
RQ(4, 1)a	6595.923	6595.9272	0.0803(7)	0.0856(86)	− 0.009(1)	− 0.009
QP(10, 6)s *	6595.616	6595.6206	0.0627(7)	0.0858(86)	− 0.014(1)	− 0.009
RQ(5, 1)s	6595.241	6595.2459	0.0774(5)	0.0786(79)	− 0.008(1)	− 0.008
RQ(5, 1)a	6595.063	6595.0682	0.0801(5)	0.0786(79)	− 0.009(1)	− 0.008

*Assigned by Lundsberg-Nielsen et al. [154], but not confirmed in Sung et al. [141].

Some caveats are in order. The supplemental line list file in Sung et al. [141] includes *empirical adjustment* of line positions and intensities of blended features if some quantum assignments are known. On occasion, the two asymmetry components of the same *J* and *K* were reset to have equal intensity and line width. An additional sanity check was also made to obtain a decent set of positions and intensities in ensemble representing the observed spectra well in the 296 − 185 K temperature range. This permitted further improvement and consistency in the line parameters, but still left some of severely blended regions less characterized, such as for the PQ(*J*, 1) branch near 6612 cm^{-1}. Further details on the quality of the individual line positions and strengths can be found in Ref. [141].

The updated $^{14}NH_3$ line list contains 45 302 lines which replace the 27 994 lines in previous editions.

2.12. HNO$_3$ (molecule 12)

For nitric acid, we have updated the pure rotational band of the ground state and added hyperfine structure from the JPL catalog [159] in the microwave region. Pure-rotational bands of v_6, v_7, v_8, v_9, $v_5/2v_9$ (mixed) states have also been added using the JPL catalog, which is largely based on the work of Petkie et al. [160, 161]. The total partition sum, Q_{total} (296 K) = 214120, was used for the conversion to HITRAN format. As mentioned in the introduction, the line positions for this molecule in the MW region are provided in a way that allows accommodation

of more decimal places. The usual HITRAN line position error code has been extended to incorporate more significant digits from the JPL catalog. Three more numbers have been added, namely 7 ($\geq$0.0000001 and $\leq$0.000001 cm^{-1}), 8 ($\geq$0.00000001 and $\leq$0.0000001 cm^{-1}), and 9 (better than 0.00000001 cm^{-1}). The air- and self- broadened half widths were adopted from the work of Gomez et al. [162].

New to HITRAN is the second-most abundant isotopologue of nitric acid, $H^{15}NO_3$. The ν_6 and $2\nu_9$ vibrational bands (in the 11-μm region) for this isotopologue were added using the work of Perrin and Mbiaké [163]. The total partition sum, Q_{total} (296 K) = 35468.0, was adopted from the same reference. Air- and self-broadened half widths and temperature dependence were adopted from the work of Flaud et al. [164]. The line list for the pure rotational band of the ground state of $H^{15}NO_3$ was adapted from the JPL catalogue.

2.13. OH (molecule 13)

Some errors in the quantum notation of the line list for the hydroxyl radical were identified in HITRAN2008 and were corrected in this edition.

2.14. HF (molecule 14)

A thorough evaluation of all the hydrogen halide line parameters that have existed in previous HITRAN editions was carried out at the HITRAN project. Accurate line positions, line intensities and Einstein *A*-coefficients were calculated for all ro-vibrational transitions (fundamental, overtone, and hot bands) for hydrogen halides in HITRAN. In addition, the deuterated isotopologues of these species have been entered into HITRAN for the first time. It should be noted that besides the terrestrial atmospheric and environmental issues that knowledge of the spectroscopy of the hydrogen halides addresses, the deuterated species has implications for

planetary research, for example Ref. [165]. Many of the updates are similar for the hydrogen halides (HF, HCl, HBr, HI); we give an overview in this section on HF. Some specifics to the other hydrogen halides are given in their respective sections (2.15-2.17). More details about the updates to the hydrogen halides can be found in Li et al. [166].

The new calculation employs the recently developed semi-empirical dipole moment functions and very accurate potential energy functions that include the parameters characterizing the Born-Oppenheimer breakdown effects [166]. Table 13 shows the choice of the maximum v, J levels for the different hydrogen halides, mainly based on the highest ro-vibrational level that is measured experimentally in high resolution. For example, $v = 22$, $J = 80$ for $D^{35,37}Cl$ means the nearby v, J level was measured experimentally for $D^{35,37}Cl$. The evaluation of the calculated line position and intensities can be found in Refs. [166-168]

<center>Approximate location of Table 13</center>

Table 13. The maximum v ,J range of the calculation for hydrogen halides.

	$H^{19}F$	$D^{19}F$	$H^{35,37}Cl$	$D^{35,37}Cl$	$H^{79,81}Br$	$D^{79,81}Br$	$H^{127}I$	$D^{127}I$
v_{max}	19	26	17	22	7	5	7	5
J_{max}	40	40	40	80	40	40	40	40

For the fundamental band of HF, the air-broadening parameters, γ_{air}, in the HITRAN2008 compilation turned out to be fitted not with a Voigt profile, but with the Galatry profile based on the Pine and Looney [169] measurements. However, the Dicke narrowing parameter was not provided in the previous database. The corresponding collisional, or Dicke, narrowing parameters have been cast into a separate columnar table that is easily linked to the main part of HITRAN using the unique combination of molecule number, isotopologue number, and quantum identifications. A header is supplied at the top of the columns to further clarify the quantities in

the table. For the pure rotational bands ($\Delta v = 0$), γ_{air} values from the HITRAN2008 listing were retained.

For the 2-0 band and beyond, N_2-and self-broadening measurements for the P(3) and P(6) lines of the 2-0 band by Chou et al. [170] were used to calibrate the Meredith and Smith measurements [171] for the 2-0 band. In the case of N_2-broadening, the calibrated results were then scaled to air by

$$\gamma_{air} = 0.9 \times \gamma_{N2}. \tag{5}$$

The self-broadening parameters, γ_{self}, of HF in the HITRAN2008 listing, which were based on Pine and Fried [172], were retained for the fundamental and $\Delta v = 1$ bands. Linear extrapolation in the vibrational level v were made using the measurements of Pine and Fried [172] and Chou et al. [170] to obtain γ_{self} for the other bands. The same γ_{air} and γ_{self} were applied to the corresponding bands of DF.

For the $\Delta v = 0, 1$ bands, the temperature-dependence of γ_{air}, n, retained values from the HITRAN2008 listing. A default value of 0.5 was used for bands with $\Delta v \geq 2$. The pressure shift, δ_{air}, also retained values from HITRAN2008 for the $\Delta v = 0, 1$ bands. Measurements by Guelachvili and Smith [173] were used for the bands with $\Delta v \geq 2$.

2.15. HCl (molecule 15)

The hyperfine structure (hfs) components for the $X^1\Sigma^+$ 0-0 $H^{35}Cl$, $H^{37}Cl$ bands were regenerated for $J \leq 15$ with improved ground-state parameters from Cazzoli and Puzzarini [174]. Similarly, hyperfine structure components for the $X^1\Sigma^+$ 0-0 $D^{35}Cl$, $D^{37}Cl$ bands were calculated using the ground-state parameters from Cazzoli and Puzzarini [175]. The sum of the relative line intensities of the HCl and DCl hfs components, calculated with the PGOPHER program [176],

was normalized to the intensity of the corresponding rotational line from the study by Li et al. [167, 168].

For the air-broadening parameters, γ_{air}, the same remarks as for HF above apply to HCl concerning the profiles of the fundamental band in HITRAN2008. Pine and Looney N_2-measurements were multiplied by a factor of 0.960 to obtain the air broadening parameters for the 0-0 band. Only the R(3) transition measurement by Park et al. [177] was applied directly. In a similar fashion, high accuracy measurements ($\pm$1% for N_2- and O_2- broadening) for the P(4) and R(3) lines of 2-0 band by De Rosa et al. [178] were used to scale Pine and Looney measurements with a factor of 1.089. The scaled values were used for bands with $\Delta v \geq 2$.

For γ_{self} in the $\Delta v = 0, 1$ bands, Pine and Fried [172] measurements were combined with Hurtmans et al. [179] accurate measurement for the P(14) line to extrapolate to high-J lines. For the $\Delta v = 2$ bands, Pine and Fried measurements were scaled with measurements ($\pm$3% uncertainty) of Ortwein et al. [180] and De Rosa et al. [178]. Ogilvie and Lee [181] and Zughul et al. [182] measurements were used for the $\Delta v = 3$ and $\Delta v \geq 4$ bands, respectively. Tudorie et al. [183] refitting of the γ_{self} measurements by Eaton and Thompson [184] were used for all bands of DCl.

Pine and Looney [169] values of the temperature-dependence exponent, n, were used for all the bands.

2.16. HBr (molecule 16)

The line positions of the hfs components for the $X^1\Sigma^+$ (0-0) and (1-0) $H^{79}Br$, $H^{81}Br$ bands were retained from the HITRAN2008 listing. However, the high-J rotational line positions without hfs structure of the same bands were recalculated using the semi-empirical potential

from Coxon and Hajigeorgiou [185]. The sum of the relative line intensities of the hfs components was normalized to the intensity of the corresponding rotational line from the study by Li et al. [168].

Values of γ_{air} from the HITRAN2008 listing were retained for hydrogen bromide. The same values were applied to DBr. However, Benedict and Herman [186] calculated values of γ_{self} were used for all bands of DBr. No data were available for the temperature dependence of the half widths of hydrogen bromide; a default value of 0.5 was used. No data were available for the shift as well.

2.17. HI (molecule 17)

Figure 7 shows an example of the significant improvements for line positions of HI compared with HITRAN2008 for the first, second, and third overtones as a function of the running index *m*.

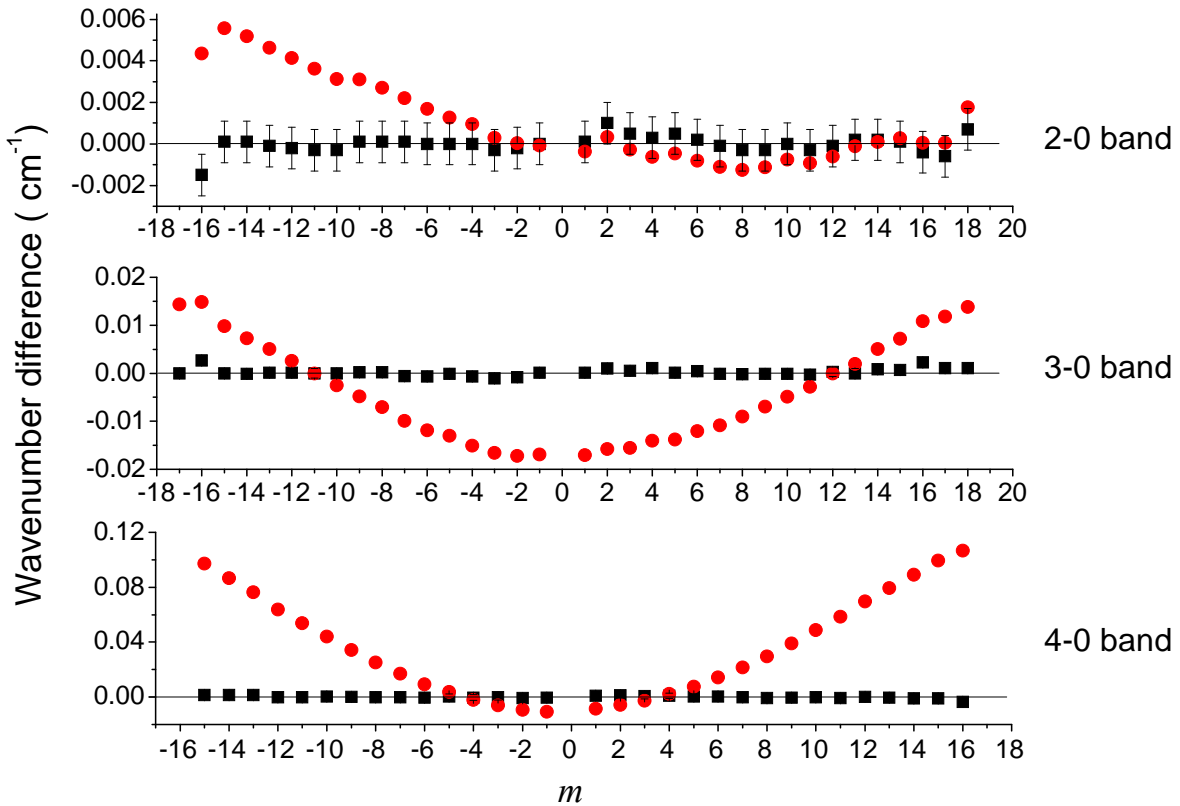Approximate location of Figure 7

Figure 7. Comparison of the line positions of HI from the present study (black squares) and HITRAN2008 (red dots) with the observations of Guelachvili [187] as a reference. The large deviation of HITRAN2008 is due to extrapolation from the lower vibrational level.

The calculated line positions for the 0-0 $D^{127}I$ band, including the hyperfine structure components, were adopted from the work by Varberg et al. [188]. The sum of the relative line intensities of the hfs components of HI and DI, calculated using the PGOPHER program, was normalized to the intensity of the corresponding rotational line from the study by Li et al. [168].

For the fundamental, first, second, third overtone bands (corresponding to $\Delta v = 1, 2, 3, 4$), γ_{N_2} from Domanskaya et al. [189] was scaled to air by Eq. (5). For the pure rotational band, the values from the fundamental band were used. For $\Delta v \geq 1$ bands, the values from the 4-0 band were used. Values of γ_{air} for HI were used for DI.

Hartmann et al. [190] measurements for γ_{self} were used for the $\Delta v = 1, 2$ bands. Bulanin et al. [191] recent γ_{self} measurements were used for $\Delta v \geq 3$ bands. Values of γ_{self} for HI were used for DI. No data were available for the temperature dependence of the half width of hydrogen bromide; a default value of 0.5 was used. Domanskaya et al. [189] measurements for the N_2 shift were adopted for HI. No data were found for the DI air shifts.

2.18. ClO (molecule 18)

Previous HITRAN intensities for the fundamental band of chlorine monoxide were introduced in a paper by Goldman et al. [192] and were based on the measurements of Burkholder et al. [193]. The intensities of all the fundamental band lines from both HITRAN isotopologues (^{35}ClO and ^{37}ClO) were adding up to a total band strength of 9.68 cm^{-2}atm^{-1} with a linear Hermann-Wallis (HW) rotational distribution (1 + 0.00563m), where m is equal to $-J''$ for the P branch, J'' for the Q branch, and $J''+1$ for the R branch. In a later experimental work, Birk and Wagner [194] derived number densities of the unstable ClO from pure rotational line intensities by consecutive mid- and far-infrared measurements. The mid infrared line strength analysis yielded a band strength of 9.01 cm^{-2} atm^{-1}. They have also shown that a quadratic expression ($1+0.00684m+1.56\times10^{-4}m^2$) is more appropriate to account for HW vibration-rotation interaction (see Fig. 4 of Ref. [194]). Consequently, the HITRAN2012 intensities have been corrected to match the results of Ref. [194].

In addition, the air-broadened half widths and their temperature dependence in the fundamental band were changed using the same method that was applied in HITRAN2008 [1] to the pure rotational band. A rough estimate for the self-broadening half width (0.1 cm^{-1} atm^{-1}) was assigned to all ClO lines in the database.

2.19. OCS (molecule 19)

The line positions and intensities in the pure rotational band for all of the HITRAN carbonyl sulfide isotopologues were updated using parameters from the Cologne Database for Molecular Spectroscopy [83]. The intensities were converted using the procedure described in the appendix of the HITRAN2008 paper, which includes scaling of the partition functions.

It was found that due to a programming error some of the air- and self-broadening half widths for all isotopologues of carbonyl sulfide were in error by as much as 50% in the HITRAN2008 edition. In addition, a typographical error in the b_3 coefficient for the O_2-broadening Padé approximant given in Ref. [195] was found. These errors have now been fixed, yielding much improved broadening parameters.

2.20. H_2CO (molecule 20)

The pure-rotational data for formaldehyde was updated with the most recent entries in the CDMS catalogue [83]. The intensities were converted using the procedure described in the appendix of the HITRAN2008 paper, which includes scaling of the partition functions.

 In addition, the line-shape parameters throughout the entire H_2CO line list were updated based on the data from Jacquemart et al. [196].

2.21. HOCl (molecule 21)

Unchanged.

2.22. N_2 (molecule 22)

It was discovered that the HITRAN2008 quadrupole line-intensities for the nitrogen molecule had not been correctly converted from the *ab initio* work of Li and Le Roy {[197]. The correction applied here yielded about a 2% change in intensities. We have also updated the line positions to the ones derived from the semi-empirical potential energy function of Le Roy et al.

[198]. New parameters have been validated using retrievals from the ACE satellite [199] and proved to be an improvement [200].

In addition, based on the works of Refs. [197] and [198], we have also added vibrational bands up to 4 - 0 for the principal isotopologue and pure rotational and fundamental bands of $^{14}N^{15}N$. It may be interesting to determine the $^{14}N/^{15}N$ ratios in different astrophysical objects using molecular nitrogen directly rather than rely on the ammonia spectra.

The excellent quality of the ab initio intensities of Ref. [197] and line positions derived from Ref. [198] has also been validated in CRDS experiments [112] where S-branch transitions of second overtone were measured. In principle from the work of Li and Le Roy one can obtain the complete database for $^{14}N_2$, $^{14}N^{15}N$ and $^{15}N_2$ lines for the transitions involving $v \leq 4$ [197].

2.23. HCN (molecule 23)

Unchanged.

2.24. CH$_3$Cl (molecule 24)

The pure rotational band of methyl chloride was converted from the JPL catalogue [159] into the HITRAN format. HITRAN2008 intensities in the 640-2600 cm^{-1} region, that originate from Nikitin et al. [201], were rescaled to be in a better agreement with existing experimental [202-204] data. Theoretical data were used [205] when no experimental values were available, and for some of the hot bands that were not measured or calculated, the PNNL cross-sections were used to estimate the band strengths [206] to provide quantitative information. The scaling factors for band strengths ranged from 5 to 650 and were isotopologue dependent. Thus this update results in a significant change to the CH$_3$Cl data in this region in comparison with HITRAN2008. The 3 μm region was completely replaced using data from Bray et al. [207].

Finally the representation of the rotational quanta was changed to accommodate not just magnitude but also the sign of *l*-quantum number which is now given for all transitions of CH_3Cl.

2.25. H_2O_2 (molecule 25)

Unchanged.

2.26. C_2H_2 (molecule 26)

The 7.7 μm region was completely updated based on the work of Gomez et al. [208, 209]. In addition, the line positions of most of the $v_1 + v_3$ band of the principal isotopologue were updated using the recommended values from the web site http://www.bipm.org/utils/common/pdf/mep/M-e-P_C2H2_1.54.pdf as well as Ref. [210].

The C_2HD isotopologue was introduced into HITRAN for the first time with microwave values originating from the CDMS catalogue [83], while parameters in the 416-789 cm^{-1} region were taken from the work of Jolly et al. [211].

Finally, some minor corrections were applied: the vibrational assignment of the line at 735.54341 cm^{-1} was corrected, and quantum assignments were corrected for the 23 Q-branch lines of the $3v_4 + v_5 - v_5$ band at 1950 cm^{-1}.

2.27. C_2H_6 (molecule 27)

Ethane is an important constituent not only in the atmosphere of the earth and comets, but also in the atmospheres of Jupiter, Saturn, Neptune, and Titan as revealed by its 12-μm emission features (e.g., see Ref. [212]). The v_9 fundamental of ethane is the strongest band seen in Titan observed in the 10-μm terrestrial window and is often used to detect and monitor its abundance in planetary atmospheres. In the HITRAN2008 database [1], the previously existing spectral line

parameters for this band were replaced by Vander Auwera et al. [213] with a new line list for the ν_9, $3\nu_4$, $\nu_4 + \nu_9 - \nu_4$, and $+ 2\nu_4 + \nu_9 - 2\nu_4$ bands. The line positions and intensities in Ref. [1] were generated based upon the global fit analysis of the four lowest vibrational states of ethane [214, 215].

Since the release of HITRAN2008 [1], two new high-resolution experimental line-parameters measurements [216, 217] have been reported in the region of the ν_9 band of $^{12}C_2H_6$. The results from Refs. [216, 217] confirmed that while the line positions agreed to within 1×10^{-4} cm^{-1} with values in Ref. [1], the line intensities were on average 15% lower. This observation was verified by comparisons made in several measured sub-band intensities between Ref. [1] and Refs. [216, 217]. Therefore, in the new HITRAN database, the line positions were retained to be the same as in HITRAN2008, while the intensities have been reduced by 15% compared to HITRAN2008.

Constant default values assumed for all transitions for air- and self-broadened half-width coefficients in Ref. [1] have been replaced with calculated values using the linear expressions for the ν_9 Q branch transitions [216, 217] for all branches in all bands. The Lorentz air-broadened half-width coefficients are computed from the reported N_2-broadened Lorentz half-width coefficients [216, 217] by assuming Eq. (5). The constant temperature dependence exponent of unity that was assumed for all lines in Ref. [1] has been replaced with calculated values based upon the new measurements [216, 217] and corrected to air by

$$n_{air} = 0.9 \times n_{N2}. \qquad (6)$$

The accuracy code for line positions in the aforementioned update is 4 (0.0001-0.001 cm^{-1}), 5% for the intensities, 10-15% for the half width coefficients, and 10-20% for the temperature dependence exponents. A short spectral region in the $^rQ(J, K=0)$ sub-band near the band head

region is shown in Fig. 8 as an example to illustrate the quality of the fit obtained for retrieving the various spectral line parameters in Ref. [217].

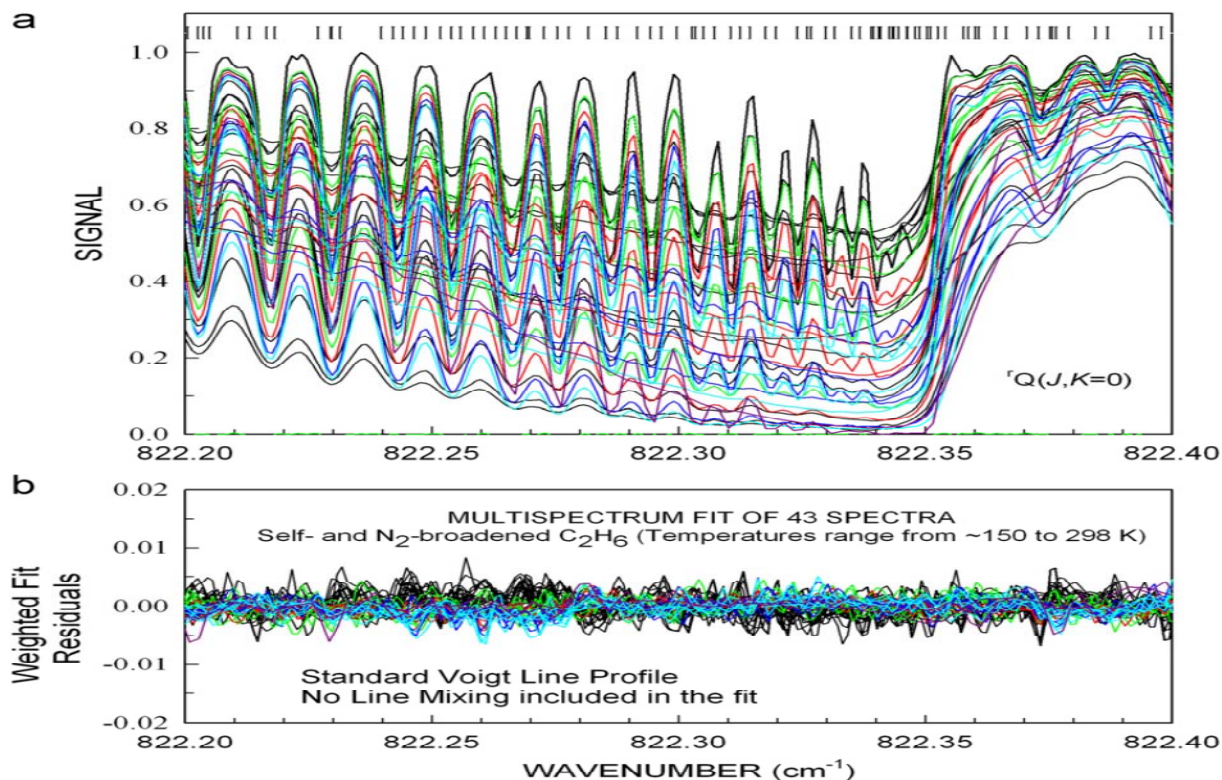Approximate location of Figure 8

Figure 8.   Example of multispectrum fit (top panel) near the band head and the excellent residuals (bottom panel).

Calculated C_2H_6 line positions, intensities, and quantum assignments between 1330 and 1610 cm^{-1} (7-μm region) from Di Lauro et al. [218] have also now been included in HITRAN. The spectrum is very complex, and there are a multitude of resonances and interactions that must be included in order to analyze high resolution spectra.   The accuracy of many predicted positions at 7 μm are enhanced using *empirical* upper state energies, E', tabulated as a function of the ethane quantum numbers by adding to the measured positions of assigned lines the corresponding lower state energies E''. The altered positions have the HITRAN accuracy code = 4 (0.0001 – 0.001 cm^{-1}). A more conservative accuracy code = 2 (0.01 – 0.1 cm^{-1}) is set for the

remaining predicted positions. The intensities are predicted, and the integrated strength is normalized to match the available laboratory spectra used by di Lauro et al. (which was also used to renormalize the prior predictions at 12 μm [1]. Self- and N_2-broadened C_2H_6 half widths and N_2-broadened temperature dependences have been added using the linear expressions for ν_9 Q-branch transitions reported by Devi et al. [216, 217] for all types of transitions (P, Q, R) of both the parallel and perpendicular bands. The accuracies for widths are conservatively set to 10 to 20% (HITRAN code = 4). The accuracies for the temperature dependence exponents of the widths are thought to be 10 to 25%.

Table 14 is an overview of the 12- and 7-μm bands of ethane in the new line list.

Approximate location of Table 14

Table 14. Band-by-band summary of the 12- and 7-μm line list for ethane.

Band	ν_0 (cm^{-1})	ν_{min} (cm^{-1})	ν_{max} (cm^{-1})	Number of lines	$\sum_{int}$	J_{max}	K_{max}
			12-μm region				
$3\nu_4$	790.9	706.8572	775.3455	43	0.0000566	45	2
ν_9	821.3	706.6015	942.1680	7188	641.548	45	22
$\nu_9 + \nu_4 - \nu_4$	832.2	717.8110	951.5441	7188	159.381	45	22
$\nu_9 + 2\nu_4 - 2\nu_4$	843.9	727.2776	961.1450	7188	46.923	45	22
			7-μm region				
ν_6	1379.2	1330.2862	1604.5903	2252	117.044	44	19
$2\nu_4 + \nu_9$	1388.2	1371.3452	1604.6207	42	0.440	40	18
ν_8	1471.8	1330.7725	1610.7034	8443	1331.374	45	20
$\nu_4 + \nu_8 - \nu_4$	1471.9	1330.3300	1610.3803	5093	341.043	45	20
$2\nu_4 + \nu_{12} - \nu_4$		1373.9485	1567.3138	781	19.044	37	14
$\nu_4 + \nu_{12}$	1480.6	1379.8273	1591.0744	3263	165.200	46	12

Note: ν_0 is the band center, ν_{min} and ν_{max} are the beginning and the ending wavenumbers of the range of transitions included in each band, and $\sum_{int}$ is the summed intensities in units of 10^{-21} cm^{-1}/(molecule cm^{-2}) at 296 K.

In this edition of HITRAN, IR cross-sections for the 3-µm region have been added. See Section 3.1 for the discussion and available pseudo-line list option. There has been some additional recent work on line assignments [219] and band models [220] in the 3.3-µm region, but these results are not yet ready for inclusion in the HITRAN database.

It should be noted that the $^{13}C^{12}CH_6$ isotopologue had not been added to the official release of HITRAN2008 despite the text in Ref. [1]; this additional isotopologue has now been included (for the 12-µm region). Finally, the symmetry labeling of some of the ethane lines in the official HITRAN2008 release were found to be erroneous. This situation has now been remedied.

2.28. PH$_3$ (molecule 28)

Phosphine FIR line parameters have been introduced into HITRAN for the first time and originate from the CDMS catalogue [83]. The dataset is slightly different from the one uploaded to CDMS in October 2008. The creation of the 2008 version was prompted by the very accurate Lamb-dip and Doppler-limited measurements up to 534 GHz and near 800 GHz, respectively [221]. The Lamb-dip measurements resolved the H and P hyperfine structure to a very large extent. Also included in the fit were transitions between the A_1 and A_2 components of $K = 3,6,9,...$ transitions with hyperfine information as far as available [222], $\Delta K = 3$ transitions [223-226] as well as regular $\Delta K = 0$ rotational transitions measured at sub-millimeter [226] and far-infrared wavelengths [227]. The entry was deemed to be satisfactory for radio-astronomical observations in the interstellar medium, but may not be extensive enough for studies of giant planets or brown dwarfs or for benchmarking against large-scale quantum-chemical calculations. Therefore, the same data set was used in a February 2013 update to create an entry with considerably lowered intensity cut-offs. It is superior to the fit published in Ref. [221] which only employed data from that work as well as $\Delta K = 0$ additional rotational transitions from Ref.

[225]. The details of the present fit which results in this HITRAN2012 update is given in Ref. [228]. As it is mentioned in introduction the line positions for this molecule in the MW region are provided in the way which allows accommodation of more decimal places.

Current quantum notation existing in HITRAN will be reconsidered in the future to provide unique assignments of rotational levels and avoid assignments that appear identical for different lines or seemingly contradicting selection rules. This problem, however, does not affect the actual spectroscopic data and simulations that employ them.

2.29. COF_2 (molecule 29)

A simultaneous fit of high-resolution THz and infrared spectra of carbonyl fluoride [229] allowed improving the line positions in HITRAN and, more importantly, creating a more complete line list for this molecule. Apart from fundamentals, the dataset now also includes hot bands in the v_6 band region (12.9 μm) as well as v_6 lines of the $^{13}COF_2$ isotopologue, which has been introduced into HITRAN for the first time.

2.30. SF_6 (molecule 30)

Unchanged.

2.31. H_2S (molecule 31)

The knowledge of reliable reference spectral data for hydrogen sulfide is important for the monitoring of the quality of air [230], especially near oil refineries. H_2S can also serve as a biomarker on exoplanets [231]. A substantial update of the pure-rotational transitions and introduction of the NIR transitions was carried out to aid these research fields.

2.31.1 Pure rotational transitions in the 45 to 360 cm^{-1} region

New room-temperature, Fourier transform measurements performed by Azzam et al [232] have been used to replace and augment the pure rotational transitions of hydrogen sulfide in the 45 to 360 cm^{-1} region. These measurements significantly extended previous experimental studies in this region [233-235] for the isotopologues $H_2^{32}S$, $H_2^{33}S$ and $H_2^{34}S$. Pure-rotational transitions within the excited ν_2 vibrational state of $H_2^{32}S$ were observed for the first time and assigned using an *ab initio* line list [236] with most assignments confirmed by combination differences based on the HITRAN data for the ν_2 vibrational band. The new experimental data were combined with lower frequency measurements to obtain new sets of Hamiltonian parameters which were used to generate a line list for the entire 45 to 360 cm^{-1} region giving a total of 4794 transitions which replace the existing data for this region. See the paper by Azzam et al [232] in this issue for further details.

2.31.2 Addition of new transitions in the 4472 and 11330 cm^{-1} regions

The compilation for hydrogen sulfide has been extended by adding 28973 transitions between 4471.7 and 11329.6 cm^{-1}. All the new transitions fall into specific spectral regions (polyads) corresponding to the first and second hexads (4471 - 6695 cm^{-1}), the first decade (7053-8039 cm^{-1}), and the first and second pentadecades (9385 - 11330 cm^{-1}). Two minor isotopologues are also included. The new information is summarized in Table 15 which gives the spectrometer used for the measurements, the numbers of studied isotopologues and included absorption lines, the estimated accuracies for positions and intensities, and the vibrational bands included for $H_2^{32}S$.

Approximate location of Table 15

Table 15. Overview of the positions and intensities for higher polyads of H_2S.

Polyad (cm^{-1})	Source of data	Number of isotopo-logues	Number of lines	Position accuracies (cm^{-1})	Intensity accuracies[+]	Vibrational bands
1st hexad 4471 –5665	Kitt Peak FTS	3	11678	0.0005–0.005	5-10%, 10-20% and worse	200-000 101-000 002-000 120-000 021-000 040-000 210-010 111-010
2nd hexad 5671 – 6695	Kitt Peak FTS	3	7016	0.0005 –0.005	5-10%, 10-20% and worse	210-000 111-000 012-000 130-000 031-000 050-000 121-010 220-010
1st decade 7053 – 8039	Kitt Peak FTS	1	3343	0.0005 –0.005	15-20% and worse	300-000 201-000 102-000 003-000 220-000 121-000
1st pentadecad 9385 – 10266	ICLAS-VECSEL	3	4071	better than 0.01	25-30% and worse	301-000 202-000 221-000 122-000 141-000
2nd pentadecad 10777 – 11329	ICLAS	3	2865	0.005	15-20% and worse	311-000 212-000 330-000

[+] "worse" accuracies (meaning different by a factor of two) apply to the weakest lines.

The extended line list contains both pure experimental and calculated line positions and intensities. The calculated positions are obtained only from the experimental upper-state energy levels based on known quantum assignments and have accuracies comparable to the experimental ones. The intensities were measured and predicted with a range of accuracies that depend on the spectral region (see Table 15). Consistent with earlier versions of HITRAN, constant broadening coefficients are applied: γ_{air}, γ_{self}, and δ_{air} of 0.074, 0.158 and 0.0 cm^{-1}atm^{-1} at 296 K, respectively; 0.75 was adopted for the temperature dependence of the air-broadened half width. Detailed laboratory investigations are needed to characterize the variation of air and self broadening as a function of the ro-vibrational quantum numbers for the range of atmospheric temperatures.

2.31.2.1 Data obtained by Fourier transform spectrometer

The new H_2S analyses between 4450 and 8050 cm^{-1} were based on the high-resolution (0.0056 and 0.011 cm^{-1}) laboratory spectra recorded with the McMath Fourier transform spectrometer located at Kitt Peak National Solar Observatory. The resulting peak list was assigned and modeled using the Watson-type effective Hamiltonian. Accurate line intensities for about 2900 lines were retrieved for the 1st and 2nd hexads from a dozen spectra recorded using path lengths of 1.5 to 433 m and pressures ranging from 1.5 to 30 Torr. For the strongest transitions in the two hexad regions, the averaged observed intensities were based on 6 to 10 individual spectra. These were then modeled with the effective transition moment series using 34 and 20 parameters to achieve RMS agreement close to experimental accuracy: 2.9 and 3.6%, respectively. For the 1st decade region above 7050 cm^{-1}, line intensities were either retrieved from only a few spectra, or were estimated from the peak absorption for weak lines. Of these, 920 measured intensities of transitions belonging to the 003-000, 201-000, 121-000, 102-000, 300-000, and 220-000 vibrational bands were modeled within 12% by using 21 transition moment parameters. In the case of the $H_2^{34}S$ and $H_2^{33}S$ isotopologues, the calculated intensities were based on the transition moment parameters for the main isotopologue and true rotational-vibrational wavefunctions obtained from the energy level fitting for isotopologues.

Some details about energy levels and transition intensity modeling can be found in Refs. [237-239]. A review of all published information on the $H_2^{32}S$, $H_2^{33}S$, and $H_2^{34}S$ infrared spectra is given in Ref. [240]. In particular, the $H_2^{32}S$ spectra in the 2nd hexad (5700-6650 cm^{-1}) and 1st decade (7300-7900 cm^{-1}) regions have been investigated in recent papers by Ulenikov et al. [241, 242]; however, no information about line positions and intensities has been published. In any case, the $H_2^{32}S$ transitions included in this issue of HITRAN involve a considerably large number of upper-state energy levels compared to those published in Refs. [241, 242].

The resulting list of transitions consists of 16288 transitions between 4450 and 8050 cm^{-1} belonging to 22 vibrational bands of H$_2$^{32}S, including four hot bands (see Table 15). There also are 4098 lines of H$_2$^{34}S and 1116 lines of H$_2$^{33}S included between 4700 and 6600 cm^{-1}. In total, the new H$_2$S line list contains 22037 transitions derived from the analysis of FTIR spectra.

The accuracies of the positions and intensities vary. The position accuracy of stronger isolated lines that dominate the spectrum is estimated to be 0.001 cm^{-1} and better, as confirmed by the combination difference analysis. For blended features and those that are 500 times weaker than the strongest lines in the region, the accuracy may degrade to 0.005 cm^{-1} and worse. The accuracy of presented intensities can vary within a wide interval. The most accurate data are in both hexads where experimental uncertainties vary from 1 to 7 %. For the 1st decade the accuracy of experimental intensities is 10-20% for stronger lines but worse for all experimental transitions with intensities less than 5.0×10^{-25} cm^{-1}/(cm^{-2} × molecule) at 296 K. The calculated intensities are thought to be accurate within 10-20% for intensities larger than 2.0×10^{-24} cm^{-1}/(cm^{-2} × molecule) at 296 K and worse for weaker lines. In the case of the two hexads, the calculated intensities obtained from the modeling of accurate experimental data are believed to be more reliable than those for the 1st decade region.

Very few near infrared experimental intensities of H$_2$S have been previously published near 1.6 μm for direct comparison. One recent paper [230] reported intensities of four lines near 6341 cm^{-1} using a laser spectrometer. As seen in Table 16, their new values are ~12% higher than the present intensities. Thus, further investigation is needed.

Approximate location of Table 16

Table 16. Comparison of the present observed intensities with literature data.

Position	Vibrational	$J'K_a'K_c'$ –	H$_2$S intensity [+]	Intensity ratio

(cm^{-1})	band	$J''K_a''K_c''$	HITRAN	Ref. [230]	Ref. [230] / present
6339.24518	(111) – (000)	423 – 322	2.67 ± 2.1%	2.9 ± 17%	1.09
6340.43196	(111) – (000)	413 – 312	10.7 ± 1.5%	11.6 ± 2.6%	1.08
6342.80948	(210) – (000)	606 – 515 616 – 505	4.45 ± 1.6%	5.1 ± 7.8%	1.15
6344.00001	(111) – (000)	606 – 515 616 – 505	17.4 ± 1.3%	20.0 ± 1.0%	1.15

[+] In units of 10^{-23} cm^{-1}/(cm^{-2} × molecule) at 296 K. Values in percent are experimental precisions of the measured intensities. Where two assignments are listed, the intensity represents the sum.

2.31.2.2. Data obtained by Intra-Cavity Laser Absorption Spectroscopy

High sensitive ICLAS - VECSEL (Intra-Cavity Laser Absorption Spectroscopy with a Vertical External Cavity Surface Emitting laser) and ICLAS systems were used to record weak absorption lines of hydrogen sulfide in the 9385 – 10200 [243] and the 10780-11330 cm^{-1} [244] spectral regions, respectively. In total, 3385 transitions involving eight highly excited upper states were recorded and assigned. The relative experimental intensities were approximately derived from the peak absorption and then scaled to the FTS data of Ref. [245].

The accuracy of line positions in the 9385-10200 cm^{-1} region was estimated to be better than 0.01 cm^{-1}. The experimental intensities are believed to be accurate within 25-30% for stronger lines, while for the weakest lines the uncertainty in measured intensities can reach up to 100%. The transition moment parameters were obtained by fitting to 1183 observed transition intensities. An rms deviation of 18% was achieved by varying 25 parameters.

For the 10780 to 11330 cm^{-1} interval, the position accuracy of 0.005 cm^{-1} was estimated in the process of spectra calibration and then confirmed by the combination differences analysis. Six transition moment parameters were derived by fitting to 337 relatively strong, well isolated line intensities, which reproduce 82% of the fitted intensities within 15%.

Finally a line list including 3385 experimentally measured lines was combined with 3551 weaker transitions whose intensities were predicted using the derived transition moment parameters; the calculated positions were estimated from the experimental upper-state energy levels.

The graphical summary of the new information on hydrogen sulfide absorption included in HITRAN2012 is shown in Fig. 9.

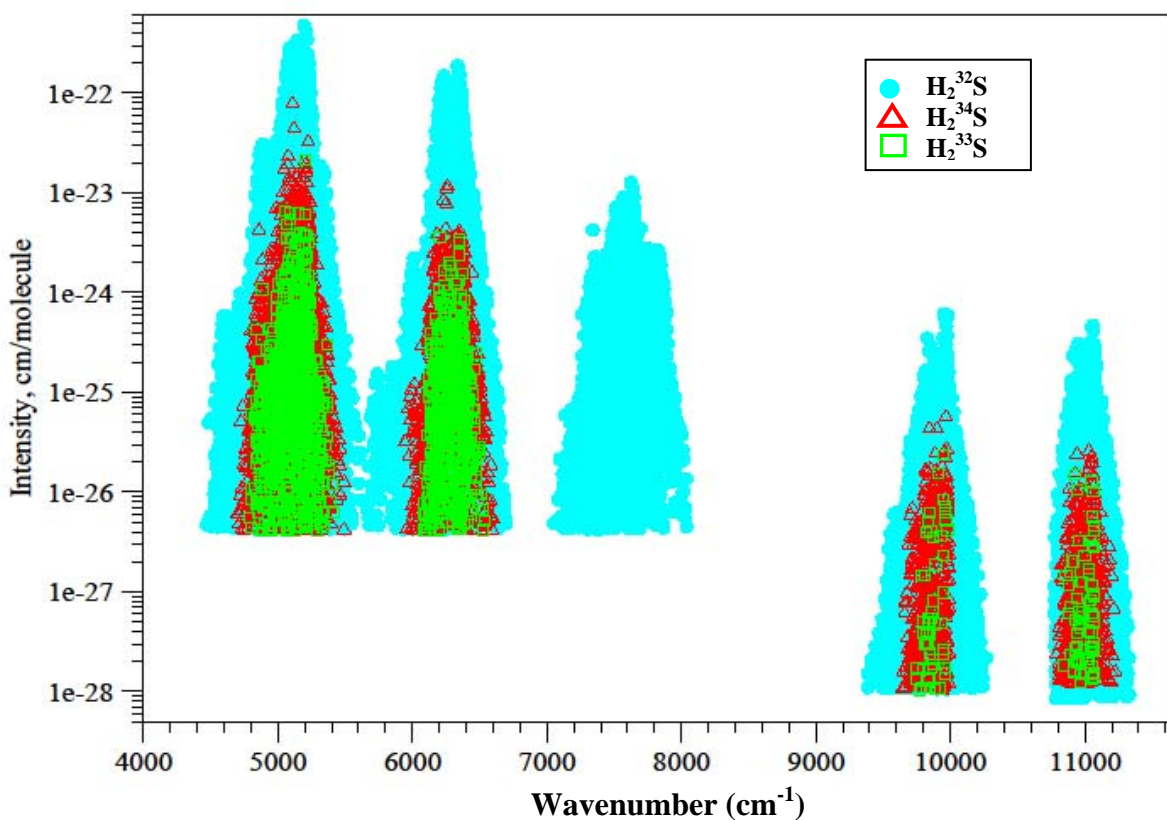Approximate location of Figure 9

Figure 9. New absorption lines of hydrogen sulfide added for the HITRAN2012 database. Transitions of $H_2{}^{32}S$, $H_2{}^{34}S$, and $H_2{}^{33}S$ are shown, respectively, by circles (in cyan), triangles (in red), and squares (in green). Intensities in $cm^{-1}/(cm^{-2} \times molecule)$ at 296 K are given for natural abundance.

This extension of the H$_2$S parameters can enable more in situ and remote sensing in the near-IR, particularly with sensitive laser-based techniques. As seen in the characterization of accuracies, the listed line positions are usually well within the full Doppler widths of H$_2$S so that the quantum assignments should be unambiguous. However, the line intensities may not be sufficiently reliable for applications desiring to measure atmospheric abundances with the highest accuracies. Much more is needed to characterize accurate pressure broadening at all wavelengths for hydrogen sulfide.

2.32. HCOOH (molecule 32)

Unchanged.

2.33. HO$_2$ (molecule 33)

Unchanged.

2.34. O ("molecule" 34)

Unchanged.

2.35. ClONO$_2$ (molecule 35)

Unchanged.

2.36. NO$^+$ (molecule 36)

Unchanged.

2.37. HOBr (molecule 37)

Unchanged.

2.38. C$_2$H$_4$ (molecule 38)

Unchanged.

2.39. CH₃OH (molecule 39)

Unchanged.

2.40. CH₃Br (molecule 40)

Unchanged.

2.41. CH₃CN (molecule 41)

Unchanged.

2.42. CF₄ (molecule 42)

Unchanged.

2.43. C₄H₂ (molecule 43)

Diacetylene, the simplest member of the polyacetylene family, is a molecule of relevant astrophysical interest. In the interstellar medium, it plays a major role in the synthesis of complex hydrocarbons and cyanopolyynes through ion–neutral or neutral–neutral reactions with C^+ or CN [246]. C_4H_2 is also a well known constituent of the stratosphere of the giant planets and their moons [98, 247, 248], where it acts as a UV shield and is thought to take part in the photochemical reaction network initiating the organic aerosols (tholines) present in the atmospheres of these solar system bodies [249].

The v_8 perpendicular band of diacetylene at 16 μm has been detected in the proto-planetary nebulae CRL 618 and CRL 2688 by ISO [250], and also outside our galaxy in a similar object embedded in the Large Magellanic Cloud (SMP LMC 11) using the IRS spectrograph on board Spitzer [251]. As concerns our Solar System, the first identification of diacetylene dates back to

1981, in Titan's atmosphere by Voyager with its IRIS spectrometer [252]. Subsequently, its detection was made in the atmospheres of Saturn [247], Jupiter [253], Uranus [254], and Neptune [255]. All these detections were made through the v_8 band observed by ISO/SWS, Spitzer/IRS and Cassini/CIRS.

The infrared spectrum of diacetylene is dominated by three strong features at 3300 cm^{-1} (v_4), 1240 cm^{-1} ($v_6 + v_8$), and 627 cm^{-1} (v_8) [256-258]. This latter band is particularly relevant for astrophysical and planetary studies as it is detectable in emission in a large variety of environments. Despite this, the region below 1000 cm^{-1} was the subject of only one high-resolution study [258] until very recently, when comprehensive investigations of the low-energy band system were undertaken [259-261].

The C$_4$H$_2$ line positions and relative intensities presented here were calculated from the results of the high-resolution analysis of the v_8 fundamental, the $v_7 + v_9$ combination band, the $v_3 - v_9$ and $v_8 - v_6$ difference bands, plus the hot bands $v_8 + v_9 - v_9$, $v_7 + 2v_9 - v_9$ and $v_8 + v_9 - v_6 - v_9$ [260, 261]. Over 1200 infrared lines measured in Ref. [261] were fitted together with the ro-vibrational transitions recorded in the millimeter-wave range [260] for the bend-bend difference bands. The model adopted for the analysis includes the rotational and vibrational l-type resonances active between the various l-sublevels of the multiple bending excited states, and also considers the two anharmonic interactions which couple $v_3 = 1$ with the $v_8 = v_9 = 1$ combination band and the $v_3 = 2$ overtone states through the normal coordinate cubic potential constants ϕ_{389} and ϕ_{377}. The resulting Hamiltonian matrix was block-factorized and diagonalized to derive the energy eigenvalues and the relative transition intensities.

The C$_4$H$_2$ relative line intensities of the bands in the microwave region were scaled to the band intensities calculated from the transition dipole moments measured by Matsumura et al.

[262]. We note that in the microwave region, the line list presented here is the first compilation available for scientists, and should prove useful in searching for this molecule in different astrophysical objects with instruments including the SMA (Submilleter Array) [263] and Herschel [264].

Band intensities in the v_8 region were scaled to those reported by Jolly et al. [259]. Lines from the bands involving vibrational states that were not observed in Refs. [260, 261] were taken from Jolly et al. [259]. The new line list spans the region 0 to 758 cm^{-1} and contains 124126 transitions (for only the principal isotopologue).

For the line-shape parameters, no broadening measurements nor calculations were available; for this edition default constant values were adopted ($\gamma_{air} = 0.10$ cm^{-1} atm^{-1}, $\gamma_{self} = 0.20$ cm^{-1} atm^{-1}, $n = 0.75$, $\delta_{air} = 0$ cm^{-1} atm^{-1}).

2.44. HC$_3$N (molecule 44)

Cyanoacetylene is present in the atmosphere of Titan [252] and in molecular clouds [265]. It is therefore important to have reliable spectroscopic reference data for this molecule. The line list of HC$_3$N covering the spectral regions of the v_5 (460-550 cm^{-1}) and v_6 (620-750 cm^{-1}) fundamentals has been adapted from Jolly et al. [266]. The line list also contains some of the hot bands.

The transitions with $\Delta v = 0$ in the ground, $v_6 = 1$ and $v_7 = 1$ states (in the microwave region) have been adopted from the CDMS catalogue [83]. Interestingly, the ro-vibrational energy levels in the $v_7 = 1$ states in the CDMS catalogue are systematically shifted by $+0.5863$ cm^{-1} with respect to the energy levels from Ref. [266], while there is no difference between the rotational energy levels in the ground state. Since in the work of Jolly et al. spectroscopic constants for all

vibrational levels were derived in a global fit which included unpublished lines from the $\nu_6+\nu_7-\nu_7$ and $\nu_6+\nu_7$ bands which allows determination of the position of the $\nu_7=1$ with respect to the ground state accurately, we have made the energy levels from CDMS database consistent with the ones from Jolly et al [266].

To accommodate representation of seven vibrational modes, three of which are doubly degenerate (ν_5, ν_6 and ν_7) in the fifteen-field "global" quanta space in post-HITRAN2004 format, vibrational quantum numbers are given as follows. In FORTRAN notation it is 2x, 7I1, 3I2. Here each of the integers (I1) corresponds to ν_1, ν_2,… ν_7, whereas each of the integers (I2) corresponds to ℓ_5, ℓ_6 and ℓ_7. The line list so far is limited to the principal isotopologue and contains 180332 lines.

2.45. H_2 (molecule 45)

Molecular hydrogen (H_2) is the most abundant gas in the atmosphere of gaseous giants. The quadrupole fundamental and overtone transitions needed to be incorporated into the database. The rotational lines of these bands are very sparse and relatively weak which makes them good candidates for probing very deep and dense Jovian atmospheres. The two most abundant isotopologues of the hydrogen molecule are making their debut in HITRAN. The details of the compilation of these line lists are given below.

The "non-local", non-adiabatic effects are important for H_2 and HD; thus there is no natural way to present the energy as a simple 1-D potential. Fortunately, the theoretical approach developed by Komasa et al. [267] have proved to be very effective. The line positions of the electric quadrupole-allowed transitions for H_2 in the ground electronic state were generated using the dissociation energies calculated by Komasa et al. [267]. The line positions of electric dipole-

allowed transitions for HD in the electronic ground state were generated using the dissociation energies calculated by Pachucki et al. [268]. A summary of the spectral range and the number of lines is given in Table 2. The maximum vibrational levels for H_2 and HD are 14 and 17, respectively; the maximum rotational levels, J_{max}, are 30 and 35 respectively for H_2 and HD.

Combining the isotopologue-dependent "best adiabatic" point-wise potential of Schwartz and Le Roy [269] (downloaded from http://leroy.uwaterloo.ca/potentials.html) and an ab initio electric quadrupole moment function of Wolniewicz et al. [270], the matrix elements of quadrupole allowed transitions were calculated for H_2 using Le Roy's LEVEL program [5]. Similarly, the dipole matrix elements of HD were calculated, based on the dipole moment function from Ref. [271]. The corresponding line intensities were subsequently calculated from these matrix elements.

The theoretical results we used here had been in excellent agreement with recent cavity ring down experiments [272-275], but in fact supersede them in accuracy and, more importantly, in the extent of the data. Therefore these ab initio results have been adopted for hydrogen line positions in HITRAN. The same discussion applies to the calculation of the intensities.

In the future, electric quadrupole lines of HD will be added to the database once the electric quadrupole moment function become available. The quadrupole moment function in either point-wise or functional form will be used in the calculation of line intensities. With this we would like to re-emphasize the importance of providing such data in theoretical or experimental papers.

The Voigt line shapes are known to be particularly inadequate for the case of broadening of hydrogen lines [276, 277]. Even for non-Voigt line shapes no complete sets of broadening parameters are currently available. So far only default Voigt values are used in HITRAN: $\gamma_{air} =$

0.05 cm^{-1}atm^{-1}; γ_{self} = 0.05 cm^{-1}atm^{-1}; and n =0.75. One should also keep in mind that no shifts are provided at the moment.

2.46. CS (molecule 46)

Carbon monosulfide is a new addition to the HITRAN database. CS detection has been a source of interest for the study of comets and planetary atmospheres. The abundance has been measured, for instance, in the Hyakutake and Hale-Bopp comets [278]. It has also been detected in the atmosphere of Jupiter after the collision with the Schumacher-Levy comet [279]. Data for four isotopologues (^{12}C^{32}S, ^{12}C^{33}S, ^{12}C^{34}S, ^{13}C^{32}S) are now included in the HITRAN database in the microwave region, while infrared data are provided only for the first two isotopologues. The line positions and lower-state energies were obtained from the Cologne Database for Molecular Spectroscopy (CDMS) catalogue [83]. Intensities were calculated from theoretical Einstein A-coefficients that were provided in the paper by Chandra et.al. [280]. The conversion from Einstein A-coefficients to HITRAN intensities is described in the paper by Šimecková et al. [3].

To the best of our knowledge, no experimental broadening parameters exist for carbon monosulfide, so rough estimates of their values had to be made. To make reasonable estimates of the behavior and values of the broadening parameters of carbon monosulfide, a comparison between carbon dioxide and carbon monoxide broadening parameters (found in the HITRAN database [1]) were made. Using the *J*-dependent scaling factors obtained for the carbon oxides, the experimental values for nitrogen [281] and self-broadening [282] of carbon disulfide were scaled to obtain broadening parameters for CS. The temperature-dependence exponent for the nitrogen-broadening was estimated to be a standard 0.75, as no experimental data exist.

2.47. SO$_3$ (molecule 47)

Sulfur trioxide spectroscopic line parameters have been included for the first time in the 2012 HITRAN edition. SO_3 occurs naturally in volcanic emissions and is also a pollutant emitted by smoke-stacks and other industrial exhausts [283]. In the terrestrial atmosphere, SO_3 rapidly forms sulfuric acid with its association with acid rain. SO_3 is also thought to be present in the atmosphere of Venus [284].

SO_3 is a planar, non-polar molecule. However with sufficient rotational excitation the molecule can distort and undergo pure rotational transitions. Lines in this centrifugally-induced pure rotational spectrum were observed by Meyer et al [285]; in this case the *ab initio* transition intensities of Underwood et al [286] have been used as there is no intensity information in the experiment.

Parameters in the infrared region are based on a series of infrared spectra recorded by Maki and co-workers [287-291]. These spectra, which in general were recorded at two pressures, only provide relative intensities. Recently Underwood et al. [286] performed detailed *ab initio* electronic structure and variational nuclear motion calculations for $^{32}S^{16}O_3$. Comparisons between their absolute, calculated intensities and the measured, relative intensities give good agreement for the strong bands and reasonable agreement for the weaker ones. The line parameters provided have therefore used the ab initio calculations to scale the measured intensities to absolute values. Details of this scaling procedure can be found in Underwood et al. [286].

No measurements or calculations for the line-shape parameters were available, therefore the usual default values were chosen. The new line list for SO_3 contains 10881 lines covering the region up to 2850 cm^{-1}. Only the main $^{32}S^{16}O_3$ isotopologue has been considered.

3. Infrared absorption cross-sections

Infrared absorption cross sections for this edition of the HITRAN compilation are listed in Table 17. This portion of the database supplies cross sections of molecules for which high-resolution (line-by-line) spectral line parameters are incomplete or unavailable; generally these are large polyatomic molecules for which generating line parameters is very difficult or undesirable at this time due to the lack of detail concerning hot bands and/or characterization of other relevant phenomena such as pressure-induced effects. Note that all absorption cross sections in HITRAN have units of cm^2 molecule^{-1}.

Approximate location of Table 17

Table 17. Summary of molecules represented by IR cross-section data in *HITRAN*

Molecule	Common Name	Temperature Range (K)	Pressure Range (torr)	Number of T,P sets	Spectral Coverage (cm^{-1})
SF$_6$	Sulfur hexafluoride	180-295	20-760	32	925-955
ClONO$_2$	Chlorine nitrate	189-297	0-117	25	750–830
		189-297	0-117	25	1260-1320
		213-296	0	2	1680-1790
CCl$_4$	Carbon tetrachloride	208-297	8-760	32	750-812
N$_2$O$_5$	Dinitrogen pentoxide	205-293	0	5	540-1380
HNO$_4$	Peroxynitric acid	220	0	1	780-830
C$_2$F$_6$	Hexafluoroethane, CFC-116	181-296	25-760	43	1061-1165
		181-296	25-760	43	1220-1285
CCl$_3$F	CFC-11	190-296	8-760	55	810-880
		190-296	8-760	55	1050-1120
CCl$_2$F$_2$	CFC-12	190-296	8-760	52	850-950
		190-296	8-760	52	1050-1200
CClF$_3$	CFC-13	203-293	0	6	765-805
		203-293	0	6	1065-1140
		203-293	0	6	1170-1235
CF$_4$	CFC-14	180-296	8-761	55	1250-1290
C$_2$Cl$_2$F$_3$	CFC-113	203-293	0	6	780-995
		203-293	0	6	1005-1232
C$_2$Cl$_2$F$_4$	CFC-114	203-293	0	6	815-860
		203-293	0	6	870-960
		203-293	0	6	1030-1067
		203-293	0	6	1095-1285
C$_2$ClF$_5$	CFC-115	203-293	0	6	955-1015
		203-293	0	6	1110-1145
		203-293	0	6	1167-1260
CHCl$_2$F	HCFC-21	296	1	1	785-840
CHClF$_2$	HCFC-22	181-297	0-765	29	760-860
		181-296	22-761	31	1070-1195
		253-287	0	3	1060-1210

		253-287	0	3	1275-1380
$CHCl_2CF_3$	HCFC-123	253-287	0	3	740-900
		253-287	0	3	1080-1450
		287	0	1	675-715
$CHClFCF_3$	HCFC-124	287	0	1	790-920
		287	0	1	1035-1430
		253-287	0	3	710-790
CH_3CCl_2F	HCFC-141b	253-287	0	3	895-1210
		253-287	0	3	1325-1470
$CHCl_2CF_2CF_3$	HCFC-225ca	253-287	0	3	695-865
		253-287	0	3	1010-1420
$CClF_2CF_2CHClF$	HCFC-225cb	253-287	0	3	715-1375
CH_2F_2	HFC-32	203-297	0-750	17	995-1236
		203-297	0-750	17	1385-1475
		287	0	1	700-745
CHF_2CF_3	HFC-125	287	0	1	840-890
		287	0	1	1060-1465
CHF_2CHF_2	HFC-134	203-297	0-750	9	600-1700
		253-287	0	3	815-865
CFH_2CF_3	HFC-134a	190-296	20-760	32	1035-1130
		190-296	20-760	33	1135-1340
		253-287	0	3	935-1485
		203-297	0-750	9	580-630
CF_3CH_3	HFC-143a	203-297	0-750	9	750-1050
		203-297	0-750	9	1100-1500
		253-287	0	3	840-995
CH_3CHF_2	HFC-152a	253-287	0	3	1050-1205
		253-287	0	3	1320-1490
		213-323	760	5	599-624
		213-323	760	5	676-704
SF_5CF_3	Trifluoromethyl	213-323	760	5	740-766
	sulfur pentafluoride	213-323	760	5	860-920
		213-323	760	5	1150-1280
		213-323	760	5	1280-2600
$CH_3C(O)OONO_2$	PAN	295	0.08	1	1650-1901
		276-324	760	3	624-784
		276-324	760	3	867-1159
CH_3CN	Acetonitrile	276-324	760	3	1175-1687
	(methyl cyanide)	276-324	760	3	2217-2343
		276-324	760	3	2786-3261
		276-324	760	3	3881-4574

New data introduced since HITRAN2008 [1.1]

C_2H_6	Ethane	194-297	49-763	14	2545-3315
CH_3OH	Methanol	204-295	50-761	12	877-1167
		204-296	51-761	12	2600-3250
CH_3CN	Acetonitrile	203-297	50-760	12	880-1700
		208-296	50-760	11	2550-3300
C_3H_8	Propane	195-296	40-763	12	2540-3300
CH_3COCH_3	Acetone	194-298	50-700	19	830-1950
		195-296	49-759	12	2615-3300
$CH_3C(O)OONO_2$	PAN	250-295	0	3	560-1400
		250	0	1	1590-2200
CH_3CHO	Acetaldehyde	200-297	50-762	16	2400-3400

CH$_3$CClF$_2$	HCFC-142b	223-283	0	7	650-1500
BrONO$_2$	Bromine nitrate	218-296	0	2	770-843
ClOOCl	Chlorine peroxide	225-250	15-33	4	500-835

Notes: These data are in the main directory. Additional redundant data for CFC-11, CFC-12, HFC-125, and HFC-143a are stored in a supplemental sub-directory. Rescaling of data for HCFC-141b for the 1325-1470 cm^{-1} region at 270 K has been performed as described in Section 3.8.

The cross section format remains the same as HITRAN 2008. Absorption cross sections are contained in files by molecule appended with the extension ".xsc", and named by the molecular formula followed by "_IRxx", where xx indicates the last two digits of the year in which the data were first introduced or updated. Files may contain many temperature–pressure sets over a number of spectral regions, as indicated by headers throughout the file. Headers provide the molecule name, the wavenumber range (cm^{-1}), the number of data points, the temperature (K) and pressure (Torr) of the laboratory measurement, the maximum value of the cross section (cm^2 molecule^{-1}), and the resolution (cm^{-1}) of the measurement. Absorption cross sections with negative values (generally occurring when there is measurement noise close to the baseline) are set to zero. For a number of datasets, the original experimental files are also provided with "_alt" appended to the filename.

There have been significant additions to the IR-absorption-cross-section section of HITRAN2008, in particular data for a number of important organic molecules are now included, largely from the work of Harrison et al. [292-299]. Updates to the database are indicated in the last ten entries to Table 17, and are described below.

3.1. C$_2$H$_6$

Ethane is the most abundant non-methane hydrocarbon in the atmosphere and a strong absorber in the troposphere. Its line parameters have been present in the HITRAN database for a number of years; however the line parameters in the 3-μm region (v_7 band) are incomplete, in

particular many P and R branch lines are absent. The ν_7 band has been identified as the most desirable for remote-sensing of ethane because it occurs in a reasonably uncongested spectral region and is associated with a C-H stretch vibrational mode (C-H stretches correspond to the most intense features in the IR spectra of aliphatic hydrocarbons). The ν_7 band is particularly accessible to remote-sensing instruments that measure atmospheric absorption using the sun as a light source. On the other hand, instruments detecting in the thermal infrared can only make use of the weaker ν_9 band (780-868 cm^{-1}).

Infrared absorption cross sections for ethane that cover the spectral range 2545 – 3315 cm^{-1} have been added to the database [292]. Spectra of ethane/dry synthetic air mixtures inside a 26-cm cell were recorded at a number of pressure–temperature combinations using a high-resolution FTIR spectrometer (Bruker IFS 125 HR) at 0.015 cm^{-1} resolution (calculated as the Bruker instrument resolution of 0.9/MOPD). These cross sections include the structure that is missing from the line list and provides a higher degree of accuracy for tropospheric sounding than can currently be obtained using a line-by-line calculation. These cross sections have been used to create a set of "pseudo-lines", effective spectral lines that empirically reproduce the pressure- and temperature-dependencies of spectral absorption without any recourse to quantum-mechanical assignments. They provide a convenient means of interpolating (and extrapolating) cross sections such that the derived absorption varies smoothly with temperature and pressure. The user will find these more useful for remote sensing purposes until the line list near 3 μm is greatly improved. Visit http://mark4sun.jpl.nasa.gov/pseudo.html to obtain the pseudo-line list.

3.2. CH$_3$OH

Methanol is the second most abundant organic molecule in the terrestrial atmosphere after methane. Around two-thirds of methanol emissions arise from plant growth, with the rest

coming from plant decay, atmospheric oxidation of methane and other hydrocarbons, biomass burning and biofuels, and vehicles and industrial activities.

Two new infrared absorption cross section datasets have been added to the database, covering the spectral ranges 877-1167 cm^{-1} and 2600-3250 cm^{-1} [298]. Spectra of methanol/dry synthetic air were recorded with a high-resolution FTIR spectrometer (Bruker IFS 125 HR) at 0.015 cm^{-1} resolution ($\equiv$0.9/MOPD) using a coolable White cell with a maximum pathlength of 19.32 m. Methanol data near 3.4 μm are included in HITRAN for the first time. Line parameters near 10 μm have been included in HITRAN since 2004; this band system is principally associated with the strong fundamental ν_8 mode at 1033 cm^{-1} (CO stretch). The new cross sections near 10 μm provide a higher level of accuracy at lower temperatures and reveal a number of problems with the line list, which was derived from a set of room-temperature spectra. When simulating spectra using the HITRAN line list, the integrated intensity of the band system drops by about one quarter from 300 to 200 K. This is at odds with the new 10 μm data, which provide no evidence for temperature dependence. Therefore, using the existing HITRAN line list for remote sensing will impact the accuracy of the retrievals. A methanol pseudo-line list near 10 μm, using the same procedure described above for ethane near 3 μm, is currently planned.

3.3. CH$_3$CN

Acetonitrile (CH$_3$CN) is a minor constituent of the Earth's atmosphere, with the majority of emissions arising from biomass burning. The lifetime of acetonitrile is of the order of 6 months, making this molecule a useful tracer for troposphere-stratosphere transport.

In addition to line parameters for the ν_4 band, HITRAN2008 contained a number of acetonitrile absorption cross sections between 624 and 4574 cm^{-1} recorded at a resolution of 0.112 cm^{-1} and a pressure of 760 Torr nitrogen at 276, 298, and 323 K. On their own, these are not useful for retrieving concentrations from spectra recorded in the upper troposphere/lower stratosphere (UTLS) because they do not cover the appropriate range of atmospheric temperatures and pressures. This problem has been remedied by the addition of a number of new pressure-temperature sets of infrared absorption cross sections to HITRAN. These datasets cover the spectral ranges 880 – 1700 cm^{-1} [297] and 2550 – 3300 cm^{-1} [296]. Spectra of acetonitrile/dry synthetic air were recorded by a high-resolution FTIR spectrometer (Bruker IFS 125 HR) at 0.015 cm^{-1} resolution ($\equiv$0.9/MOPD) using a coolable White cell with a maximum pathlength of 19.32 m. The cross sections in the MWIR region, in particular the $^r Q_0$ branch of the ν_6 band at 1462.96-1463.60 cm^{-1}, have recently been used as the basis for an ACE-FTS (Atmospheric Chemistry Experiment) acetonitrile research product [299].

3.4. $CH_3CH_2CH_3$

Propane is the second most abundant non-methane hydrocarbon in the atmosphere (after ethane). However, thus far there have been no global measurements using IR remote-sensing techniques. Infrared absorption cross sections for propane have been introduced for the first time into HITRAN; they cover the spectral range 2540 – 3300 cm^{-1} [293], where propane has its strongest-intensity vibrational modes (C-H stretch). Spectra of propane/dry synthetic air mixtures inside a 26-cm cell were recorded at twelve pressure–temperature combinations using a high-resolution FTIR spectrometer (Bruker IFS 125 HR) at 0.015 cm^{-1} resolution ($\equiv$0.9/MOPD).

3.5. CH_3COCH_3

Infrared absorption cross sections for propanone (acetone) have been introduced for the first time into HITRAN. Acetone is the simplest member of the ketone family, and one of the most abundant volatile organic compounds (VOCs) in the free troposphere. The largest source of atmospheric acetone is the oxidation of organic precursors, e.g. alkanes. Other sources include biomass burning and biogenic emissions, including plant growth and decay, and a minor contribution from anthropogenic emissions.

Two new datasets have been added to the database, covering the spectral ranges $830 - 1950$ cm^{-1} [295] and $2615 - 3300$ cm^{-1}; the mid-IR cross sections have been combined with older measurements taken by Waterfall [300] to create a combined dataset. For the new measurements, spectra of acetone/dry synthetic air were recorded by a high-resolution FTIR spectrometer (Bruker IFS 125 HR) at 0.015 cm^{-1} resolution ($\equiv 0.9$/MOPD) using a coolable White cell with a maximum path length of 19.32 m. These mid-IR data have been used, for example, to retrieve acetone concentrations from spectra recorded by the MIPAS (Michelson Interferometer for Passive Atmospheric Sounding) instrument onboard Envisat [301]. Additionally, an ACE research product has recently been developed [302].

3.6. $CH_3C(O)OONO_2$

Infrared absorption data at 295 K for peroxyacetyl nitrate (abbreviated as PAN) became available in HITRAN2008. PAN, a reservoir for reactive NO_x, has a number of sources, including photochemical smog and biomass burning. Due to thermal stability of PAN at lower temperatures, it can be transported over long distances in the middle and upper troposphere; the consequence of this is the long-distance transport of pollution.

Additional infrared absorption cross sections for PAN ($560 - 1400$ cm^{-1}) have been included in HITRAN. The original data [303, 304] have been adapted to correct the baselines so that they

agree better with each other and the intensities have been normalized to the room temperature value [305]; the data in HITRAN (at 250, 273 and 295 K), therefore, differ slightly from those in the original references. PAN cross sections are also available over the range $1590 - 2200$ cm^{-1} at 250 K and $1650 - 1900$ cm^{-1} at 295K. The user should use these two cross sections with care due to an obvious discrepancy in the baseline between the two measurements.

3.7. CH$_3$CHO

Ethanal, also known as acetaldehyde, is a trace molecular species found in the terretrial atmosphere. Sources include photochemical production, the oxidation of hydrocarbons, biogenic emission from plant decay, anthropogenic combustion and biomass burning. So far there have been no measurements using IR remote-sensing techniques. Infrared absorption cross sections for acetaldehyde in the 3μm region [306] have been introduced for the first time into HITRAN. The spectra were recorded at a number of temperatures and pressures appropriate for atmospheric conditions.

3.8. HCFC-141b

HITRAN infrared cross-sections for the hydrochlorofluorocarbon HCFC-141b (1,1-Dichloro-1-fluoroethane) originate from Clerbaux et al. [307]. It was found recently that the set of cross-sections in the 1325-1470 cm^{-1} region at 270 K differed from the ones in the original publication. The reason for this discrepancy is unclear. The HITRAN cross-sections in this pressure-temperature set have now been multiplied by 1.75 to bring them into consistency with the original publication.

3.9. HCFC-142b

New temperature-dependent absorption cross-sections of HCFC-142b (1-Chloro-1,1-difluoroethane) have been added to the HITRAN compilation. The data cover the 650-1500 cm^{-1} spectral region, and come from the work of Le Bris and Strong [308]. These data replace the sets of HCFC-142b IR cross-sections that previously existed in HITRAN.

3.10. $BrONO_2$

IR absorption cross sections for bromine nitrate were recently introduced into HITRAN. $BrONO_2$ is an important species in stratospheric bromine chemistry and is part of the photochemistry in stratospheric ozone depletion. It is the most important reservoir species for inorganic stratospheric bromine.

The cross-sections are given at 218K and 296K. The latter set is based on laboratory measurements, whereas the set for 218K was obtained by scaling the 296 K experimental data. The values are explained in more detail in the paper about the atmospheric detection of $BrONO_2$ by the MIPAS instrument [309].

3.11. ClOOCl

Chlorine peroxide (ClOOCl) is known to play an important role in the antarctic and arctic perturbed chemistry leading to the well-known ozone hole [310]. The first proof that ClOOCl, being a product of the ClO self reaction, has a peroxide like structure which is the only Cl_2O_2 isomer capable of destroying ozone in a catalytic cycle was shown by Birk et al. [311]. The first direct observation of this species by balloon-borne mid-infrared limb sounding in the arctic [312] is based on the absorption cross sections now entered into the HITRAN data base. This latter paper also contains details about the laboratory measurements of the absorption cross-sections.

The agreement of the total chlorine budget using these absorption cross-sections with the total inorganic chlorine load of the atmosphere indicates the validity of the data.

Four sets of absorption cross sections are given for combinations of temperatures 213 K and 243 K and total pressures 20 hPa and 40 hPa in the mixture of nitrogen and helium. The total uncertainty of the absorption cross sections is 12%. Figure 10 shows the absorption cross sections for 213 K and 20 hPa. There are three bands visible. So far the weakest band in the range 720-790 cm^{-1} was used for retrieval. The middle band is blended by CO_2 and cannot be used for atmospheric measurements. In the absorption cross sections, this band is contaminated by CO_2 arising from the technical chlorine used in the synthesis. Best suited for atmospheric measurements would be the band between 500 and 600 cm^{-1} since this band is three times stronger than the band at 720-790 cm^{-1}. So far no limb sounder is available covering this region.
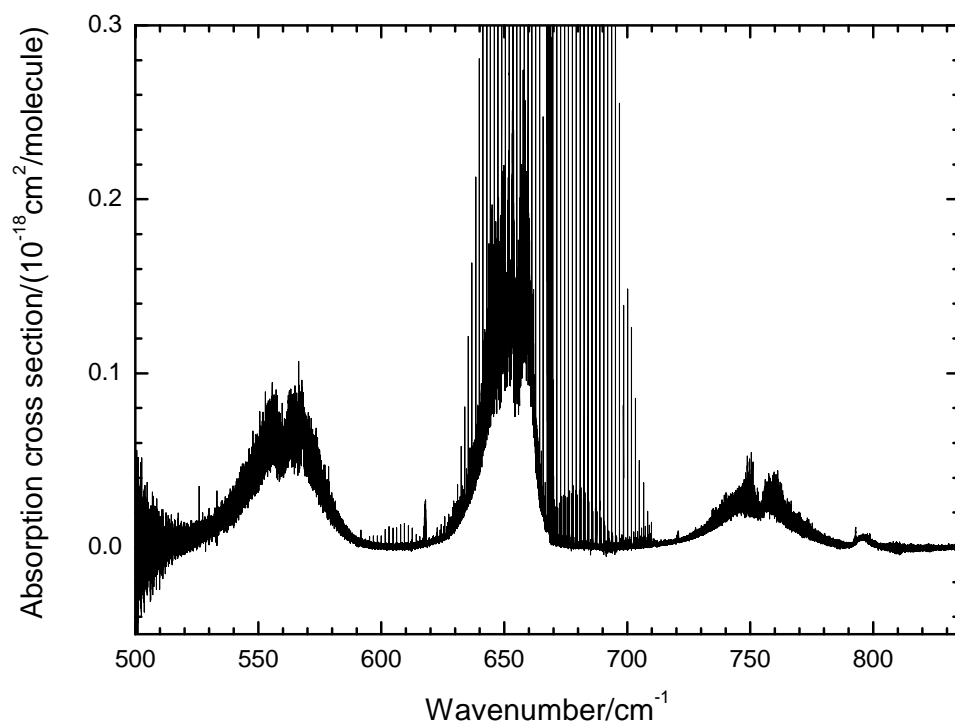
Approximate location of Fig. 10

Figure 10. Absorption cross sections of ClOOCl at 213 K and 20 hPa.

4. Ultraviolet data sets

4.1. H₂CO

A study of the previous ultraviolet absorption cross sections for formaldehyde in HITRAN was carried out as recommended by the HITRAN Advisory Committee. The cross sections introduced into the new edition of HITRAN have been derived from two existing sets, one using a Fourier transform spectrometer, and one using a grating instrument. The new re-scaled data are based on the work of Chance and Orphal [313].

5. Aerosol refractive indices

Aerosols and clouds influence radiative transfer in the terrestrial atmosphere [314], participate in chemistry reactions in both the liquid and solid phases [310], and complicate remote-sensing retrievals of gaseous species. Light scattering and absorption by aerosols and clouds is dependent upon how particle size distributions are distributed in a three-dimensional manner, the compositions (i.e. refractive indices) of the aerosols and cloud particles, and by the shapes of the particles. HITRAN2012 contains refractive indices in the visible, infrared, and millimeter spectral ranges of many of the materials which comprise the compositions of aerosols and clouds. Table 18 lists the HITRAN2012 indices.

Approximate location of Table 5.1

Table 18. Refractive indices included in HITRAN 2012.

Compound	Measurement Specifics	Reference
Water	27°C, 10–5000 cm^{-1}	[315]
Water	0.67–2.5 μm	[316]
Ice	266 K, 0.04 μm – 2 m	[316]
Ice	0.67–2.5 μm	[317]
Water, ice, sodium chloride, sea salt, water soluble aerosol, ammonium sulfate,	Room temperature, 0.2–40 μm	[318]

carbonaceous aerosol, volcanic dust, sulfuric acid, meteoric dust, quartz, hematite, sand

Sulfuric acid (H_2SO_4/H_2O)	Room temperature, 25–96% H_2SO_4	[319]
Sulfuric acid (H_2SO_4/H_2O)	Room temperature, 75 and 90% H_2SO_4	[320]
Sulfuric acid (H_2SO_4/H_2O)	215 K, 499–6996 cm^{-1}	[321]
Sulfuric acid (H_2SO_4/H_2O)	200–300 K, 825–4700 cm^{-1}	[322]
Sulfuric acid (H_2SO_4/H_2O)	213–293 K, 432–5028 cm^{-1}	[323]
Nitric acid (H_2SO_4/HNO_3)	Room temperature, 250–2987 cm^{-1}	[324]
Nitric acid (H_2SO_4/HNO_3)	220 K, 754–4700 cm^{-1}	[325]
Nitric acid (H_2SO_4/HNO_3)	213–293 K, 432–5028 cm^{-1}	[323]
Amorphous nitric acid (NAM, NAD, NAT)	153 K, 482–7000 cm^{-1}	[326]
NAM	179 K, 482–6002 cm^{-1}	[326]
NAD	184 K, 482–6981 cm^{-1}	[326]
NAD	160–190 K, 700–4700 cm^{-1}	[327]
αNAT	181 K, 482–6989 cm^{-1}	[326]
βNAT	196 K, 482–6364 cm^{-1}	[326]
NAT	160 K, 711–4004 cm^{-1}	[328]
Burning vegetation	525–5000 cm^{-1}	[329]
Burning vegetation	0.35 – 1.5 μm	[330]
Carbon flame	0.4 – 0.7 μm, 25 – 600° C	[331]
Flame soot	0.2 – 38 μm	[332]
Brown carbon	0.2 – 1.2 μm	[333]
Organic acids (Oxalic, malonic, succinic, pinonic, pyruvic, phthalic)	0.25 – 1.1 μm	[334]
Organic haze	0.525 nm	[335]
SOA (proxy)	0.525 nm	[336]
Minerals (clay, illite, kaolin, montmorillonite)	2.5 – 200 μm	[337]
Minerals (granite, montmorillonite)	5 – 40 μm	[338]
Saharan dust	0.30 – 0.95 μm	[339]
Saharan dust	0.35 – 0.65 μm	[340]
Volcanic ash	0.45 – 25 μm	[341]

Additions to HITRAN2012 focus upon absorptive aerosol species. Absorptive aerosol is of interest since it can perturb the radiation field close to the Earth's surface, thereby perturbing the temperature profile structure and convective processes [342]. The dimensionless complex refractive index

$$m = m_{real} + \mathrm{i}\, m_{imag} \qquad (7)$$

has positive real m_{real} and imaginary m_{imag} components. A plane light wave of wavelength λ is attenuated along the propagation x axis according to

$$E = E_0 \exp(-2\pi m_{imag}\mathrm{x}/\lambda)\, \exp(\mathrm{i}2\pi m_{real}\mathrm{x}/\lambda - \mathrm{i}2\pi ct/\lambda) \qquad (8)$$

with time t and the speed of light c. Thus, it is the imaginary refractive index which determines the amount of light absorption in a medium.

New HITRAN indices include secondary organic acid (proxy) [336], carbonaceous indices [331, 332] mineralogical indices, Saharan dust (as a function of hematite content) [339], brown carbon [333], volcanic ash indices [341], and vegetation-fire indices derived from field measurements [330]. Organic acids, which scatter primarily and are precursors to secondary organic aerosols, are also tabulated [333].

HITRAN2012 contains indices based upon field measurements of aerosols in their natural setting in addition to laboratory measurements. Since the composition of aerosol is chemically very diverse and evolves daily, it is useful to include field measurements of aerosol refractive indices in HITRAN. Figure 11 illustrates this point by presenting the composite AFCRL carbonaceous aerosol indices [318], Sutherland-Khana burning vegetation indices [329], and the Magi indices of biomass fires inferred from aircraft measurements during the SAFARI 2000 field experiment [330]. Since the imaginary refractive index is responsible for light absorption,

90

differences in the imaginary index of various materials are of primary interest. The range in the

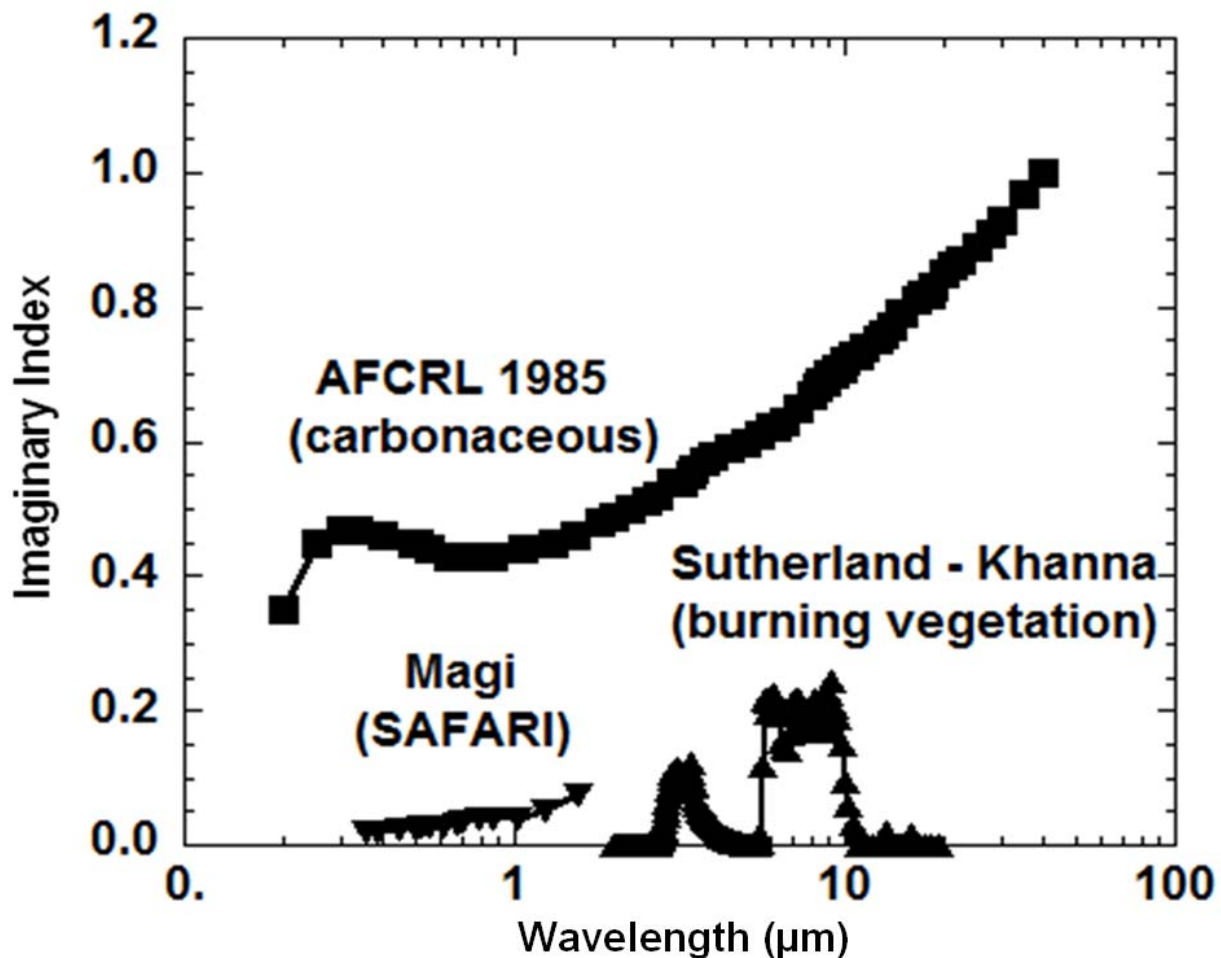imaginary indices in Fig. 11 – a factor of 10 – is considerable.

Figure 11. Imaginary indices of three carbon containing materials that illustrate the wide range of absorptive characteristics of naturally occurring combustion products.

A new development for HITRAN2012 is the introduction of the HITRAN-RI program [343]

that will reside on the HITRAN website. This program, written in the IDL (Interactive Design

Language) and Fortran 90 programming languages, allows the user to access and use the

HITRAN2012 indices in Mie calculations. Output ASCII files of the indices, particle size

distributions, and spectra (extinction, scattering, absorption, single scattering albedo,

backscattering, and asymmetry parameters) are created by the program. The IDL version of the program also produces output Postscript graphics files. The user specifies the size distribution and the indices of the particles by editing a simple ASCII input file. The wavelength dependence of the refractive indices of two data sets can be compared to each other. The user can obtain composite indices of multiple-component aerosols by applying one of several available mixing rules. There are test cases which serve an instructional purpose for those not familiar with Mie calculations. Subdirectories associated with HITRAN-RI contain pdfs of the reference papers, and the indices are specified in both ASCII and netCDF formats. The ASCII files are useful to quickly obtain the real and imaginary indices at a specific wavelength, while the netCDF files are used by the HITRAN – RI program in user friendly calculations.

6. Collision-Induced Absorption

Collision-induced absorption (CIA) is caused by a transient dipole moment being created during collisions of molecules. The absorption features underlie many of the traditional electric dipole, magnetic dipole, and quadrupole transitions that have been the traditional mainstay of HITRAN. They not only are valuable for radiative-transfer calculations for the terrestrial atmosphere, but are applicable to simulations of radiance in planetary and stellar atmospheres. Experimental and theoretical sources have now been assembled and cast into a consistent format of cross-sections for this new edition of HITRAN. The details of the sets of collision pairs, their spectral and temperature ranges, and their sources are described in Ref. [344].

In this first presentation of CIA in the HITRAN compilation, fourteen different collisional pairs are given, N_2-N_2, N_2-H_2, N_2-CH_4, H_2-H_2, H_2-He, H_2-CH_4, H_2-H, He-H, O_2-O_2, O_2-N_2, O_2-CO_2, CO_2-CO_2, CH_4-CH_4, and CH_4-Ar. In the future, other complexes of interest will be

included, improved data will replace less accurate data, and the CIA datasets will be extended to cover other spectral regions and temperature domains when possible.

7. Global data and software

7.1. Options for accessing, filtering, and managing HITRAN data

The Java-based JavaHawks software that accompanied previous editions of HITRAN is no longer maintained and, although one can still use it for most of the molecules, it will not be able to handle new molecules or new isotopologues that have been recently introduced. It will also fail to select vibrational bands which were introduced into HITRAN after the year 2004.

HITRAN on the Web (hitran.iao.ru) is an efficient online HITRAN browsing and plotting tool developed at the Institute of Atmospheric Optics in Tomsk, Russia and the Harvard-Smithsonian Center for Astrophysics taking advantage of the S&MPO ozone database software [76] and adapted functionalities of the JavaHawks software. Inside HITRAN on the web, the HITRAN data are treated as a relational database under control of the MySQL database management system. The site software is written in the PHP language using the Zend Framework. The modules for spectra simulations are written on C. Application software was developed using the Model-View-Controller (MVC) approach. Within MVC, the data model of an application, the user interface, and the operating logic are considered as separate components, so that updating of one of the components has minimum influence on others.

The HITRAN on the Web browsing tool allows selections and manipulations with HITRAN data that are most desired by the users of the database. The "HITRAN survey" option allows selecting lines of chosen molecules within a desired spectral range. A more sophisticated interactive system is provided in the individual "Molecules" section. In particular, it allows for

the selection of multiple spectral bands and their plotting in different colors, predicting spectra at different temperatures, and implementation of user-selected isotopic abundances. Other important features include: 1) easy access to the abstracts of publications used as sources of data for the spectroscopic parameters and absorption cross-sections in HITRAN; 2) selection of data based on the uncertainty index; 3) advanced plotting options that are also applicable to the cross-sections (see Figure 12, for example) that is generated using this online tool); 4) convenient presentation of relative band intensities and spectral range they cover and many other important features. One of the presentations, describing the use of the database, is given as supplementary material to this paper.
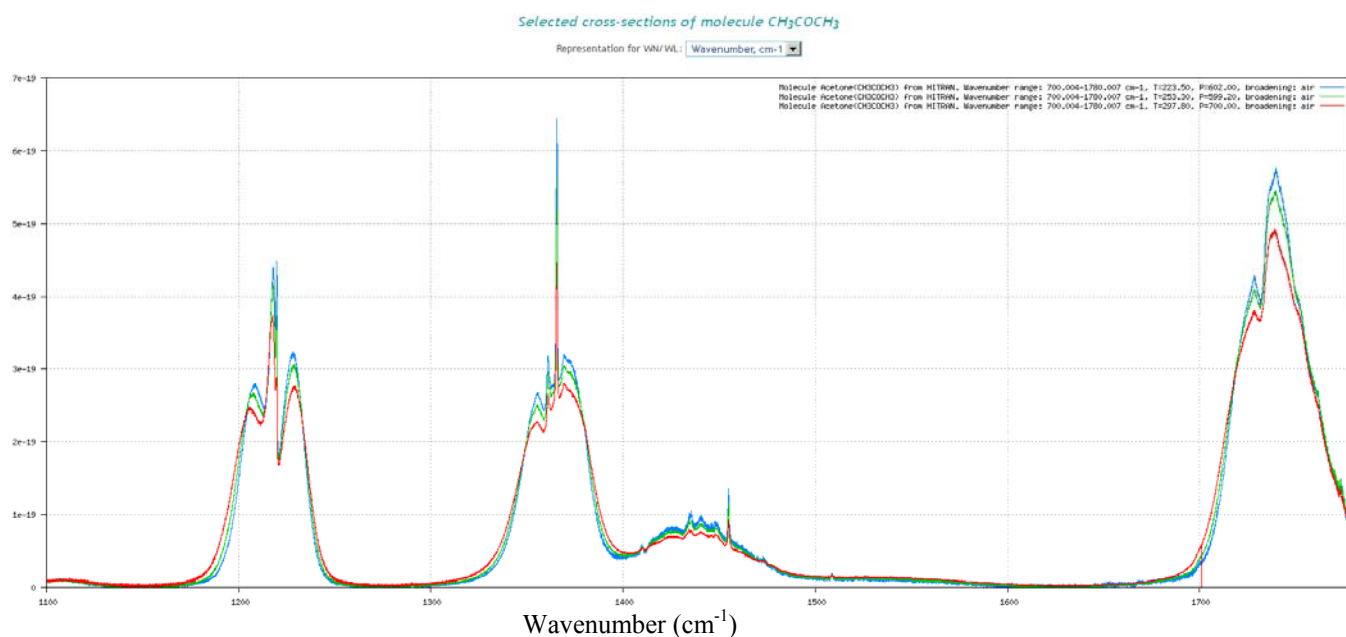
Approximate location of Figure 12

Figure 12. HITRAN on the web plot of selected cross-sections of acetone (CH_3COCH_3). Y axis in absorption (cm^2 $molecule^{-1}$).

Another development for accessing the HITRAN database is the development of a user interface based on the relational database discussed in the next section.

7.2. Database structures

Under the auspices of the Virtual Atomic and Molecular Data Centre (VAMDC) project [345], an initiative was created to cast the HITRAN database into a relational database structure that would be interoperable with other major databases in the fields of atomic, molecular, and plasma physics. This structure has many advantages over the fixed-field, text-based format that has existed since the inception of HITRAN four decades ago. First of all it addresses some of the deficiencies encountered by the old structure, including (1) the limited ability to expand the fields to account for the quantum identification of complex states, for example polyatomic molecules with many vibrational modes, dynamic molecules with torsional modes, hyperfine coupling to more than one nucleus; (2) the limited ability to expand the line shape parameters, including line broadening by other collisional partners, their temperature dependences, line-shape formalisms other than Voigt profile, line mixing, etc.; (3) the inconvenient methods of flagging unavailable data (for example setting the lower-state energy to negative unity to flag an unassigned transition); and (4) the restriction of field length that prevents accomodating parameters with a greater number of significant figures. The advantages of a relational database for HITRAN are myriad. It is easy to extend. More complex molecular states can be represented with as many quantum numbers as necessary. Parameters for alternative line shapes (for example Galatry) can easily be implemented. Additional broadeners, now needed for planetary atmospheres, can be efficiently added. Field size is not an issue, so all significant digits of a parameter can be stored.

Other advantages of the relational database for HITRAN include the ability to simply establish a data provenance, that is, each parameter can be given a time stamp; it is not removed when replaced by newer data and can easily be reproduced at a later time if necessary. The database allows for a structured query language which greatly facilitates validation and data

mining for semantic information. References to sources of data, which have previously been stored in a separate file, are now part of the database and easily accessed (this is similar to the feature available in the HITRAN on the Web system discussed in Section 7.1).

Under continued development, the new database structure has the ability to filter and return HITRAN data in different output formats, including the older ones familiar to many users. Details of this endeavor can be found in Hill et al. [346].

7.3. Global data

Certain data that are general in scope to HITRAN appear in a separate folder of the compilation that we call Global Data. These data are necessary information including: (1) the isotopic abundance values chosen for the HITRAN intensities (required by the user to normalize their values); and (2) the partition sums of the isotopologues as used by HITRAN. Table 19 is the table of chosen molecular quantities provided with the HITRAN compilation.

Approximate location of Table 19

Table 19. Values of isotopic abundance chosen for isotopologues in HITRAN.

Molecule	Isotopo-logue	Abundance	Q(296K)	g_j	Mass (g)
(1) H_2O	161	9.973×10^{-1}	1.74×10^2	1	18.01056
	181	1.999×10^{-3}	1.75×10^2	1	20.01481
	171	3.719×10^{-4}	1.04×10^3	6	19.01478
	162	3.107×10^{-4}	8.59×10^2	6	19.01674
	182	6.230×10^{-7}	8.75×10^2	6	21.02098
	172	1.158×10^{-7}	5.22×10^3	36	20.02096
(2) CO_2	626	9.842×10^{-1}	2.87×10^2	1	43.98983
	636	1.106×10^{-2}	5.78×10^2	2	44.99319
	628	3.947×10^{-3}	6.09×10^2	1	45.99408
	627	7.340×10^{-4}	3.55×10^3	6	44.99405
	638	4.434×10^{-5}	1.23×10^3	2	46.99743
	637	8.246×10^{-6}	7.16×10^3	12	45.99740
	828	3.957×10^{-6}	3.24×10^2	1	47.99832
	728	1.472×10^{-6}	3.78×10^3	6	46.99829

	838	4.446×10^{-8}	6.54×10^2	2	49.00168
	837	1.654×10^{-8}	7.42×10^3	12	48.00165
	666	9.929×10^{-1}	3.48×10^3	1	47.98475
	668	3.982×10^{-3}	7.47×10^3	1	49.98899
(3) O_3	686	1.991×10^{-3}	3.65×10^3	1	49.98899
	667	7.405×10^{-4}	4.33×10^4	6	48.98896
	676	3.702×10^{-4}	2.14×10^4	6	48.98896
	446	9.903×10^{-1}	5.00×10^3	9	44.00106
	456	3.641×10^{-3}	3.36×10^3	6	44.9981
(4) N_2O	546	3.641×10^{-3}	3.46×10^3	6	44.9981
	448	1.986×10^{-3}	5.31×10^3	9	46.00531
	447	3.693×10^{-4}	3.10×10^4	54	45.00528
	26	9.865×10^{-1}	1.07×10^2	1	27.99492
	36	1.108×10^{-2}	2.24×10^2	2	28.99827
(5) CO	28	1.978×10^{-3}	1.12×10^2	1	29.99916
	27	3.679×10^{-4}	6.59×10^2	6	28.99913
	38	2.223×10^{-5}	2.36×10^2	2	31.00252
	37	4.133×10^{-6}	1.38×10^3	12	30.00249
	211	9.883×10^{-1}	5.90×10^2	1	16.0313
	311	1.110×10^{-2}	1.18×10^3	2	17.03466
(6) CH_4	212	6.158×10^{-4}	4.78×10^3	3	17.03748
	312	6.918×10^{-6}	1.60×10^3	6	18.04083
	66	9.953×10^{-1}	2.16×10^2	1	31.98983
(7) O_2	68	3.991×10^{-3}	4.52×10^2	1	33.99408
	67	7.422×10^{-4}	2.64×10^3	6	32.99405
	46	9.940×10^{-1}	1.14×10^3	3	29.99799
(8) NO	56	3.654×10^{-3}	7.89×10^2	2	30.99502
	48	1.993×10^{-3}	1.20×10^3	3	32.00223
(9) SO_2	626	9.457×10^{-1}	6.34×10^3	1	63.9619
	646	4.195×10^{-2}	6.37×10^3	1	65.9577
(10) NO_2	646	9.916×10^{-1}	1.36×10^4	3	45.9929
(11) NH_3	4111	9.959×10^{-1}	1.73×10^3	3	17.02655
	5111	3.661×10^{-3}	1.15×10^3	2	18.02358
(12) HNO_3	146	9.891×10^{-1}	2.14×10^5	6	62.99564
	156	$3.636\times10{-3}$	3.55×104	4	63.99268
(13) OH	61	9.975×10^{-1}	8.04×10^1	2	17.00274
	81	2.000×10^{-3}	8.09×10^1	2	19.00699

	62	1.554×10^{-4}	2.09×10^{2}	3	18.00892
(14) HF	19	9.998×10^{-1}	4.15×10^{1}	4	20.00623
	29	1.557×10^{-4}	1.16×10^{2}	6	21.0124
(15) HCl	15	7.576×10^{-1}	1.61×10^{2}	8	35.97668
	17	2.423×10^{-1}	1.61×10^{2}	8	37.97373
	25	1.180×10^{-4}	4.63×10^{2}	12	36.98285
	27	3.774×10^{-5}	4.64×10^{2}	12	38.9799
(16) HBr	19	5.068×10^{-1}	2.00×10^{2}	8	79.92616
	11	4.931×10^{-1}	2.00×10^{2}	8	81.92412
	29	7.894×10^{-5}	5.86×10^{2}	12	80.93234
	21	7.680×10^{-5}	5.87×10^{2}	12	82.93029
(17) HI	17	$9.998\times10\text{-}1$	3.90×10^{2}	12	127.9123
	27	1.557×10^{-4}	1.15×10^{3}	18	128.9185
(18) ClO	56	7.559×10^{-1}	3.27×10^{3}	4	50.96377
	76	2.417×10^{-1}	3.33×10^{3}	4	52.96082
(19) OCS	622	9.374×10^{-1}	1.22×10^{3}	1	59.96699
	624	4.158×10^{-2}	1.25×10^{3}	1	61.96278
	632	1.053×10^{-2}	2.48×10^{3}	2	60.97034
	623	7.399×10^{-3}	4.95×10^{3}	4	60.96637
	822	1.880×10^{-3}	1.31×10^{3}	1	61.97123
(20) H_2CO	126	9.862×10^{-1}	2.85×10^{3}	1	30.01057
	136	1.108×10^{-2}	5.84×10^{3}	2	31.01392
	128	1.978×10^{-3}	2.99×10^{3}	1	32.01481
(21) HOCl	165	7.558×10^{-1}	1.93×10^{4}	8	51.97159
	167	2.417×10^{-1}	1.96×10^{4}	8	53.96864
(22) N_2	44	9.927×10^{-1}	4.66×10^{2}	1	28.00615
(23) HCN	124	9.851×10^{-1}	8.95×10^{2}	6	27.0109
	134	1.107×10^{-2}	1.84×10^{3}	12	28.01425
	125	3.622×10^{-3}	6.21×10^{2}	4	28.00793
(24) CH_3Cl	215	7.489×10^{-1}	1.16×10^{5}	4	49.99233
	217	2.395×10^{-1}	1.18×10^{5}	4	51.98938
(25) H_2O_2	1661	9.950×10^{-1}	9.82×10^{3}	1	34.00548
(26) C_2H_2	1221	9.776×10^{-1}	4.14×10^{2}	1	26.01565
	1231	2.197×10^{-2}	1.66×10^{3}	8	27.01901
	1222	3.046×10^{-4}	1.58×10^{3}	6	27.02183
(27) C_2H_6	1221	9.770×10^{-1}	7.09×10^{4}	1	30.04695

	1231	2.195×10^{-2}	8.00×10^{4}	2	31.05031
(28) PH_3	1111	9.995×10^{-1}	3.25×10^{3}	2	33.99724
(29) COF_2	269	9.865×10^{-1}	7.00×10^{4}	1	65.99172
	369	1.108×10^{-2}	3.78×10^{4}	2	66.99508
(30) SF_6	29	9.502×10^{-1}	1.62×10^{6}	1	145.9625
	121	9.499×10^{-1}	5.03×10^{2}	1	33.98772
(31) H_2S	141	4.214×10^{-2}	5.04×10^{2}	1	35.98352
	131	7.498×10^{-3}	2.01×10^{3}	4	34.98711
(32) HCOOH	126	9.839×10^{-1}	3.91×10^{4}	4	46.00548
(33) HO_2	166	9.951×10^{-1}	4.30×10^{3}	2	32.99766
(34) O	6	9.976×10^{-1}	6.72	1	15.99492
(35) $ClONO_2$	5646	7.496×10^{-1}	4.79×10^{6}	12	96.95667
	7646	2.397×10^{-1}	4.91×10^{6}	12	98.95372
(36) NO^+	46	9.940×10^{-1}	3.12×10^{2}	3	29.99799
(37) HOBr	169	5.056×10^{-1}	2.83×10^{4}	8	95.92108
	161	4.919×10^{-1}	2.82×10^{4}	8	97.91903
(38) C_2H_4	221	9.773×10^{-1}	1.10×10^{4}	1	28.0313
	231	2.196×10^{-2}	4.52×10^{4}	2	29.03466
(39) CH_3OH	2161	9.859×10^{-1}	3.53×10^{4}	2	32.02622
(40) CH_3Br	219	5.010×10^{-1}	2.08×10^{4}	4	93.94181
	211	4.874×10^{-1}	2.08×10^{4}	4	95.93976
(41) CH_3CN	2124	9.739×10^{-1}	8.87×10^{4}	3	41.02655
(42) CF_4	29	9.889×10^{-1}	1.21×10^{5}	1	87.99362
(43) C_4H_2	21	9.560×10^{-1}	9.83×10^{3}	6	50.01090
(44) HC_3N	1224	9.633×10^{-1}	5.14×10^{4}	6	51.0109
(45) H_2	11	9.997×10^{-1}	7.67×10^{0}	1	2.01565
	12	1.557×10^{-4}	3.00×10^{1}	6	3.02182
(46) CS	22	9.396×10^{-1}	2.57×10^{2}	1	43.97104
	24	4.168×10^{-2}	2.61×10^{2}	1	45.96679
	32	1.056×10^{-2}	5.43×10^{2}	2	44.97437
	23	7.417×10^{-3}	1.03×10^{3}	4	44.97040
(46) SO_3	26	9.434×10^{-1}	7.96×10^{3}	1	79.95682

Besides giving the value of the partition sum at the HITRAN standard temperature of 296K, a program is provided with the compilation to compute the partition sum of the isotopologues at temperatures from 70 to 3000K. Note that the definitions of partition sum in HITRAN is very general and includes state-independent statistical weights. Thus the values themselves may appear rather large; however, the partition sums usually appear as ratios, so extra factors in the definitions cancel out. Descriptions of the methodology for deriving the HITRAN partition sums can be found in Refs. [347, 348].

7. Conclusions

The improvements to a new HITRAN database release have been elaborated upon. The new edition has incorporated improved line position, intensity, and line-shape parameters for many of the previously existing molecules and isotopologues. Several new molecules and isotopologues have been added to the compilation, with special consideration for applications beyond those associated with the terrestrial atmosphere.

Applications over the past few years, especially high-resolution, high signal-to-noise satellite remote-sensing missions, have put new demands on the standard database. Thus one can see in this new edition of HITRAN a concentrated effort to not only provide more accurate data, but to expand the database to include more vibration-rotation bands, weaker transitions, and refined line-shape parameters and formalisms. The compilation also includes for the first time sets of collision-induced absorption data.

HITRAN is also evolving in terms of structure. A new relational database structure has been established that allows for many expansions that would be prohibitive in the old fixed-length ASCII format of previous HITRAN editions. Interfaces on the internet have also been

established that provide the diverse group of HITRAN users with much power to filter, extract, plot, and query the database.

The compilation is free; access instructions can be obtained at http://www.cfa.harvard.edu/HITRAN.

Acknowledgments

References

[1]   Rothman LS, Gordon IE, Barbe A, Benner DC, Bernath PF, Birk M, et al. The HITRAN 2008 molecular spectroscopic database. JQSRT 2009;110:533-72.

[2]   Rothman LS, Jacquemart D, Barbe A, Chris Benner D, Birk M, Brown LR, et al. The HITRAN 2004 molecular spectroscopic database. JQSRT 2005;96:139-204.

[3]   Simecková M, Jacquemart D, Rothman LS, Gamache RR, Goldman A. Einstein *A*-coefficients and statistical weights for molecular absorption transitions in the *HITRAN* database. JQSRT 2006;98:130-55.

[4]   Oudot C, Wang L, Thomas X, Von der Heyden P, Daumont L, Régalia L. Intensity measurements of $H_2^{16}O$ lines in the spectral region 8000-9350 cm^{-1}. J Mol Spectrosc 2010;262:22-9.

[5]   Lodi L, Tennyson J, Polyansky OL. A global, high accuracy ab initio dipole moment surface for the electronic ground state of the water molecule. J Chem Phys 2011;135:034113-10.

[6]   Shillings AJL, Ball SM, Barber MJ, Tennyson J, Jones RL. An upper limit for water dimer absorption in the 750 nm spectral region and a revised water line list. Atmos Chem Phys 2011;11:4273-87.

[7]   Tallis L, Coleman M, Gardiner T, Ptashnik IV, Shine KP. Assessment of the consistency of H_2O line intensities over the near-infrared using sun-pointing ground-based Fourier transform spectroscopy. JQSRT 2011;112:2268-80.

[8]   Coudert LH, Wagner G, Birk M, Baranov YI, Lafferty WJ, Flaud J-M. The $H_2^{16}O$ molecule: Line position and line intensity analyses up to the second triad. J Mol Spectrosc 2008;251:339-57.

[9]   Ptashnik IV, Smith KM. Water vapour line intensities and self-broadening coefficients in the 5000-5600 cm^{-1} spectral region. JQSRT 2010;111:1317-27.

[10]   Jenouvrier A, Daumont L, Régalia-Jarlot L, Tyuterev VG, Carleer M, Vandaele AC, et al. Fourier transform measurements of water vapor line parameters in the 4200-6600 cm^{-1} region. JQSRT 2007;105:326-55.

[11]   Toth RA Linelists of water vapor parameters from 500 to 8000 cm^{-1}. http://mark4sun.jpl.nasa.gov/data/spec/

[12]   Wunch D, Toon GC, Blavier J-FL, Washenfelder RA, Notholt J, Connor BJ, et al. The Total Carbon Column Observing Network. Philosophical Transactions of the Royal Society A: Mathematical, Physical and Engineering Sciences 2011;369:2087-112.

[13]   Gordon IE, Rothman LS, Gamache RR, Jacquemart D, Boone C, Bernath PF, et al. Current updates of the water-vapor line list in HITRAN: A new "diet" for air-broadened half-widths. JQSRT 2007;108:389-402.

[14]   Gamache RR, Laraia AL. N_2-, O_2-, and air-broadened half-widths, their temperature dependence, and line shifts for the rotation band of $H_2^{16}O$. J Mol Spectrosc 2009;257:116-27.

[15]   Gamache RR. Lineshape parameters for water vapor in the 3.2-17.76 μm region for atmospheric applications. J Mol Spectrosc 2005;229:9-18.

[16]   Jacquemart D, Gamache R, Rothman LS. Semi-empirical calculation of air-broadened half-widths and air pressure-induced frequency shifts of water-vapor absorption lines. JQSRT 2005;96:205-39.

[17]   Ma Q, Tipping RH, Gamache RR. Uncertainties associated with theoretically calculated N_2-broadened half-widths of H_2O lines. Mol Phys 2010;108:2225-52.

[18]   Birk M, Wagner G. Temperature-dependent air broadening of water in the 1250-1750 cm$^-$^{1} range. J Quant Spectrosc Radiat Tansfer 2012;113:889-928.
[19]   Rothman LS, Gordon IE, Barber RJ, Dothe H, Gamache RR, Goldman A, et al. HITEMP, the high-temperature molecular spectroscopic database. JQSRT 2010;111:2139-50.
[20]   Barber RJ, Tennyson J, Harris GJ, Tolchenov RN. A high-accuracy computed water line list. Mon Not Astr R Soc 2006;368:1087-94.
[21]   Tennyson J, Bernath PF, Brown LR, Campargue A, Császár AG, Daumont L, et al. IUPAC critical evaluation of the rotational-vibrational spectra of water vapor, Part III: Energy levels and transition wavenumbers for $H_2^{16}O$. JQSRT 2013;117:29-58.
[22]   Furtenbacher T, Császár AG, Tennyson J. MARVEL: measured active rotational-vibrational energy levels. J Mol Spectrosc 2007;245:115-25.
[23]   Furtenbacher T, Császár AG. MARVEL: Measured active rotational-vibrational energy levels. II. Algorithmic improvements. JQSRT 2012;113:929-35.
[24]   Martin MA, Coudert L, Pirali O, Balcon O. Intensities of water vapor transitions in 0-6000 cm^{-1} region. J Chem Phys 2013;in preparation.
[25]   Gordon IE, Rothman LS, Lodi L, Tennyson J, Toon GC, Brown LR, in: *67th International Symposium on Molecular Spectroscopy*, Columbus, OH, USA, 2012.
[26]   Wagner G, Birk M. Water line intensities in the 1µm region. JQSRT 2013;in preparation.
[27]   Lisak D, Hodges JT. Low-uncertainty H_2O line intensities for the 930-nm region. J Mol Spectrosc 2008;249:6-13.
[28]   Lodi L, Tennyson J. Line lists for $H_2^{18}O$ and $H_2^{17}O$ based on empirical line positions and ab initio intensities. JQSRT 2012;113:850-8.
[29]   Shirin SV, Polyansky OL, Zobov NF, Ovsyannikov RI, Császár AG, Tennyson J. Spectroscopically determined potential energy surfaces of the $H_2^{16}O$, $H_2^{17}O$, and $H_2^{18}O$ isotopologues of water. J Mol Spectrosc 2006;236:216-23.
[30]   Tennyson J, Bernath PF, Brown LR, Campargue A, Carleer MR, Császár AG, et al. IUPAC critical evaluation of the rotational--vibrational spectra of water vapor. Part I---Energy levels and transition wavenumbers for $H_2^{17}O$ and $H_2^{18}O$. JQSRT 2009;110:573-96.
[31]   Ma Q, Tipping RH, Lavrentieva NN. Pair identity and smooth variation rules applicable for the spectroscopic parameters of H_2O transitions involving high-J states. Mol Phys 2011;109:1925-41.
[32]   Brown LR, Humphrey CM, Gamache RR. CO_2-broadened water in the pure rotation and ν_2 fundamental regions. J Mol Spectrosc 2007;246:1-21.
[33]   Clough SA, private communication, 2012.
[34]   Voronin BA, Tennyson J, Tolchenov RN, Lugovskoy AA, Yurchenko SN. A high accuracy computed line list for the HDO molecule. Mon Not Astr R Soc 2010;402:492-6.
[35]   Tennyson J, Bernath PF, Brown LR, Campargue A, Császár AG, Daumont L, et al. IUPAC critical evaluation of the rotational-vibrational spectra of water vapor. Part II: Energy levels and transition wavenumbers for $HD^{16}O$, $HD^{17}O$, and $HD^{18}O$. JQSRT 2010;111:2160-84.
[36]   Scheepmaker RA, Frankenberg C, Galli A, Butz A, Schrijver H, Deutscher NM, et al. Improved water vapour spectroscopy in the 4174-4300 cm-1 region and its impact on SCIAMACHY HDO/H2O measurements. Atmospheric Measurement Techniques Discussions 2012;5:8539-78.
[37]   Thompson DR, Benner DC, Brown LR, Crisp D, Devi VM, Jiang YB, et al. Atmospheric validation of high accuracy CO_2 absorption coefficients for the OCO-2 mission. JQSRT 2012;113:2265-76.

[38]   Yokomizo M. Greenhouse gases Observing SATellite (GOSAT) Ground Systems. Fujitsu Scientific & Technical Journal 2008;44:410-7.

[39]   Bézard B, Fedorova A, Bertaux JL, Rodin A, Korablev O. The 1.10- and 1.18-μm nightside windows of Venus observed by SPICAV-IR aboard Venus Express. Icarus 2011;216:173-83.

[40]   Toth RA, Brown LR, Miller CE, Malathy Devi V, Benner DC. Spectroscopic database of CO_2 line parameters: 4300-7000 cm^{-1}. JQSRT 2008;109:906-21.

[41]   Perevalov VI, Tashkun SA, in: *10th HITRAN Database Conference*, Cambridge, MA, USA, 2008.

[42]   Tashkun SA, Perevalov VI, Teffo JL, Bykov AD, Lavrentieva NN, in: *14th International Symposium on High Resolution Molecular Spectroscopy* Krasnoyarsk, Russia, 2003.

[43]   Jacquemart D, Gueye F, Lyulin OM, Karlovets EV, Baron D, Perevalov VI. Infrared spectroscopy of CO_2 isotopologues from 2200 to 7000 cm^{-1}:Characterizing experimental uncertainties of positions and intensities. JQSRT 2012;113:961-75.

[44]   Lyulin OM, Karlovets EV, Jacquemart D, Lu Y, Liu AW, Perevalov VI. Infrared spectroscopy of ^{17}O- and ^{18}O-enriched carbon dioxide in the 1700-8300 cm^{-1} wavenumber region. JQSRT 2012;113:2167-81.

[45]   Depraz S, Perrin MY, Rivière P, Soufiani A. Infrared emission spectroscopy of CO2 at high temperature. Part II: Experimental results and comparisons with spectroscopic databases. JQSRT 2012;113:14-25.

[46]   Song KF, Kassi S, Tashkun SA, Perevalov VI, Campargue A. High sensitivity CW-cavity ring down spectroscopy of $^{12}CO_2$ near 1.35 μm (II): New observations and line intensities modeling. JQSRT 2010;111:332-44.

[47]   Durry G, Li JS, Vinogradov I, Titov A, Joly L, Cousin J, et al. Near infrared diode laser spectroscopy of C_2H_2, H_2O, CO_2 and their isotopologues and the application to TDLAS, a tunable diode laser spectrometer for the martian PHOBOS-GRUNT space mission. Appl Phys B 2010;99:339-51.

[48]   Casa G, Wehr R, Castrillo A, Fasci E, Gianfrani L. The line shape problem in the near-infrared spectrum of self-colliding CO2 molecules: Experimental investigation and test of semiclassical models. J Chem Phys 2009;130:4306.

[49]   Villanueva GL, Mumma MJ, Novak RE, Hewagama T. Identification of a new band system of isotopic CO_2 near 3.3 μm: Implications for remote sensing of biomarker gases on Mars. Icarus 2008;195:34-44.

[50]   Villanueva GL, Mumma MJ, Novak RE, Hewagama T. Discovery of multiple bands of isotopic CO_2 in the prime spectral regions used when searching for CH_4 and HDO on Mars. JQSRT 2008;109:883-94.

[51]   Joly L, Marnas F, Gibert F, Bruneau D, Grouiez B, Flamant PH, et al. Laser diode absorption spectroscopy for accurate CO_2 line parameters at 2 μm: consequences for space-based DIAL measurements and potential biases. Appl Opt 2009;48:5475-83.

[52]   Cai TD, Wang GS, Chen WD, Zhang WJ, Gao XM. Study of CO_2 Spectroscopic Parameters at High Temperature near 1.57 μm. Spectroscopy and Spectral Analysis 2009;29:1463-7.

[53]   Castrillo A, de Tommasi E, Gianfrani L, Sirigu L, Faist J. Doppler-free saturated-absorption spectroscopy of CO_2 at 4.3 μm by means of a distributed feedback quantum cascade laser. Optics Letters 2006;31:3040-2.

[54]   Lu Y, Liu AW, Pan H, Li XF, Perevalov VI, Tashkun SA, et al. High sensitivity cavity ring down spectroscopy of $^{13}C^{16}O_2$ overtone bands near 806 nm. JQSRT 2012;113:2197-204.

[55]   Pan H, Li XF, Lu Y, Liu AW, Perevalov VI, Tashkun SA, et al. Cavity ring down spectroscopy of ^{18}O and ^{17}O enriched carbon dioxide near 795 nm. JQSRT 2013;114:42-4.

[56]   Robert S, Borkov YG, Vander Auwera J, Drummond R, Mahieux A, Wilquet V, et al. Assignment and rotational analysis of new absorption bands of carbon dioxide isotopologues in Venus spectra. JQSRT 2013;114:29-41.

[57]   Giusfredi G, Bartalini S, Borri S, Cancio P, Galli I, Mazzotti D, et al. Saturated-Absorption Cavity Ring-Down Spectroscopy. Phys Rev Letters 2010;104.

[58]   Cancio P, Bartalini S, Borri S, Galli I, Gagliardi G, Giusfredi G, et al. Frequency-comb-referenced mid-IR sources for next-generation environmental sensors. Appl Phys B 2011;102:255-69.

[59]   Tashkun SA, Velichko TI, Mikhailenko SN. Critical evaluation of measured pure-rotation and rotation-vibration line positions and an experimental dataset of energy levels of $^{12}C^{16}O$ in $X^1\Sigma^+$ state. JQSRT 2010;111:1106-16.

[60]   Lamouroux J, Gamache RR, Laraia AL, Hartmann J-M, Boulet C. Semiclassical calculations of half-widths and line shifts for transitions in the 30012-00001 and 30013-00001 bands of CO_2 II: Collisions with O_2 and air. JQSRT 2012;113:991-1003.

[61]   Lamouroux J, Gamache RR, Laraia AL, Hartmann J-M, Boulet C. Semiclassical calculations of half-widths and line shifts for transitions in the 30012-00001 and 30013-00001 bands of CO_2. III: Self collisions. JQSRT 2012;113:1536-46.

[62]   Gamache RR, Lamouroux J. The vibrational dependence of half-widths of CO_2 transitions broadened by N_2, O_2, air, and CO_2. JQSRT 2013;117:93-103.

[63]   Lamouroux J, Tran H, Laraia AL, Gamache RR, Rothman LS, Gordon IE, et al. Updated database plus software for line-mixing in CO_2 infrared spectra and their test using laboratory spectra in the 1.5-2.3 μm region. JQSRT 2010;111:2321-31.

[64]   Tyuterev VG, Tashkun SA, Schwenke DW, Jensen J, Cours T, Barbe A, et al. Variational EKE-calculations of rovibrational energies of the ozone molecules from an empirical potential function. Chem Phys Lett 2000;316:271-9.

[65]   Tyuterev VG, Tashkun SA, Schwenke DW, Barbe A. Variational calculations of high-J rovibrational states of the ozone molecule from empirically determined isotopically invariant potential energy surface. SPIE Proc Ser 2004;5311:176-84.

[66]   Funke B, López-Puertas M, García-Comas M, Kaufmann M, Höpfner M, Stiller GP. GRANADA: A Generic RAdiative traNsfer AnD non-LTE population algorithm. JQSRT 2012;113:1771-817.

[67]   Bouazza S, Barbe A, Mikhailenko S, Plateaux JJ. Line positions and intensities of the $\nu_1+2\nu_2+\nu_3$ and $2\nu_2+2\nu_3$ bands of $^{16}O_3$. J Mol Spectrosc 1994;166:365-71.

[68]   Barbe A, De Backer MR, Starikova E, Tashkun SA, Thomas X, Tyuterev VG. FTS high resolution spectra of $^{16}O_3$ in 3500 and 5500 cm^{-1} regions. First example of new theoretical modelling for a polyad of strongly coupled states. JQSRT 2012;113:829-39.

[69]   Mikhailenko S, Barbe A, Tyuterev VG, Régalia L, Plateaux JJ. Line positions and intensities of the $\nu_1+\nu_2+3\nu_3$, $\nu_2+4\nu_3$, and $3\nu_1+2\nu_2$ bands of ozone. J Mol Spectrosc 1996;180:227-35.

[70]   Barbe A, Chichery A, Tyuterev VG, Plateaux JJ. Analysis of high resolution measurements of the $\nu_1+5\nu_3$ band of ozone: Coriolis interactions with the $6\nu_3$ and $3\nu_1+\nu_2+2\nu_3$ bands. Mol Phys 1998;94:751-7.

[71]   Campargue A, Barbe A, De Backer-Barilly MR, Tyuterev VG, Kassi S. The near infrared spectrum of ozone by CW-cavity ring down spectroscopy between 5850 and 7000 cm^{-1}: new observations and exhaustive review. Physical Chemistry Chemical Physics 2008;10:2925-46.

[72]   Kassi S, Campargue A, De Backer-Barilly MR, Barbe A. The $\nu_1+3\nu_2+3\nu_3$ and $4\nu_1+\nu_2+\nu_3$ bands of ozone by CW-cavity ring down spectroscopy between 5900 and 5960 cm^{-1}. J Mol Spectrosc 2007;244:122-9.

[73]   Campargue A, Kassi S, Romanini D, Barbe A, De Backer-Barilly MR, Tyuterev VG. CW-cavity ring down spectroscopy of the ozone molecule in the 6625-6830 cm^{-1} region. J Mol Spectrosc 2006;240:1-13.

[74]   Barbe A, De Backer-Barilly MR, Tyuterev VG, Campargue A, Romanini D, Kassi S. CW-Cavity Ring Down Spectroscopy of the ozone molecule in the 5980-6220 cm^{-1} region. J Mol Spectrosc 2007;242:156-75.

[75]   Barbe A, De Backer-Barilly MR, Tyuterev VG, Kassi S, Campargue A. CW-cavity ring down spectroscopy of the ozone molecule in the 6220-6400 cm^{-1} region. J Mol Spectrosc 2007;246:22-38.

[76]   Mikhailenko SN, Babikov YL, Tyuterev VG, Barbe A. The databank of ozone spectroscopy on WEB (S&MPO). J Computational Technologies 2002;7:64-70.

[77]   Tyuterev VG, Tashkun SA, Seghir H. High-order contact transformations: General algorithm, computer implementation and triatomic tests. SPIE Proc Ser 2004;5311:164-75.

[78]   Barbe A, Mikhailenko S, Starikova E, De Backer MR, Tyuterev VG, Mondelain D, et al. Ozone spectroscopy in the electronic ground state: high-resolution spectra analyses and update of line parameters since 2003. JQSRT 2013;this issue.

[79]   Malathy Devi V, Chris Benner D, Smith MAH, Mantz AW, Sung K, Brown LR, et al. Spectral line parameters including temperature dependences of self- and air-broadening in the 2←0 band of CO at 2.3 μm. JQSRT 2012;113:1013-33.

[80]   Malathy Devi V, Chris Benner D, Smith MAH, Mantz AW, Sung K, Brown LR. Spectral line parameters including temperature dependences of air-broadening in the 2←0 bands of $^{13}C^{16}O$ and $^{12}C^{18}O$ at 2.3 μm. J Mol Spectrosc 2012;276-277:33-48.

[81]   Rosenkranz PW. Shape of 5 mm oxygen band in atmosphere. IEEE Trans Antennas Propag 1975;AP-23:498-506.

[82]   Hartmann J-M, Boulet C. Line shape parameters for HF in a bath of argon as a test of classical path models. J Chem Phys 2000;113:9000.

[83]   Müller HSP, Schlöder F, Stutzki J, Winnewisser G. The Cologne Database for Molecular Spectroscopy, CDMS: a useful tool for astronomers and spectroscopists. J Mol Struct 2005;742:215.

[84]   Brown LR, Campargue A, Kassi S, Wang L, Mondelain D, Leshchishina O, et al. Revised 2013 compilation of methane line parameters. JQSRT 2013;this issue.

[85]   Daumont L, Nikitin AV, Thomas X, Régalia L, Von der Heyden P, Tyuterev VG, et al. New assignments in the 2μm transparency window of the $^{12}CH_4$ Octad band system. JQSRT 2013;116:101-9.

[86]   Niederer HM, Albert S, Bauerecker S, Boudon V, Champion JP, Quack M. Global analysis of the infrared spectrum of $^{13}CH_4$: lines in the region 0 to 3200 cm^{-1}. Chimia 2008;62:273-6.

[87]   Niederer HM, Albert S, Bauerecker S, Boudon V, Champion JP, Quack M. Analysis of the rovibrational spectrum of methane $^{13}CH_4$ in the infrared. J Mol Spectrosc 2013;submitted.

[88]   Nikitin AV, Daumont L, Thomas X, Régalia L, Rey M, Tyuterev VG, et al. Preliminary assignments of $2\nu_3$-ν_4 hot band of $^{12}CH_4$ in the 2 μm transparency window from long-path FTS spectra. J Mol Spectrosc 2011;268:93-106.

[89]   Nikitin AV, Brown LR, Sung K, Rey M, Tyuterev VG, Smith MAH, et al. Preliminary modeling of CH_3D from 4000 to 4550 cm^{-1}. JQSRT 2013;114:1-12.

[90]   Wishnow EH, Orton GS, Ozier I, Gush HP. The distortion dipole rotational spectrum of CH_4: A low temperature far-infrared study. JQSRT 2007;103:102-17.

[91]   Boudon V, Pirali O, Roy P, Brubach J-B, Manceron L, Vander Auwera J. The high-resolution far-infrared spectrum of methane at the SOLEIL synchrotron. JQSRT 2010;111:1117-29.

[92]   Brown LR. Empirical line parameters of methane from 1.1 to 2.1 μm. JQSRT 2005;96:251-70.

[93]   Campargue A, Leshchishina O, Wang L, Mondelain D, Kassi S. The WKLMC empirical linelists (5852 - 7919 cm^{-1}) for methane between 80 K and 296 K: "final" lists in HITRAN format for atmospheric and planetary applications. J Mol Spectrosc 2013;in press.

[94]   Benner DC, Devi VM, O'Brien JJ, Shahl S, Spickler PT, Houck CP, et al. Empirical line parameters of CH_4 from 10923 to 11502 cm^{-1}. Icarus 2013;in preparation.

[95]   Abe M, Iwakuni K, Okubo S, Sasada H. Accurate transition frequency list of the ν_3 band of methane from sub-Doppler resolution comb-referenced spectroscopy. J Opt Soc Am B 2013;in press.

[96]   Zolot AM, Giorgetta FR, Baumann E, Swann WC, Coddington I, Newbury NR. Broadband frequency references in the near-infrared: Accurate dual comb spectroscopy of methane and acetylene. JQSRT 2013;118:26-39.

[97]   Sanzharov M, Vander Auwera J, Pirali O, Roy P, Brubach J-B, Manceron L, et al. Self and N_2 collisional broadening of far-infrared methane lines measured at the SOLEIL synchrotron. JQSRT 2012;113:1874-86.

[98]   Coustenis A, Achterberg RK, Conrath BJ, Jennings DE, Marten A, Gautier D, et al. The composition of Titan's stratosphere from Cassini/CIRS mid-infrared spectra. Icarus 2007;189:35-62.

[99]   Mackie CJ, Gordon IE, Rothman LS, Leshchishina O, Kassi S, Campargue A, et al. Revision of spectral parameters for the bands of oxygen that involve ground $X^3\Sigma_g^-$ and first excited $a^1\Delta_g$ electronic states. JQSRT 2013;in preparation.

[100]   Leshchishina O, Kassi S, Gordon IE, Rothman LS, Wang L, Campargue A. High sensitivity CRDS of the $a^1\Delta_g$ - $X^3\Sigma_g^-$ band of oxygen near 1.27 μm: Extended observations, quadrupole transitions, hot bands and minor isotopologues. JQSRT 2010;111:2236-45.

[101]   Leshchishina O, Kassi S, Gordon IE, Yu S, Campargue A. The band of $^{16}O^{17}O$, $^{17}O^{18}O$ and $^{17}O_2$ by high sensitivity CRDS near 1.27 μm. JQSRT 2011;112:1257-65.

[102]   Tretyakov MY, Koshelev MA, Dorovskikh VV, Makarov DS, Rosenkranz PW. 60-GHz oxygen band: precise broadening and central frequencies of fine-structure lines, absolute absorption profile at atmospheric pressure, and revision of mixing coefficients. J Mol Spectrosc 2005;231:1-14.

[103]   Golubiatnikov GY, Krupnov AF. Microwave study of the rotational spectrum of oxygen molecule in the range up to 1.12 THz. J Mol Spectrosc 2003;217:282-7.

[104]   Park K, Nolt IG, Steele TC, Zink LR, Evenson KM, Chance KV, et al. Pressure broadening of the 50.873 and 83.469 cm^{-1} molecular oxygen lines. JQSRT 1996;56:315-6.

[105]   Jennings DA, Evenson KM, Vanek MD, Nolt IG, Radostitz JV, Chance KV. Air- and oxygen-broadening coefficients for the O_2 rotational line at 60.46 cm^{-1}. Geophys Res Lett 1987;14:722-5.
[106]   Drouin BJ. Temperature dependent pressure induced linewidths of $^{16}O_2$ and $^{16}O^{18}O$ transitions in nitrogen, oxygen and air. JQSRT 2007;105:450-8.
[107]   Newman SM, Orr-Ewing AJ, Newnham DA, Ballard J. Temperature and pressure dependence of line widths and integrated absorption intensities for the O_2 a $^1\Delta_g$ - X $^3\Sigma_g^-$ (0,0) transition. J Phys Chem A 2000;104:9467-80.
[108]   Washenfelder RA, Toon GC, Blavier J-F, Yang Z, Allen NT, Wennberg PO, et al. Carbon dioxide column abundances at the Wisconsin Tall Tower site. Journal of Geophysical Research (Atmospheres) 2006;111:22305.
[109]   Gordon IE, Kassi S, Campargue A, Toon GC. First identification of the $a^1\Delta_g$ - X $^3\Sigma_g^-$ electric quadrupole transitions of oxygen in solar and laboratory spectra. JQSRT 2010;111:1174-83.
[110]   Kassi S, Leshchishina O, Gordon IE, Yu S, Campargue A. Hyperfine structure of the transitions of $^{16}O^{17}O$, $^{17}O^{18}O$ and $^{17}O_2$ by CRDS at 80 K. Chem Phys Lett 2011;502:37-41.
[111]   Mishra AP, Balasubramanian TK, Shetty BJ. Generalized electric quadrupole branch linestrengths for the infrared atmospheric oxygen bands. JQSRT 2011;112:2303-9.
[112]   Kassi S, Campargue A. Cavity ring down spectroscopy with 5×10^{-13} cm^{-1} sensitivity. J Chem Phys 2012;137:4201.
[113]   Robichaud DJ, Hodges JT, Brown LR, Lisak D, Maslowski P, Yeung LY, et al. Experimental intensity and lineshape parameters of the oxygen A-band using frequency-stabilized cavity ring-down spectroscopy. J Mol Spectrosc 2008;248:1-13.
[114]   Robichaud DJ, Hodges JT, Lisak D, Miller CE, Okumura M. High-precision pressure shifting measurement technique using frequency-stabilized cavity ring-down spectroscopy. JQSRT 2008;109:435-44.
[115]   Robichaud DJ, Hodges JT, Masłowski P, Yeung LY, Okumura M, Miller CE, et al. High-accuracy transition frequencies for the O_2 A-band. J Mol Spectrosc 2008;251:27-37.
[116]   Robichaud DJ, Yeung LY, Long DA, Okumura M, Havey DK, Hodges JT, et al. Experimental line parameters of the $b^1\Sigma_g^+ \leftarrow X^3\Sigma_g^-$(0,0) band of oxygen isotopologues at 760 nm using frequency-stabilized cavity ring-down spectroscopy. Journal of Physical Chemistry A 2009;113:13089-99.
[117]   Havey DK, Long DA, Okumura M, Miller CE, Hodges JT. Ultra-sensitive optical measurements of high-J transitions in the O_2 A-band. Chemical Physics Letters 2009;483:49-54.
[118]   Long DA, Havey DK, Okumura M, Miller CE, Hodges JT. O_2 A-band line parameters to support atmospheric remote sensing. JQSRT 2010;111:2021-36.
[119]   Long DA, Havey DK, Yu SS, Okumura M, Miller CE, Hodges JT. O_2 A-band line parameters to support atmospheric remote sensing. Part II: The rare isotopologues. JQSRT 2011;112:2527-41.
[120]   Galatry L. Simultaneous effect of Doppler and foreign gas broadening on spectral lines. Physical Review 1961;122:1218-23.
[121]   Ritter KJ, Wilkerson TD. High-resolution spectroscopy of the oxygen A-band. J Mol Spectrosc 1987;121:1-19.
[122]   Long DA, Hodges JT. On spectroscopic models of the O_2 A-band and their impact upon atmospheric retrievals. J Geophys Res-Atmos 2012;117:D12309.

[123]   Tran H, Boulet C, Hartmann JM. Line mixing and collision-induced absorption by oxygen in the A band: Laboratory measurements, model, and tools for atmospheric spectra computations. J Geophys Res-Atmos 2006;111:D15210.

[124]   Tran H, Hartmann JM. An improved O_2 A band absorption model and its consequences for retrievals of photon paths and surface pressures. J Geophys Res-Atmos 2008;113:D18104.

[125]   Long DA, Robichaud DJ, Hodges JT. Frequency-stabilized cavity ring-down spectroscopy measurements of line mixing and collision-induced absorption in the O_2 A-band. Journal of Chemical Physics 2012;137.

[126]   Richard C, Gordon IE, Rothman LS, Abel M, Frommhold L, Gustafsson M, et al. New section of the HITRAN database: Collision-induced absorption (CIA). JQSRT 2012;113:1276-85.

[127]   Long DA, Havey DK, Okumura M, Pickett HM, Miller CE, Hodges JT. Laboratory measurements and theoretical calculations of O_2 A-band electric quadrupole transitions. Physical Review A 2009;80:042513.

[128]   Gordon IE, Rothman LS, Toon GC. Revision of spectral parameters for the B- and gamma-bands of oxygen and their validation against atmospheric spectra. JQSRT 2011;112:2310-22.

[129]   Miller CE, Wunch D. Fourier transform spectrometer remote sensing of O_2 A-band electric quadrupole transitions. JQSRT 2012;113:1043-50.

[130]   Brault JW. Detection of Electric Quadrupole Transitions in the Oxygen A-Band at 7600 Å. J Mol Spectrosc 1980;80:384-7.

[131]   Yu S, Miller CE, Drouin BJ, Müller HSP. High resolution spectral analysis of oxygen. I. Isotopically invariant Dunham fit for the $X^3\Sigma_g^-$, $a^1\Delta_g$, $b^1\Sigma_g^+$ states. J Chem Phys 2012;137:4304.

[132]   Flaud JM, Lafferty WJ, Sams RL. Line Intensities for the ν_1, ν_3 and $\nu_1 + \nu_3$ bands of $^{34}SO_2$. JQSRT 2009;110:669-74.

[133]   Lafferty WJ, Flaud JM, Ngom EHA, Sams RL. $^{34}S^{16}O_2$: High-resolution analysis of the (0 3 0), (1 0 1), (1 1 1), (0 0 2) and (2 0 1) vibrational states; determination of equilibrium rotational constants for sulfur dioxide and anharmonic vibrational constants. J Mol Spectrosc 2009;253:51-4.

[134]   Lafferty WJ, Flaud J-M, Sams RL, Abib Ngom EH. High resolution analysis of the rotational levels of the (0 0 0), (0 1 0), (1 0 0), (0 0 1), (0 2 0), (1 1 0) and (0 1 1) vibrational states of $^{34}S^{16}O_2$. J Mol Spectrosc 2008;252:72-6.

[135]   Galloway JN, Aber JD, Erisman JW, Seitzinger SP, Howarth RW, Cowling EB, et al. The nitrogen cascade. BioScience 2003;53:341.

[136]   Clarisse L, Clerbaux C, Dentener F, Hurtmans D, Coheur P-F. Global ammonia distribution derived from infrared satellite observations. Nature Geosci 2009;advanced online publication.

[137]   Burgess AB, Dudhia A, Grainger RG, Stevenson D. Progress in tropospheric ammonia retrieval from the MIPAS satellite instrument. Adv Space Res 2006;37:2218-21.

[138]   Beer R, Shephard MW, Kulawik SS, Clough SA, Eldering A, Bowman KW, et al. First satellite observations of lower tropospheric ammonia and methanol. Geophys Res Lett 2008;35:L09801.

[139]   Rothman LS, Barbe A, Chris Benner D, Brown LR, Camy-Peyret C, Carleer MR, et al. The HITRAN molecular spectroscopic database: edition of 2000 including updates through 2001. JQSRT 2003;82:5-44.

[140]   Down MJ, Hill C, Yurchenko SN, Tennyson J, Brown LR, Kleiner I. Re-analysis of observed Ammonia spectra: Updating the HITRAN $^{14}NH_3$ database. J Quant Spectrosc Radiat Transf (submitted) 2013.

[141]   Sung K, Brown LR, Huang X, Schwenke DW, Lee TJ, Coy SL, et al. Extended line positions, intensities, empirical lower state energies and quantum assignments of NH_3 from 6300 to 7000 cm^{-1}. JQSRT 2012;113:1066-83.

[142]   Chen P, Pearson JC, Pickett HM, Matsuura S, Blake GA. Measurements of $^{14}NH_3$ in the $v_2=1$ state by a solid-state, photomixing, THz spectrometer, and a simultaneous analysis of the microwave, terahertz, and infrared transitions between the ground and v_2 inversion-rotation levels. J Mol Spectrosc 2006;236:116-26.

[143]   Yu S, Pearson JC, Drouin BJ, Sung K, Pirali O, Vervloet M, et al. Submillimeter-wave and far-infrared spectroscopy of high-J transitions of the ground and $v_2= 1$ states of ammonia. J Chem Phys 2010;133:174317-14.

[144]   Yurchenko SN, Barber RJ, Tennyson J. A variationally computed line list for hot NH_3. Mon Not Astr R Soc 2011;413:1828-34.

[145]   Guinet M, Jeseck P, Mondelain D, Pepin I, Janssen C, Camy-Peyret C, et al. Absolute measurements of intensities, positions and self-broadening coefficients of R branch transitions in the v_2 band of ammonia. JQSRT 2011;112:1950-60.

[146]   Fabian M, Yamada KMT. Absolute intensity of the NH_3 v_2 band. J Mol Spectrosc 1999;198:102-9.

[147]   Nemtchinov V, Sung K, Varanasi P. Measurements of line intensities and half-widths in the 10 μm bands of $^{14}NH_3$. JQSRT 2004;83:243-65.

[148]   Aroui H, Nouri S, Bouanich JP. NH_3 self-broadening coefficients in the v_2 and v_4 bands and line intensities in the v_2 band. J Mol Spectrosc 2003;220:248-58.

[149]   Yurchenko SN, Barber RJ, Yachmenev A, Thiel W, Jensen P, Tennyson J. A variationally computed T =300 K line list for NH_3. J Phys Chem A 2009;113:11845-55.

[150]   Chu Z, Chen L, Cheo PK. Absorption spectra of NH_3 using a microwave sideband CO_2-Laser spectrometer. JQSRT 1994;51:591-602.

[151]   Cacciani P, Cermak P, Cosléou J, Khelkhal M, Jeseck P, Michaut X. New progress in spectroscopy of ammonia in the infrared 1.5 μm range using evolution of spectra from 300 K down to 122 K. JQSRT 2012;113:1084-91.

[152]   Bell CL, Dhib M, Hancock G, Ritchie GAD, van Helden JH, van Leeuwen NJ. Cavity enhanced absorption spectroscopy measurements of pressure-induced broadening and shifts coefficients in the $v_1 + v_3$ combination band of ammonia. Appl Phys B 2009;94:327-36.

[153]   Cacciani P. Private communication. 2012.

[154]   Lundsberg-Nielsen L, Hegelund F, Nicolaisen FM. Analysis of the high-resolution spectrum of ammonia ($^{14}NH_3$) in the near-infrared regions, 6400 - 6900 cm^{-1}. J Mol Spectrosc 1993;162:230-45.

[155]   Xu L-H, Liu Z, Yakovlev I, Tretyakov MY, Lees RM. External cavity tunable diode laser NH_3 spectra in the 1.5 μm region. Infra Phys Tech 2004;45:3-45.

[156]   Li L, Lees RM, Xu L-H. External cavity tunable diode laser spectra of the $v_1 + 2v_4$ stretch-bend combination bands of $^{14}NH_3$ and $^{15}NH_3$. J Mol Spectrosc 2007;243:219-26.

[157]   Lees RM, Li L, Xu L-H. New VISTA on ammonia in the 1.5 μm region: Assignments for the $v_3 + 2v_4$ of $^{14}NH_3$ and $^{15}NH_3$ by isotopic shift labeling. J Mol Spectrosc 2008;251:241-51.

[158]   Urban Š, D'Cunha R, Rao NK, Papoušek D. The $\Delta K = \pm 2$ forbidden band and inversion rotation energy-levels of ammonia. Can J Phys 1984;62:1775-91.

[159]   Pickett HM, Poynter RL, Cohen EA, Delitsky ML, Pearson JC, Müller HSP. Submillimeter, millimeter and microwave spectral line catalog. JQSRT 1998;60:883-90.

[160]   Petkie DT, Helminger P, Winnewisser BP, Winnewisser M, Butler RAH, Jucks KW, et al. The simulation of infrared bands from the analyses of rotational spectra: the $2\nu_9$-ν_9 and ν_5-ν_9 hot bands of HNO_3. JQSRT 2005;92:129-41.

[161]   Petkie DT, Helminger P, Butler RAH, Albert S, De Lucia FC. The millimeter and submillimeter spectra of the ground state and excited ν_9, ν_8, ν_7, and ν_6 vibrational states of HNO_3. J Mol Spectrosc 2003;218:127-30.

[162]   Gomez L, Tran H, Perrin A, Gamache RR, Laraia A, Orphal J, et al. Some improvements of the HNO_3 spectroscopic parameters in the spectral region from 600 to 950 cm^{-1}. JQSRT 2009;110:675-86.

[163]   Perrin A, Mbiaké R. The ν_5 and $2\nu_9$ bands of the ^{15}N isotopic species of nitric acid ($H^{15}NO_3$): Line positions and intensities. J Mol Spectrosc 2006;237:27-35.

[164]   Flaud J-M, Brizzi G, Carlotti M, Perrin A, Ridolfi M. MIPAS database: Validation of HNO_3 line parameters using MIPAS satellite measurements. Atmos Chem Phys 2006;6:5037-48.

[165]   Krasnopolsky VA, Belyaev DA, Gordon IE, Li G, Rothman LS. Observations of D/H Ratios in H_2O, HCl, and HF on Venus and New DCl and DF Line Strengths. Icarus 2013;224:57-65.

[166]   Li G, Gordon IE, Hajigeorgiou PG, Coxon JA, Rothman LS. Reference spectroscopic data for hydrogen halides. Part II: the line lists. JQSRT 2013;submitted.

[167]   Li G, Gordon IE, Bernath PF, Rothman LS. Direct fit of experimental ro-vibrational intensities to the dipole moment function: Application to HCl. JQSRT 2011;112:1543-50.

[168]   Li G, Gordon IE, Le Roy RJ, Hajigeorgiou PG, Coxon JA, Bernath PF, et al. Reference spectroscopic data for hydrogen halides. Part I: Construction and validation of the ro-vibrational dipole moment functions. JQSRT 2013;in press.

[169]   Pine AS, Looney JP. N_2 and air broadening in the fundamental bands of HF and HCl. J Mol Spectrosc 1987;122:41-55.

[170]   Chou S-I, Baer DS, Hanson RK. Spectral Intensity and Lineshape Measurements in the First Overtone Band of HF Using Tunable Diode Lasers. J Mol Spectrosc 1999;195:123-31.

[171]   Meredith RE. Strengths and widths in the first overtone band of hydrogen fluoride. JQSRT 1972;12:485-503.

[172]   Pine AS, Fried A, Elkins JW. Spectral intensities in the fundamental bands of HF and HCl. J Mol Spectrosc 1985;109:30-45.

[173]   Guelachvili G, Smith MAH. Measurements of pressure-induced shifts in the 1-0 and 2-0 bands of HF and in the 2-0 bands of $H^{35}Cl$ and $H^{37}Cl$. JQSRT 1978;20:35-47.

[174]   Cazzoli G, Puzzarini C. Hyperfine structure of the J=1←0 transition of $H^{35}Cl$ and $H^{37}Cl$: improved ground state parameters. J Mol Spectrosc 2004;226:161-8.

[175]   Cazzoli G, Puzzarini C. Hyperfine structure of the J = 1←0 and J = 2←1 transitions of $D^{35}Cl$ and $D^{37}Cl$. Physical Chemistry Chemical Physics 2004;6:5133-9.

[176]   Western CM *PGOPHER, a Program for Simulating Rotational Structure*, University of Bristol, http://pgopher.chm.bris.ac.uk.

[177]   Park K, Chance KV, Nolt IG, Radostitz JV, Vanek MD, Jennings DA, et al. Pressure broadening of the 2.5 THz $H^{35}Cl$ rotational line by N_2 and O_2. J Mol Spectrosc 1991;147:521-5.

[178]   De Rosa M, Nardini C, Piccolo C, Corsi C, D'Amato F. Pressure broadening and shift of transitions of the first overtone of HCl. Appl Phys B: Lasers Opt 2001;72:245-8.

[179]   Hurtmans D, Henry A, Valentin A, Boulet C. Narrowing broadening and shifting parameters for R(2) and P(14) lines in the HCl fundamental band perturbed by N_2 and rare gases from tunable diode laser spectroscopy. J Mol Spectrosc 2009;254:126-36.

[180]   Ortwein P, Woiwode W, Wagner S, Gisi M, Ebert V. Laser-based measurements of line strength, self- and pressure-broadening coefficients of the $H^{35}Cl$ R(3) absorption line in the first overtone region for pressures up to 1 MPa. Appl Phys B: Lasers Opt 2010;100:341-7.

[181]   Ogilvie JF, Lee Y-P. Linestrengths in the 3–0 vibration-rotational band of gaseous $H^{35}Cl$ and the electric dipole moment function. Chem Phys Lett 1989;159:239-43.

[182]   Zughul M, Gelfand J, Rabitz H, DePristo AE. Pressure broadening in the 0-4 through 0-7 overtone bands of $H^{35}Cl$ and $H^{37}Cl$. JQSRT 1980;24:371-7.

[183]   Tudorie M, Földes T, Vandaele AC, Vander Auwera J. CO_2 pressure broadening and shift coefficients for the 1-0 band of HCl and DCl. JQSRT 2012;113:1092-101.

[184]   Eaton DR, Thompson HW. Pressure Broadening Studies on Vibration-Rotation Bands. II. The Effective Collision Diameters. Proceedings of the Royal Society of London Series A Mathematical and Physical Sciences 1959;251:475-85.

[185]   Coxon JA, Hajigeorgiou PG. Breakdown of the Born-Oppenheimer approximation in the ground electronic state of hydrogen halides: improved Direct Potential Fitting analyses for HF/DF/TF. HCl/DCl/TCl, HBr/DBr/TBr and HI/DI/TI. 2013;In preparation

[186]   Benedict WS, Herman R. The calculation of self-broadened line widths in linear molecules. JQSRT 1963;3:265-78.

[187]   Guelachvili G, Niay P, Bernage P. Fourier transform high-resolution measurements on the 2←0, 3←0, 4←0, 5←0 infrared absorption bands of HI and DI. J Mol Spectrosc 1981;85:253-70.

[188]   Varberg TD, Roberts JC, Tuominen KA, Evenson KM. The Far-Infrared Spectrum of Deuterium Iodide. J Mol Spectrosc 1998;191:384-6.

[189]   Domanskaya AV, Asfin RE, Maul C, Kerl K, Bulanin MO. Nitrogen-induced broadening and shifts of rotation-vibrational lines in the fundamental, first, second and third overtone bands of HI. J Mol Spectrosc 2011;265:69-73.

[190]   Hartmann JM, Bouanich JP, Boulet C, Bulanin MO, Domanskaya AV, Kerl K. Self-broadening and shifting of HI lines in the 1-0 and 2-0 infrared bands. JQSRT 2005;95:151-63.

[191]   Bulanin MO, Domanskaya AV, Kerl K, Maul C. Spectral line parameters in the (3←0) overtone band of the HI molecule and line-mixing in the band head. J Mol Spectrosc 2005;230:87-92.

[192]   Goldman A, Gillis JR, Rinsland CP, Burkholder JB. Improved line parameters for the $X^2\Pi$-$X^2\Pi$ (1-0) bands of ^{35}ClO and ^{37}ClO. JQSRT 1994;52:357-9.

[193]   Burkholder JB, Howard CJ, Hammer PD, Goldman A. Infrared line intensity measurements in the v = 0-1 band of the ClO radical. J Geophys Res 1989;94:2225-34.

[194]   Birk M, Wagner G. Experimental line strengths of the ClO fundamental. J Geophys Res 1997;102:19199-206.

[195]   Koshelev MA, Tretyakov MY. Collisional broadening and shifting of OCS rotational spectrum lines. JQSRT 2009;110:118-28.

[196]   Jacquemart D, Laraia A, Kwabia Tchana F, Gamache RR, Perrin A, Lacome N. Formaldehyde around 3.5 and 5.7-μm: Measurement and calculation of broadening coefficients. JQSRT 2010;111:1209-22.

[197]   Li H, Le Roy RJ. Quadrupole moment function and absolute infrared quadrupolar intensities for N_2. J Chem Phys 2007;126:4301.

[198]   Le Roy RJ, Huang Y, Jary C. An accurate analytic potential function for ground-state N_2 from a direct-potential-fit analysis of spectroscopic data. J Chem Phys 2006;125:164310-12.

[199]   Bernath PF, McElroy CT, Abrams MC, Boone CD, Butler M, Camy-Peyret C, et al. Atmospheric Chemistry Experiment (ACE): Mission overview. Geophys Res Lett 2005;32:5.

[200]   Boone CD, Bernath PF, Spectroscopy for the Atmospheric Chemistry Experiment (ACE). Presented at ASA/HITRAN meeting, Reims, France, August 2012.

[201]   Nikitin A, Champion JP, Burger H. Global analysis of $^{12}CH_3^{35}Cl$ and $^{12}CH_3^{37}Cl$: simultaneous fit of the lower five polyads (0-2600 cm^{-1}). J Mol Spectrosc 2005;230:174-84.

[202]   Chackerian C, Brown LR, Lacome N, Tarrago G. Methyl Chloride ν_5 Region Lineshape Parameters and Rotational Constants for the ν_2, ν_5, and $2\nu_3$ Vibrational Bands. J Mol Spectrosc 1998;191:148-57.

[203]   Kondo S, Koga Y, Nakanaga T, Saëki S. Infrared Intensities in Methyl Chloride. I. The Fundamental Bands. Bull Chem Soc Jpn 1983;56:416-21.

[204]   Kondo S, Koga Y, Nakanaga T, Saëki S. Infrared Intensities in Methyl Chloride. II. Binary Overtone and Combination Bands. Bull Chem Soc Jpn 1984;57:16-21.

[205]   Kondo S, Koga Y, Nakanaga T. Infrared Intensities in Methyl Chloride. III. Improvement of the Anharmonic Force Field and the Analysis of the Overtone and Combination Band Intensities. Bull Chem Soc Jpn 1985;58:65-72.

[206]   Johnson TJ, Sams RL, Sharpe SW, Colton R, Vo-Dinh T, in: *Society of Photo-Optical Instrumentation Engineers (SPIE) Conference Series*, 2004.

[207]   Bray C, Perrin A, Jacquemart D, Lacome N. The ν_1, ν_4 and $3\nu_6$ bands of methyl chloride in the 3.4-μm region: Line positions and intensities. JQSRT 2011;112:2446-62.

[208]   Gomez L, Jacquemart D, Lacome N, Mandin JY. Line intensities of $^{12}C_2H_2$ in the 7.7 μm spectral region. JQSRT 2009;110:2102-14.

[209]   Gomez L, Jacquemart D, Lacome N, Mandin JY. New line intensity measurements for $^{12}C_2H_2$ around 7.7 μm and HITRAN format line list for applications. JQSRT 2010;111:2256-64.

[210]   Nakagawa K, de Labachelerie M, Awaji Y, Kourogi M. Accurate optical frequency atlas of the 1.5-μm bands of acetylene. *J Opt Soc Am* 1996;13:2708-14.

[211]   Jolly A, Benilan Y, Cané E, Fusina L, Tamassia F, Fayt A, et al. Measured integrated band intensities and simulated line-by-line spectra for $^{12}C_2HD$ between 25 and 2.5 μm, and new global vibration-rotation parameters for the bending vibrations. JQSRT 2008;109:2846-56.

[212]   Nixon CA, Achterberg RK, Conrath BJ, Irwin PGJ, Teanby NA, Fouchet T, et al. Meridional variations of C_2H_2 and C_2H_6 in Jupiter's atmosphere from Cassini CIRS infrared spectra. Icarus 2007;188:47-71.

[213]   Vander Auwera J, Moazzen-Ahmadi N, Flaud J-M. Toward an Accurate Database for the 12 μm Region of the Ethane Spectrum. Astrophys J 2007;662:750-7.

[214]   Moazzen-Ahmadi N. A combined frequency analysis of the ν_3, ν_9, $3\nu_4$ and the far-infrared bands of ethane: A reassessment of the torsional parameters for the ground vibrational state. J Mol Spectrosc 2002;214:144-51.

[215]   Cooper JR, Moazzen-Ahmadi N. Global fit analysis including the $\nu_9 + \nu_4 - \nu_4$ hot band of ethane: Evidence of an interaction with the ν_{12} fundamental. J Mol Spectrosc 2006;239:51-8.

[216]   Malathy Devi V, Rinsland CP, Chris Benner D, Sams RL, Blake TA. Multispectrum analysis of the ν_9 band of $^{12}C_2H_6$: Positions, intensities, self- and N_2-broadened half-width coefficients. JQSRT 2010;111:1234-51.

[217]   Devi VM, Benner DC, Rinsland CP, Smith MAH, Sams RL, Blake TA, et al. Multispectrum measurements of spectral line parameters including temperature dependences of

N$_2$- and self-bropadened half-width coefficients in the region of the ν$_9$ band of ^{12}C$_2$H$_6$. JQSRT 2010;111:2481-504.

[218]   di Lauro C, Lattanzi F, Brown LR, Sung K, Vander Auwera J, Mantz AW, et al. High resolution investigation of the 7 μm region of the ethane spectrum. Planetary and Space Science 2012;60:93-101.

[219]   Lattanzi F, di Lauro C, Vander Auwera J. Toward the understanding of the high resolution infrared spectrum of C$_2$H$_6$ near 3.3 μm. J Mol Spectrosc 2011;267:71-9.

[220]   Villanueva GL, Mumma MJ, Magee-Sauer K. Ethane in planetary and cometary atmospheres: Transmittance and fluorescence models of the ν$_7$ band at 3.3 μm. Journal of Geophysical Research-Planets 2011;116.

[221]   Cazzoli G, Puzzarini C. The Lamb-dip spectrum of phosphine: The nuclear hyperfine structure due to hydrogen and phosphorus. J Mol Spectrosc 2006;239:64-70.

[222]   Davies PB, Neumann RM, Wofsy SC, Klemperer W. Radio-frequency spectrum of phosphine (PH$_3$). J Chem Phys 1971;55:3564-8.

[223]   Belov SP, Burenin AV, Polyansky OL, Shapin SM. A new approach to the treatment of rotational spectra of molecules with small moments of inertia applied to the PH$_3$ molecule in the ground state. J Mol Spectrosc 1981;90:579-89.

[224]   Chu FY, Oka T. "Forbidden" rotational spectra of phosphine and arsine. J Chem Phys 1974;60:4612-8.

[225]   Helms DA, Gordy W. "Forbidden" rotational spectra of symmetric-top molecules: PH$_3$ and PD$_3$. J Mol Spectrosc 1977;66:206-18.

[226]   Belov SP, Burenin AV, Gershtein LI, Krupnov AF, Markov VN, Maslovsky AV, et al. Rotational spectrum and spectroscopic constants of the phosphine molecule in the ground vibrational state. J Mol Spectrosc 1981;86:184-92.

[227]   Fusina L, Carlotti M. The far-infrared spectrum and spectroscopic parameters of PH$_3$ in the ground state. J Mol Spectrosc 1988;130:371-81.

[228]   Müller HSP. Spectroscopic parameters of phosphine. JQSRT 2013;this issue.

[229]   Cohen EA, Drouin BJ, Brown LR, Oh JJ. Terahertz and infrared spectra of carbonyl fluoride, COF$_2$: Vibration-rotation analyses of the four lowest bands, 2ν$_6$, and ν$_6$ hot bands; ^{13}COF$_2$ ground state and ν$_6$ band. JQSRT 2013;114:13-9.

[230]   Ciaffoni L, Cummings BL, Denzer W, Peverall R, Procter SR, Ritchie GAD. Line strength and collisional broadening studies of hydrogen sulphide in the 1.58 μm region using diode laser spectroscopy. Appl Phys B: Lasers Opt 2008;92:627-33.

[231]   Kaltenegger L, Sasselov D. Detecting Planetary Geochemical Cycles on Exoplanets: Atmospheric Signatures and the Case of SO$_2$. Astrophys J 2010;708:1162-7.

[232]   Azzam A, Yurchenko SN, Tennyson J, Martin M-A, Pirali O. THz spectroscopy of hydrogen sulphide. JQSRT 2013;this issue.

[233]   Flaud JM, Camy-Peyret C, Johns J. The far-infrared spectrum of hydrogen-sulfide - the (000) rotational-constants of H$_2$^{32}S, H$_2$^{33}S and H$_2$^{34}S. Can J Phys 1983;61:1462-73.

[234]   Yamada KMT, Klee S. Pure Rotational Spectrum of H$_2$S in the Far-Infrared Region Measured by FTIR Spectroscopy. J Mol Spectrosc 1994;166:395-405.

[235]   Belov SP, Yamada KMT, Winnewisser G, Poteau L, Bocquet R, Demaison J, et al. Terahertz Rotational Spectrum of H$_2$S. J Mol Spectrosc 1995;173:380-90.

[236]   Azzam A, Yurchenko SN, Tennyson J. Ab initio vibration-rotation transition intensities for H$_2$S; a room temperature line list. J Mol Spectrosc (in preparation).

[237]   Brown LR, Naumenko OV, Polovtseva ER, Sinitsa LN. *Hydrogen sulfide absorption spectrum in the 5700-6600 cm^{-1} spectral region.* Proc. of SPIE 14th Symposium on High-Resolution Molecular Spectroscopy. Editors Sinitsa L.N., Mikhailenko S.N. 2003;5311:59-67.

[238]   Brown LR, Naumenko OV, Polovtseva E R, Sinitsa LN. *Absorption spectrum of H$_2$S between 7200 and 7890 cm^{-1}.* Proc. of SPIE Tenth Joint International Symposium on Atmospheric and Ocean Optics. Atmospheric Physics. Part I: Radiation Propagation in the Atmosphere and Ocean. July 2004. V. 5396. P.42-48. Editors Matvienko GG, Krekov GM. February 2004, Krasnoyarsk, Russia

[239]   Naumenko O, Polovtseva ER. Database of the hydrogen sulfide absorption in the 4400-11400 cm^{-1} region. Atmos Oceanic Opt 2003;16:900-6.

[240]   Polovtseva ER, Lavrentiev NA, Voronina SS, Naumenko OV, Fazliev AZ. Information system for molecular spectroscopy. 5. Ro-vibrational transitions and energy levels of the hydrogen sulfide molecule. Atmos Oceanic Opt 2012;25:157-65.

[241]   Ulenikov ON, Liu AW, Bekhtereva ES, Gromova OV, Hao LY, Hu SM. High-resolution Fourier transform spectrum of H$_2$S in the region of the second hexade. J Mol Spectrosc 2005;234:270-8.

[242]   Ulenikov ON, Liu AW, Bekhtereva ES, Gromova OV, Hao LY, Hu SM. On the study of high resolution rovibrational spectrum of H$_2$S in the region of 7300-7900 cm^{-1}. J Mol Spectrosc 2004;226:57-70.

[243]   Ding Y, Naumenko O, Hu S-M, Zhu Q, Bertseva E, Campargue A. The absorption spectrum of H$_2$S between 9540 and 10000 cm^{-1} by intracavity laser absorption spectroscopy with a vertical external cavity surface emitting laser. J Mol Spectrosc 2003;217:222-38.

[244]   Naumenko O, Campargue A. Local mode effects in the absorption spectrum of H$_2$S between 10780 and 11330 cm^{-1}. J Mol Spectrosc 2001;209:242-53.

[245]   Bykov AD, Naumenko OV, Smirnov MA, Sinitsa LN, Brown LR, Crisp J, et al. The infrared spectrum of H$_2$S from 1 to 5 μm. Can J Phys 1994;72:989-1000.

[246]   Cherchneff I, Glassgold AE. The Formation of Carbon Chain Molecules in IRC +10216. Astrophysical J Lett 1993;419:L41.

[247]   de Graauw T, Feuchtgruber H, Bézard B, Drossart P, Encrenaz T, Beintema DA, et al. First results of ISO-SWS observations of Saturn: detection of CO$_2$, CH$_3$C$_2$H, C$_4$H$_2$ and tropospheric H$_2$O. Astron Astrophys 1997;321:L13-L6.

[248]   Fouchet T, Bézard B, Encrenaz T. The Planets and Titan Observed by ISO. Space Science Reviews 2005;119:123-39.

[249]   Waite JH, Young DT, Cravens TE, Coates AJ, Crary FJ, Magee B, et al. The Process of Tholin Formation in Titan's Upper Atmosphere. Science 2007;316:870-5.

[250]   Cernicharo J, Heras AM, Tielens AGGM, Pardo JR, Herpin F, Guélin M, et al. Infrared Space Observatory's Discovery of C$_4$H$_2$, C$_6$H$_2$, and Benzene in CRL 618. Astrophysical J Lett 2001;546:L123-L6.

[251]   Bernard-Salas J, Peeters E, Sloan GC, Cami J, Guiles S, Houck JR. The Spitzer IRS spectrum of SMP LMC 11. Astrophysical J Lett 2006;652:L29-L32.

[252]   Kunde VG, Aikin AC, Hanel RA, Jennings DE, Maguire WC, Samuelson RE. C$_4$H$_2$, HC$_3$N and C$_2$N$_2$ in Titan's atmosphere. Nature 1981;292:686-8.

[253]   Kunde VG, Flasar FM, Jennings DE, Bézard B, Strobel DF, Conrath BJ, et al. Jupiter's Atmospheric Composition from the Cassini Thermal Infrared Spectroscopy Experiment. Science 2004;305:1582-7.

[254]   Burgdorf M, Orton G, van Cleve J, Meadows V, Houck J. Detection of new hydrocarbons in Uranus' atmosphere by infrared spectroscopy. Icarus 2006;184:634-7.

[255]   Meadows VS, Orton G, Line M, Liang M-C, Yung YL, van Cleve J, et al. First Spitzer observations of Neptune: Detection of new hydrocarbons. Icarus 2008;197:585-9.

[256]   Dang-Nhu M, Guelachvili G, Ramsay DA. Absolute line intensities of the 5-μm ν_5-fundamental band of diacetylene. J Mol Spectrosc 1991;146:513-5.

[257]   McNaughton D, Bruget DN. The high-resolution infrared spectrum of diacetylene and structures of diacetylene, triacetylene and dicyanoacetylene. J Mol Struct 1992;273:11-25.

[258]   Arié E, Johns JWC. The bending energy levels of C_4H_2. J Mol Spectrosc 1992;155:195-204.

[259]   Jolly A, Fayt A, Benilan Y, Jacquemart D, Nixon CA, Jennings DE. The ν_8 Bending Mode of Diacetylene: From Laboratory Spectroscopy to the Detection of ^{13}C Isotopologues in Titan's Atmosphere. Astrophys J 2010;714:852-9.

[260]   Bizzocchi L, Degli Esposti C, Dore L. Submillimetre-wave spectrum of diacetylene and diacetylene-d2. Mol Phys 2010;108:2315-23.

[261]   Bizzocchi L, Tamassia F, Esposti CD, Fusina L, Canè E, Dore L. High-resolution infrared spectroscopy of diacetylene below 1000 cm^{-1}. Mol Phys 2011;109:2181-90.

[262]   Matsumura K, Kawaguchi K, Hirota E, Tanaka T. Stark modulation infrared diode laser spectroscopy of the $\nu_6 + \nu_8$ band of diacetylene. J Mol Spectrosc 1986;118:530-9.

[263]   Ho PTP, Moran JM, Lo KY. The Submillimeter Array. Astrophysical J Lett 2004;616:L1-L6.

[264]   Pilbratt GL, Riedinger JR, Passvogel T, Crone G, Doyle D, Gageur U, et al. Herschel Space Observatory. An ESA facility for far-infrared and submillimetre astronomy. Astron Astrophys 2010;518:L1.

[265]   Snell RL, Schloerb FP, Young JS, Hjalmarson A, Friberg P. Observations of HC_3N, HC_5N, and HC_7N in molecular clouds. Astrophys J 1981;244:45-53.

[266]   Jolly A, Benilan Y, Fayt A. New infrared integrated band intensities for HC_3N and extensive line list for the ν_5 and ν_6 bending modes. J Mol Spectrosc 2007;242:46-54.

[267]   Komasa J, Piszczatowski K, Lach G, Przybytek M, Jeziorski B, Pachucki K. Quantum Electrodynamics Effects in Rovibrational Spectra of Molecular Hydrogen. J Chem Theory Comput 2011;7:3105-15.

[268]   Pachucki K, Komasa J. Rovibrational levels of HD. Physical Chemistry Chemical Physics 2010;12:9188-96.

[269]   Schwartz C, Leroy RJ. Nonadiabatic eigenvalues and adiabatic matrix-elements for all isotopes of diatomic hydrogen. J Mol Spectrosc 1987;121:420-39.

[270]   Wolniewicz L, Simbotin I, Dalgarno A. Quadrupole transition probabilities for the excited rovibrational states of H_2. Astrophysical Journal Supplement Series 1998;115:293-313.

[271]   Pachucki K, Komasa J. Electric dipole rovibrational transitions in the HD molecule. Phys Rev A 2008;78:52503.

[272]   Kassi S, Campargue A. Electric quadrupole and dipole transitions of the first overtone band of HD by CRDS between 1.45 and 1.33 μm. J Mol Spectrosc 2011;267:36-42.

[273]   Campargue A, Kassi S, Pachucki K, Komasa J. The absorption spectrum of H_2: CRDS measurements of the (2-0) band, review of the literature data and accurate ab initio line list up to 35 000 cm^{-1}. Physical Chemistry Chemical Physics (Incorporating Faraday Transactions) 2012;14:802.

[274]   Cheng C-F, Sun YR, Pan H, Wang J, Liu A-W, Campargue A, et al. Electric-quadrupole transitions of H_2 determined to 10^{-9} precision. Phys Rev A 2012;85:24501.

[275]   Hu S-M, Pan H, Cheng C-F, Sun YR, Li X-F, Wang J, et al. The v=3 ← S(0)-S(3) electric quadrupole transitions of H_2 near 0.8 μm. Astrophys J 2012;749:76.

[276]   Gupta M, Owano T, Baer DS, O'Keefe A. Quantitative determination of the Q(1) quadrupole hydrogen absorption in the near infrared via off-axis ICOS. Chem Phys Lett 2006;418:11-4.

[277]   Tran H, Hartmann JM, Chaussard F, Gupta M. An isolated line-shape model based on the Keilson-Storer function for velocity changes. II. Molecular dynamics simulations and the Q(1) lines for pure H_2. J Chem Phys 2009;131.

[278]   Canaves MV, de Almeida AA, Boice DC, Sanzovo GC. On the chemistry of CS and NS in cometary comae. Adv Space Res 2007;39:451-7.

[279]   Moreno R, Marten A, Matthews HE, Biraud Y. Long-term evolution of CO, CS and HCN in Jupiter after the impacts of comet Shoemaker-Levy 9. Planetary and Space Science 2003;51:591-611.

[280]   Chandra S, Kegel WH, Le Roy RJ, Hertenstein T. Einstein A-coefficients for vib-rotational transitions in CS. Astron Astrophys, Suppl Ser 1995;114:175.

[281]   Blanquet G, Walrand J, Bouanich J-P. N_2 broadening of carbon disulfide $^{12}C^{32}S_2$ in the v_3 and $3v_3$ - v_1 bands. J Mol Spectrosc 1999;198:408-15.

[282]   Misago F, Lepère M, Bouanich J-P, Blanquet G. Self-broadening coefficients in the v_3 - v_1 band of CS_2. J Mol Spectrosc 2009;254:16-9.

[283]   Rawlins WT, Hensley JM, Sonnenfroh DM, Oakes DB, Allen MG. Quantum cascade laser sensor for SO_2 and SO_3 for application to combustor exhaust streams. Appl Opt 2005;44:6635-43.

[284]   Zhang X, Liang M-C, Montmessin F, Bertaux J-L, Parkinson C, Yung YL. Photolysis of sulphuric acid as the source of sulphur oxides in the mesosphere of Venus. Nature Geosci 2010;3:834-7.

[285]   Meyer V, Sutter DH, Dreizler H. The centrifugally-induced pure rotational spectrum and the structure of sulfur-trioxide: a microwave Fourier-transform study of a nonpolar molecule Z Naturforsch A 1991;46:710-4.

[286]   Underwood DS, Tennyson J, Yurchenko SN. An ab initio variationally computed room-temperature line list for SO_3. Phys Chem Chem Phys (submitted) 2013.

[287]   Kaldor A, Maki AG, Dorney AJ, Mills IM. Assignment of v_2 and v_4 of SO_3. J Mol Spectrosc 1973;45:247-52.

[288]   Ortigoso J, Escribano R, Maki AG. The v_2 and v_4 IR bands of SO_3. J Mol Spectrosc 1989;138:602-13.

[289]   Maki A, Blake TA, Sams RL, Vulpanovici N, Barber J, Chrysostom ETH, et al. High-resolution infrared spectra of the v_2, v_3, v_4 and $2v_3$ bands of $^{32}S^{16}O_3$. J Mol Spectrosc 2001;210:240-9.

[290]   Sharpe SW, Blake TA, Sams RL, Maki A, Masiello T, Barber J, et al. The v_3 and $2v_3$ bands of $^{32}S^{16}O_3$, $^{32}S^{18}O_3$, $^{34}S^{16}O_3$ and $^{34}S^{18}O_3$. J Mol Spectrosc 2003;222:142-52.

[291]   Maki A, Blake TA, Sams RL, Frieh J, Barber J, Masiello T, et al. Analysis of some combination-overtone infrared bands of $^{32}S^{16}O_3$. J Mol Spectrosc 2004;225:109-22.

[292]   Harrison JJ, Allen NDC, Bernath PF. Infrared absorption cross sections for ethane (C_2H_6) in the 3 μm region. JQSRT 2010;111:357-63.

[293]   Harrison JJ, Bernath PF. Infrared absorption cross sections for propane (C_3H_8) in the 3 μm region. JQSRT 2010;111:1282-8.

[294]   Harrison JJ, Allen NDC, Bernath PF. Infrared absorption cross sections for acetone (propanone) in the 3 μm region. JQSRT 2011;112:53-8.

[295]   Harrison JJ, Humpage N, Allen NDC, Waterfall AM, Bernath PF, Remedios JJ. Mid-infrared absorption cross sections for acetone (propanone). JQSRT 2011;112:457-64.

[296]   Allen NDC, Harrison JJ, Bernath PF. Acetonitrile (CH_3CN) infrared absorption cross sections in the 3 μm region. JQSRT 2011;112:1961-6.

[297]   Harrison JJ, Bernath PF. Mid- and long-wave infrared absorption cross sections for acetonitrile. JQSRT 2012;113:221-5.

[298]   Harrison JJ, Allen NDC, Bernath PF. Infrared absorption cross sections for methanol. JQSRT 2012;113:2189-96.

[299]   Harrison JJ, Bernath PF. ACE-FTS observations of acetonitrile in the lower stratosphere. Atmos Chem Phys 2013;13:3323-44.

[300]   Waterfall AM. Measurement of Organic Compounds in the Upper Troposphere using Infrared Remote Sensing. DPhil thesis, University of Oxford, 2004.

[301]   Moore DP, Remedios JJ, Waterfall AM. Global distributions of acetone in the upper troposphere from MIPAS spectra. Atmos Chem Phys 2012;12:757-68.

[302]   Boone CD. Private communication. 2012.

[303]   Allen G, Remedios JJ, Smith KM. Low temperature mid-infrared cross-sections for peroxyacetyl nitrate (PAN) vapour. Atmos Chem Phys 2005;5:3153-8.

[304]   Allen G, Remedios JJ, Newnham DA, Smith KM, Monks PS. Improved mid-infrared cross-sections for peroxyacetyl nitrate (PAN) vapour. Atmos Chem Phys 2005;5:47-56.

[305]   Tereszchuk KA, Moore DP, Harrison JJ, Boone CD, Park M, Remedios JJ, et al. Observations of peroxyacetyl nitrate (PAN) in the upper troposphere by the Atmospheric Chemistry Experiment Fourier Transform Spectrometer (ACE-FTS). Atmos Chem Phys 2013;13:1575-607.

[306]   Tereszchuk KA, Bernath PF. Infrared absorption cross-sections for acetaldehyde (CH_3CHO) in the 3 μm region. JQSRT 2011;112:990-3.

[307]   Clerbaux C, Colin R, Simon PC, Granier C. Infrared cross sections and global warming potentials of 10 alternative hydrohalocarbons. J Geophys Res 1993;98:10491.

[308]   Le Bris K, Strong K. Temperature-dependent absorption cross-sections of HCFC-142b. JQSRT 2010;111:364-71.

[309]   Höpfner M, Orphal J, von Clarmann T, Stiller G, Fischer H. Stratospheric $BrONO_2$ observed by MIPAS. Atmos Chem Phys 2009;9:1735-46.

[310]   Brasseur G, Solomon S. Aeronomy of the middle atmosphere (third edition), Atmos. Oceanograph. Sci. Lib., Springer, Dordrecht, The Netherlands, 369 ff., 2005.

[311]   Birk M, Friedl RR, Cohen EA, Pickett HM, Sander SP. The rotational spectrum and structure of chlorine peroxide. J Chem Phys 1989;91:6588-97.

[312]   Wetzel G, Oelhaf H, Kirner O, Ruhnke R, Friedl-Vallon F, Kleinert A, et al. First remote sensing measurements of ClOOCl along with ClO and $ClONO_2$ in activated and deactivated Arctic vortex conditions using new ClOOCl IR absorption cross sections. Atmos Chem Phys 2010;10:931-45.

[313]   Chance K, Orphal J. Revised ultraviolet absorption cross sections of H_2CO for the HITRAN database. JQSRT 2011;112:1509-10.

[314]   Thomas GE, Stamnes K, *Radiative Transfer in the Atmosphere and Ocean*. Cambridge University Press Cambridge, 1999.

[315]   Downing HD, Williams D. Optical constants of water in the infrared. J Geophys Res 1975;80:1656-61.

[316]   Kou L, Labrie D, Chylek P. Refractive indices of water and ice in the 0.65- to 2.5-μm spectral range. Appl Opt 1993;32:3531-40.

[317]   Warren SG, Brandt RE. Optical constants of ice from the ultraviolet to the microwave: A revised compilation. J Geophys Res [Atmos] 2008;113:D14220.

[318]   Fenn RW, Clough SA, Gallery WO, Good RE, Kneizys FX, Mill JD, Rothman LS, Shettle EP. Optical and infrared properties of the atmosphere. In: Jursa AS, editor. Handbook of geophysics and the space environment [chapter 18]. Springfield: National Technical Information Service; 1985.

[319]   Palmer KF, Williams D. Optical Constants of Sulfuric Acid; Application to the Clouds of Venus? Appl Opt 1975;14:208-19.

[320]   Remsberg EE, Lavery D, Crawford B. Optical constants for sulfuric and nitric acids. J Chem Eng Data 1974;19:263-5.

[321]   Tisdale RT, Glandorf DL, Tolbert MA, Toon OB. Infrared optical constants of low-temperature H_2SO_4 solutions representative of stratospheric sulfate aerosols. J Geophys Res [Atmos] 1998;103:25353-70.

[322]   Niedziela RF, Norman ML, DeForest CL, Miller RE, Worsnop DR. A Temperature- and Composition-Dependent Study of H_2SO_4 Aerosol Optical Constants Using Fourier Transform and Tunable Diode Laser Infrared Spectroscopy. J Phys Chem A 1999;103:8030-40.

[323]   Biermann UM, Luo BP, Peter T. Absorption Spectra and Optical Constants of Binary and Ternary Solutions of H_2SO_4, HNO_3, and H_2O in the Mid Infrared at Atmospheric Temperatures. J Phys Chem A 2000;104:783-93.

[324]   Querry MR, Tyler IL. Reflectance and complex refractive indices in the infrared for aqueous solutions of nitric acid. J Chem Phys 1980;72:2495-9.

[325]   Norman ML, Qian J, Miller RE, Worsnop DR. Infrared complex refractive indices of supercooled liquid HNO_3/H_2O aerosols. J Geophys Res [Atmos] 1999;104:30571-84.

[326]   Toon OB, Tolbert MA, Koehler BG, Middlebrook AM, Jordan J. Infrared optical constants of H2O ice, amorphous nitric acid solutions, and nitric acid hydrates. J Geophys Res [Atmos] 1994;99:25631-54.

[327]   Niedziela RF, Miller RE, Worsnop DR. Temperature- and Frequency-Dependent Optical Constants for Nitric Acid Dihydrate from Aerosol Spectroscopy. J Phys Chem A 1998;102:6477-84.

[328]   Richwine LJ, Clapp ML, Miller RE, Worsnop DR. Complex refractive indices in the infrared of nitric acid trihydrate aerosols. Geophys Res Lett 1995;22:2625-8.

[329]   Sutherland RA, Khanna RK. Optical Properties of Organic-based Aerosols Produced by Burning Vegetation. Aerosol Sci Technol 1991;14:331-42.

[330]   Magi BI, Fu Q, Redemann J. A methodology to retrieve self-consistent aerosol optical properties using common aircraft measurements. J Geophys Res [Atmos] 2007;112:D24S12.

[331]   Stagg BJ, Charalampopoulos TT. Refractive indices of pyrolytic graphite, amorphous carbon, and flame soot in the temperature range 25° to 600°C. Combust Flame 1993;94:381-96.

[332]   Chang H, Charalampopoulos TT. Determination of the Wavelength Dependence of Refractive Indices of Flame Soot. Proceedings: Mathematical and Physical Sciences 1990;430:577-91.

[333]   Alexander DTL, Crozier PA, Anderson JR. Brown Carbon Spheres in East Asian Outflow and Their Optical Properties. Science 2008;321:833-6.

[334]   Lund Myhre CE, Nielsen CJ. Optical properties in the UV and visible spectral region of organic acids relevant to tropospheric aerosols. Atmos Chem Phys 2004;4:1759-69.

[335]   Hasenkopf CA, Beaver MR, Trainer MG, Langley Dewitt H, Freedman MA, Toon OB, et al. Optical properties of Titan and early Earth haze laboratory analogs in the mid-visible. Icarus 2010;207:903-13.

[336]   Zarzana KJ, De Haan DO, Freedman MA, Hasenkopf CA, Tolbert MA. Optical Properties of the Products of α-Dicarbonyl and Amine Reactions in Simulated Cloud Droplets. Environmental Science & Technology 2012;46:4845-51.

[337]   Querry MR *Optical constants of minerals and other materials from the millimeter to the ultraviolet*; Chemical Research, Development Engineering Center: Aberdeen, 1987.

[338]   Toon OB, B. Pollack J, Sagan C. Physical Properties of the Particles Composing the Martian Dust Storm of 1971-1972. Icarus 1977;30:663-96.

[339]   Wagner R, Ajtai T, Kandler K, Lieke K, Linke C, Muller T, et al. Complex refractive indices of Saharan dust samples at visible and near UV wavelengths: a laboratory study. Atmos Chem Phys 2012;12:2491-512.

[340]   Sinyuk A, Torres O, Dubovik O. Combined use of satellite and surface observations to infer the imaginary part of refractive index of Saharan dust. Geophys Res Lett 2003;30:1081.

[341]   Grainger RG, et al. Measuring Volcanic Plume and Ash Properties from Space. In: Remote Sensing of Volcanoes and Volcanic Processes: Integrating Observation and Modeling (Pyle D, Mather T, edit.). London: Special Publ Geo Soc; 2013.

[342]   Ramanathan V, Carmichael G. Global and regional climate changes due to black carbon. Nature Geosci 2008;1:221-7.

[343]   Massie S, Hervig M. HITRAN 2012 Refractive Indices. JQSRT 2013.

[344]   Richard C, Gordon IE, Rothman LS, Abel M, Frommhold L, Gustafsson M, et al. New section of the HITRAN database: Collision-induced absorption (CIA). JQSRT 2012;113:1276-85.

[345]   Dubernet ML, Boudon V, Culhane JL, Dimitrijevic MS, Fazliev AZ, Joblin C, et al. Virtual atomic and molecular data centre. JQSRT 2010;111:2151-9.

[346]   Hill C, Gordon IE, Rothman LS, Tennyson J. A new relational database structure and online interface for the HITRAN database. JQSRT 2013;this issue.

[347]   Laraia AL, Gamache RR, Lamouroux J, Gordon IE, Rothman LS. Total internal partition sums to support planetary remote sensing. Icarus 2011;215:391-400.

[348]   Fischer J, Gamache RR, Goldman A, Rothman LS, Perrin A. Total internal partition sums for molecular species in the 2000 edition of the HITRAN database. JQSRT 2003;82:401-12.

JQSRTJQSRTJQSRTJQSRTJQSRTJQSRTJQSRTJQSRTJQSRTJQSRT